WILLIAMS, LEE B., Ph.D. Chitin Nanofiber Alignment: Optical and Quantitative Analysis. (2014)
Directed by Dr. Dennis R. LaJeunesse. 133 pp.

Polymers are an important material in modern life. Most of our modern world is made of polymeric materials. When we think of polymers, the synthetic plastics we use on a regular basis typically come to mind, but not all polymers are synthetics. The natural world is made up of polymers; we are made up of biological polymers. In fact, polynucleotides, polypeptides, and polysaccharides are all important polymers essential for life as we know it. Chitin is a valuable biopolymer that is an easily attainable, sustainable natural material and has the potential to become more commercially important in the near future. Chitin is the second most abundant biopolymer on the planet. This exquisitely abundant natural resource is found in the exoskeletons of arthropods, the beaks of cephalopods, the radulae of mollusca, and the cell wall of fungi. As a biopolymer, chitin is robust and strong, biologically compatible, and insoluble in all common polar solvents. Chitin shows resilience to wear, but it is completely biodegradable and enzymatically digested by chitinases. It provides much the same properties to insect cuticle as cellulose provides in the cell walls of plants: strength, rigidity, protection, and a basis for a mechanically resilient composite material. However, the organization of chitin in these structures, especially at the nanoscale, remains undescribed, as do the mechanisms that govern this organization. For this thesis I will determine and characterize the patterns of chitin alignment in an insect cuticle, characterize the linear polarization associated with specific cuticle structures, determine the role that chitin organization plays in this property, and determine the underlying rules of chitin nanofiber alignment.

CHITIN NANOFIBER ALIGNMENT: OPTICAL AND QUANTITATIVE ANALYSIS

by

Lee B. Williams

A Dissertation Submitted to
the Faculty of the Graduate School at
The University of North Carolina at Greensboro
in Partial Fulfillment
of the Requirements for the Degree
Doctor of Philosophy

Greensboro
2014

Approved by

_____
Committee Chair

To my wife, Allison, and my family – who have supported my endeavours.

APPROVAL PAGE

This dissertation written by Lee B. Williams has been approved by the following committee of the Faculty of The Graduate School at The University of North Carolina at Greensboro.

Committee Chair _____
Dennis R. LaJeunesse

Committee Members _____
Daniel Herr

_____
Albert Hung

_____
Joseph Starobin

_____
Date of Acceptance by Committee

_____
Date of Final Oral Examination

TABLE OF CONTENTS

LIST OF TABLES

Page

LIST OF FIGURES

Page

CHAPTER I

INTRODUCTION

The overarching scope of this research lies in the understanding and the furthering of the understanding of the organization of chitin. Chitin is a valuable biopolymer that is an easily attainable and sustainable natural material and has the potential to become more commercially valuable in the near future. This work will focus on the chitin as organized by insects, more specifically, in the wings of the seventeen year cicada, *Magicicada septendecim*. *M. septendecim* is a cicada that emerges in large broods every seventeen years.

1.1 Polymers

Polymers are an important material in modern life. Most of our modern world is made of polymeric materials. In the simplest terms and the literal translation of the word, a polymer is made up of many units: "Poly" from the Greek word for many and "mer" from Greek meros, which means part. So, a polymer is made up of many parts. In the chemical sense, a polymer is made up of many monomers. Polymers can be homopolymers and heteropolymers. Homopolymers are polymer chains made up of one kind of monomer while heteropolymers consist of more than one type of monomer. A few examples of common polymers that are used daily would be things like polyethylene (PE) that is found in plastic bags, polyethylene terephthalate (PET) that makes up soda bottles, and polypropylene (PP) that can be found a list of items too long to enumerate. To sum up, all of the items used in daily life know as plastics are in the polymers category. In the examples above, the first part of the word is

"poly", as, in there are many propylenes and many ethylenes and so on. The polymer is made up of a chain of covalently linked monomers to create the unit. The chemical composition of the monomers involved in a polymer are a major factor in determining the overall characteristics of the polymer.

Often polymers are described by the number of parts of the chain. The molecular weight governs some of the material properties of the polymer, such as tensile strength and melt flow viscosity. When polymers are made through a chemical synthesis route in a factory for commercial use, the number of units of a distribution of chains falls along a bell shaped curve. The narrower the bell shape, the higher quality the polymer, but the curve is always bell shaped. This means that synthetic polymer also has a distribution of molecular weight in a single sample. A spread in molecular weight is the cause of variations in the materials properties of plastics. The idealized situation is one in which all chains have the same number of units and molecular weight and the bell shaped curve is reduced to a Dirac delta function. The idealized situation is more readily achieved with biosynthesized polymers. An example of which is spider's silk. The fine threads produced by spiders are known to be very strong and tough.

The architecture of polymers is varied, as they can be long, straight chains or branched in a variety of manners. Polymers of the same monomer can be branched or unbranched. An example of this case is with polyethylene. Both high density polyethylene (HDPE) and low density polyethylene (LDPE) have the same basic monomeric chemical structure,$(C_2H_4)_nH_2$. HDPE is unbranched whereas LDPE has a percentage of branching on the carbon atoms. The branching greatly effects the

material properties of the final polymer: tensile strength, density, clarity, and thermal stability.

Generally, the polymers used in daily life are melt-processed plastics. Melt processing simply means that the feed stock to be used is melted and the melt manipulated in a manner according to end use. Plastics can be extruded and drawn to create fibers, blown into films, or injection molded into parts. Once the melt has cooled, the final form of the polymer is set. Plastics can be remelted and recycled. Prior to this end processing, the plastics must be compounded with other materials to impart special features and characteristics. The features and characteristics may include clarifying agents, flame retardants, colorants, and so on.

1.2 Biopolymers

When we think of polymers, the synthetics we use regularly do typically come to mind; but not all polymers are synthetic. The natural world is made up of polymers; we are made up of biological polymers. In fact, polynucleotides, polypeptides, and polysaccharides are all important polymers essential for life as we know it.

Biopolymers are abundant, have great economic potential and are an environmentally valuable resource. They are biologically derived, which means that with proper management they can be a renewable resource. As resource management becomes more important due our dwindling stocks of petroleum based plastics and other polymeric materials, it will be increasingly important going forward to develop and maintain diverse resources such as biopolymers [10]. As mentioned before, biopolymers are more consistent in their chain length, a therefore have more consistent material properties.

The production of biologically synthesized polymers follow a similar route to plastics. The major difference being the manner in which the polymer is processed. Biologically produced, or biopolymers, are produced by a cell, one at a time. This eliminates the bell shaped curve, each chain looks just like the one produced before it and the one produced after. Also, biopolymers are also mostly solution processed by the cells to allow for enzymatic action, catalysis, and secretion and manipulation. Biopolymers still undergo a sort of compounding process to mix in other, non-polymeric materials to add desired traits and characteristics.

Biopolymers fall into three main categories: nucleic acids, proteins, and polysaccharides. The nucleic acids make up the RNA and DNA required for life and can range in size from 21 nucleotides to the 247 million base pairs found in human chromosome 1. Proteins are made up of single or multiple chains of amino polypeptides. The proteins are large molecules containing greater than 30 polypeptides. Polysaccharides are composed of repeating sugar units that can have as few as ten monomers up to around 3000 monomers repeated.

1.2.1 Polysaccharides

An important branch of the biopolymer tree are the polysaccharides. The polysaccharides are made up of many units of monosaccharides, such as glucose and fructose, linked by a glycosidic bond. The polysaccharides are important both structurally and as energy storage. Examples of energy storage polysaccharides would be starch and glycogen. Examples of structural polysaccharides would be cellulose, hyaluronan, and chitin.

The three examples of structural polysaccharides (cellulose, hyaluronan, and chitin) are long chain, unbranched polymers. They are created in the cell by a class of mem-

brane associated synthase protein complexes [40, 50]. The synthases are a group of trans membrane proteins that catalyze and link monomers together to form a polysaccharide chain. The monomers of the nascent polysaccharide are linked one at a time as they pass through the transferase and are excreted into the extra-cellular area.

1.2.2 Lineages of Polysaccharides

Chitin repeats are linked via a glycosidic bond. The glycosidic bond is a covalent bond that exists between a hemiacetal and another molecule. These molecules are termed "glycosides". The reaction of the anomeric carbon (the carbonyl carbon) (Figure 1) in a carbohydrate with the hydroxyl group of another compound yields the breaking of the carbonyl double bond and the addition of a single bond and water. In the case of chitin, both molecules, the hemiacetal and the alcohol, are N-acetylated glucosamine molecules; in the case of cellulose, the glycosidic bond is between two glucose molecules. The glycosidic bond is common in nature. Many natural systems use it as a means of storing energy. The bound chains of glucose are relatively inert and require the action of enzymes to cleave off the glucose or maltose molecules that supply energy to living organisms. The lactol (such as glucose or N-acetylglucosamine) is the ring analog of a hemiacetal; the linear forms of aldehydes are less stable than the ring form. For instance, D-glucose, the chain aldehyde form of glucose, forms a six member ring of α- and β-D-glucopyranose (Figure 2). The α and β prefix is used to denote the location of the hydroxyl group located at the anomeric carbon, C1, with respect to the hydroxyl group located at C5. If the -OH at C1 is a trans configuration with regards to the -OH at C5, i.e. on the opposite side of the plane of the ring, it is α-D-glucopyranose. If the -OH at C1 is in a cis

configuration with the -OH at C5, on the same side of the plane of the ring, it is β-D-glucopyranose.

1.2.3 Starches

Starch and glycogen are both polysaccharides used in the storage of energy. Starch is derived from plants and glycogen from animals. They are both heavily branched polysaccharides of glucose. The starches and glycogens yield glucose upon hydrolysis for use by the cells as a source of energy. Energy storage polysaccharides are an important resource in the making of beer. The starches stored in the barley kernel are extracted from the grain by steeping in hot water. Along with the starches, the enzyme, β – amylase, is also extracted from the husk of the grain. The β – amylase acts on the starch as a two–cutter by hydrolyzing every other glycosidic bond, yielding maltose. Maltose is readily fermented by the yeast *Saccharomyces cerevisiae* into alcohol, carbon dioxide, and other byproducts.

1.2.4 Cellulose

Of the structural polysaccharides, the longest running biopolymers used by humans is cellulose. The most common place to find cellulose is in wood. Cellulose is a major constituent in the cell walls of plants and is responsible for the rigidity of woody plants and lumber [15]. For thousands of years, lumber has been used as a building material to shelter from nature or to adorn the sacred [23, 64]. One of the first composite materials used by humans was based on cellulose. Wattle and daub construction has been around since the neolithic period and is still employed in building today [19]. This manner of construction uses wood sticks or staves covered over with a mud or clay based plaster.

As a polymer, cellulose is a long, unbranched chain of repeating glucopyranose rings. The length of the chain depends upon the origin of the cellulose [34]. Cellulose is also produced by algae and bacteria. Bacterial cellulose tends to be the longest and purest [28]. These long chains of cellulose are chemically stable and can be degraded by cellulase to obtain cellobiose, and further to glucose by β –glucosidase. The cellulose chain is insoluble in water and can be extracted from pulp wood by boiling to create a soupy suspension of cellulose in water, which can be dried in sheets to create paper. Though this method of paper production is simplified and antiquated, the notion that cellulose makes up the bulk of paper is no less true.

1.2.5 Chitin

Chitin is the second most abundant biopolymer on the planet [52]. This exquisitely abundant natural resource is found in the exoskeletons of arthropods, the beaks of cephalopods, the radulae of mollusca, and the cell wall of fungi [6, 42, 47, 49]. Chitin is very much underutilized; most is thrown out with the discards of last evening's dinner. As a biopolymer, chitin is robust and strong, biologically compatible, and insoluble in all common polar solvents. Chitin shows resilience to wear, but it is completely biodegradable and enzymatically digested by chitinases [46].

Chemically, chitin is similar to cellulose - the material found in plants, trees, and algae(Figure 1). Whereas cellulose is a repeating polymer of β (1,4) D-glucose units, chitin is comprised of β (1,4) linked N-acetylglucosamine, replacing a hydroxyl group on each monomer with an acetyl amine group. The chemical formula of chitin is written as $(C_8H_13O_5N)_n$ (Figure 3). Chitin is formed when an amine group is substituted for the hydroxyl group at the C2 carbon on the glucopyranose and is acetylated. When multiple repeats of the chitin molecule are linked together via

the $\beta(1,4)$ glycosidic bonds, the formation of long chains occurs. These long chains are the normal manner in which chitin is found in nature. The length of the chain produced is dependent upon the species that creates it and has been shown to be influenced by the NodC gene [34]. Hydrogen bonding between the individual chains is quite prevalent due to the acetyl amine groups on the chitin monomers resulting in a very strong and stable polymer. This hydrogen bonding is the basis for chitin's relative insolubility in most common solvents. Modification to chitin can result in greater water solubility. Deacteylation of chitin results in the formation of chitosan.

A water soluble derivative of chitin is chitosan(Figure 4). Chitosan is a commercially available material that is commonly used as a fining agent in wines and beers. Chitosan is produced naturally in cuticle, to a lesser degree than chitin. It can be manufactured by treating chitin with a strong alkali to remove the acetyl group from the chitin.

1.2.6 Insect Cuticles: Structural Applications of Chitin

Chitin can be thought of as the animal kingdom's analogue to cellulose [3]. It provides much the same functions as cellulose in plant cell walls: strength, rigidity, protection, and a basis for a mechanically resilient composite material [60]. Chitin, as a biopolymer, is found in the cuticle of insects and other arthropods, the beaks of squid , the radulae of Mollusca, and the cell walls of fungi[6, 42, 47, 49]. The cuticle of the arthropod is an amazing composite material that has been around for at least 500 million years. The cuticle is a layered composite of chitin and an extracellular matrix that is composed of minerals, lipids, and proteins. The cuticle has two layers: the procuticle and the epicuticle. The procuticle is in turn composed of two distinct layers: the endocuticle and the exocuticle. The cuticular layer is built upon the epidermal

cells of the organism. The epidermis excretes the chitin and the extracellular matrix. The extracellular matrix guides and organizes the chitin and solidifies it into a hard shell. The cuticle can take on many textures, as it can be hard and brittle and also soft and supple. This wide range of material features is due to the way in which the cuticle is organized and what is making up the extra-cellular matrix.

An issue with chitin is that it is insoluble in most solvents. It strongly hydrogen bonds with itself to produce a crystalline structure that is quite chemically inert [48]. It is a simple matter to remove the extra-cellular matrix to purify chitin, but once it is in a purified state it is exceptionally stable. This can be a double-edged sword in terms of using it in any useful manner. It can be degraded in strong acid to break it down into the constituent monosaccharides, which leave none of the desirable properties of chitin. It can be dissolved into a calcium solvent, which is also used in the dissolution of nylons, or into fluorinated alcohols. Both solvents dissolve the chitin due to the disruption of hydrogen bonding, and both have their pitfalls when it comes to chitin manipulation.

Chitin use is generally limited to the use of its water soluble derivative, chitosan. Chitosan is a de-acetylated form of chitin that naturally occurs in cuticle, or it can be produced by treating chitin with an acid. Typically to produce a chitin product, chitosan will be used as a starting point and acetylated to produce chitin. This method is inefficient and leaves a certain amount of the material as chitosan in the finished product.

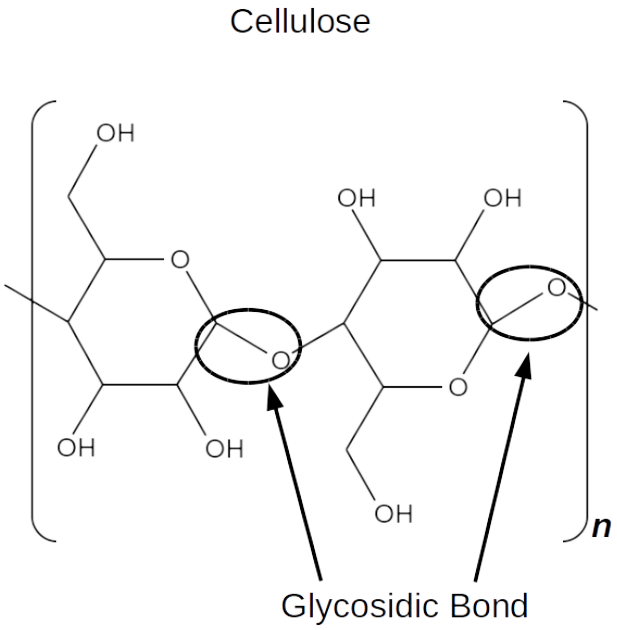

Figure 1. Stick Diagram of Cellulose. Cellulose is the most common biopolymer on Earth. Arrows are indicating the glycosidic bonds that bind polysaccharides.

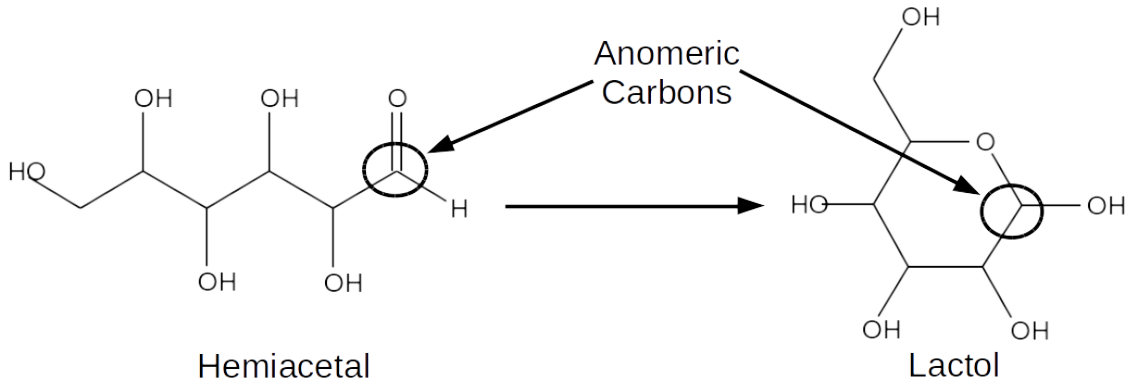

Figure 2. Hemiacetals and Lactols. The linear hemiacetal forms a lactol when the hydroxyl group interacts with the carbonyl group, forming a ring compound; which is thermodynamically more stable.

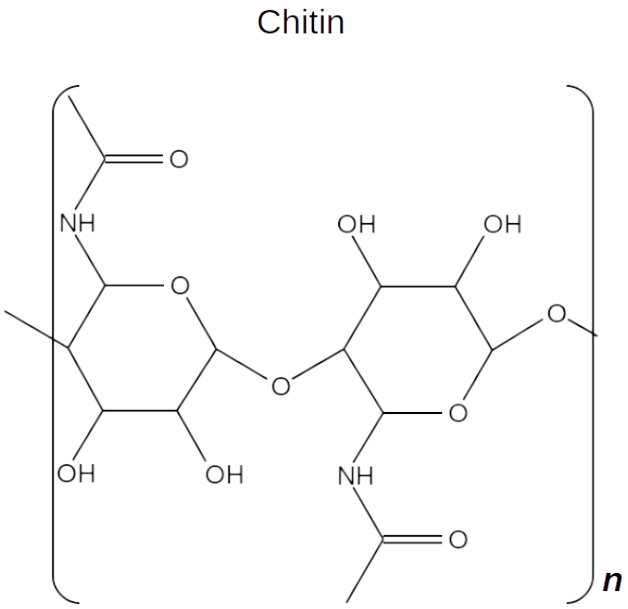

Figure 3. The Stick Diagram of Chitin. Chitin is the second most abundant biopolymer on Earth.

Chitosan

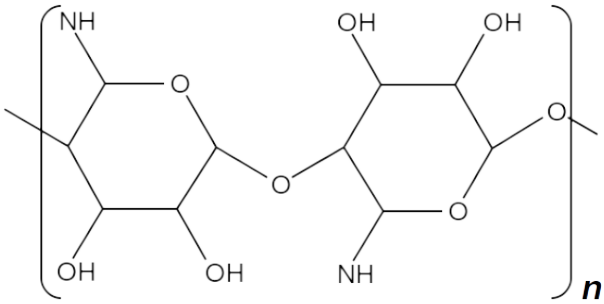

Figure 4. The Stick Diagram of Chitosan. Chitosan is a modified, water soluble form of chitin.

1.3 Cicadas and Insect Cuticle

The song of the cicada can be identified on any summer evening by the long, rasping drone that they use to call mates. The cicada flight is rather graceless, they more bumble through the air clumsily than fly and dart about like a bee or wasp. It is in the anecdotal observation of the flight of the cicada, it becomes apparent that the overlapping, flapping of the wings does more than keep them airborne in flight. As the cicada flies and flutters its wings to keep aloft, it becomes visually curious. There seems to be a blurring effect as the wings cross one another in the line of sight.

1.3.1 Chitin Crystal Structure

The crystal structure of chitin was first discussed by Meyer and Pankow in 1935 and further refined by Carlstrom in 1957 [12]. The introduction of the amine groups adds a larger degree of hydrogen bonding with one chitin chain and another. This hydrogen bonding leads to the crystal structure of chitin. Chitin exhibits three distinct crystalline polymorphs, α, β, and γ. Of these three, the α form of chitin is the most abundant. The α-chitin is an orthorhombic crystal structure of the space group P212121, which has lattice constants (a, b, c) of (4.749Å, 18.89Å, 10.33Å). The c lattice parameter is in the chitin chain direction(Figure 5). The powder diffraction of α-chitin show distinct diffraction peaks at 9.390 degres (020), 19.340 degrees (110), and 26.570 degrees (130) 2θ (the numbers in parenthesis being the (h k l) values of the planes represented). The most pronounced is the (110) family of planes.

1.3.2 Mechanical Properties of Insect/Arthropod Cuticle

The mechanical properties of the arthropod cuticle are quite remarkable. Cuticle ranges from hard and tough to soft and supple and it all incorporates chitin in the

matrix of its structure. An example of the former is the hard, protective shell of the beetle elytra, which is a derivative of the forewing that has evolved to form a protective covering for the flight wing. An example of the latter is the segments of the caterpillar, which allow it to flex and move. The vast and varied areas of a stress - strain plot that insect cuticle occupies shows it to be a wonderful structure, and this is in no small part due to the chitin of which it is comprised. Cuticle has a Young's Modulus that ranges from 1kPa to 150GPa[60].

Cuticle is a composite material. Although composites of natural materials have been known to mankind for thousands of years, artificial composites are a relatively new manner of construction, having seen a great deal of use since the early 1900s [13, 41]. The past one hundred years, or even thousands of years, pales in the comparison to the length of time the natural world has been producing composites. Arthropods developed during the Cambrian period- over 500 million years ago [17].

The natural composite of cuticle is by no means a simple affair, either. Arthropoda build their cuticle sequentially. Each layer is excreted from the epidermis and as each subsequent layer is excreted, the layer preceding it temporally moves up and away from the epidermis and is compacted [59]. The chitin fibrils are approximately 2 - 5nm in diameter and can be up to 300 nm long. The chitin is organized into bundles that are between 50 – 300nm in diameter and up to 1 micron long. These bundles are then organized into larger fibers (Figure 6). The extracellular matrix is composed of proteins that aid in the organization of the chitin fibers as they are moved out from the epidermis, which are later sclerotized and pigmented. The bundles of chitin fibers are organized into planar sheets of fibers bound in the extracellular matrix. The fibers in the sheets are laid up in a general, singular direction, giving an organized,

parallel orientation. As each new sheet is created, the fibers' orientation is rotated slightly, 7 – 8 degrees, off the axis of the preceding sheet. As more sheets are added, a helicoidal structure known as a Bouligand structure is created (Figure 6). Bouligand structure is the term applied when there are enough layers to rotate through 180 degrees. The lay up of each successive layer gives multi-directional strength, much like that of plywood or modern fiberglass construction.

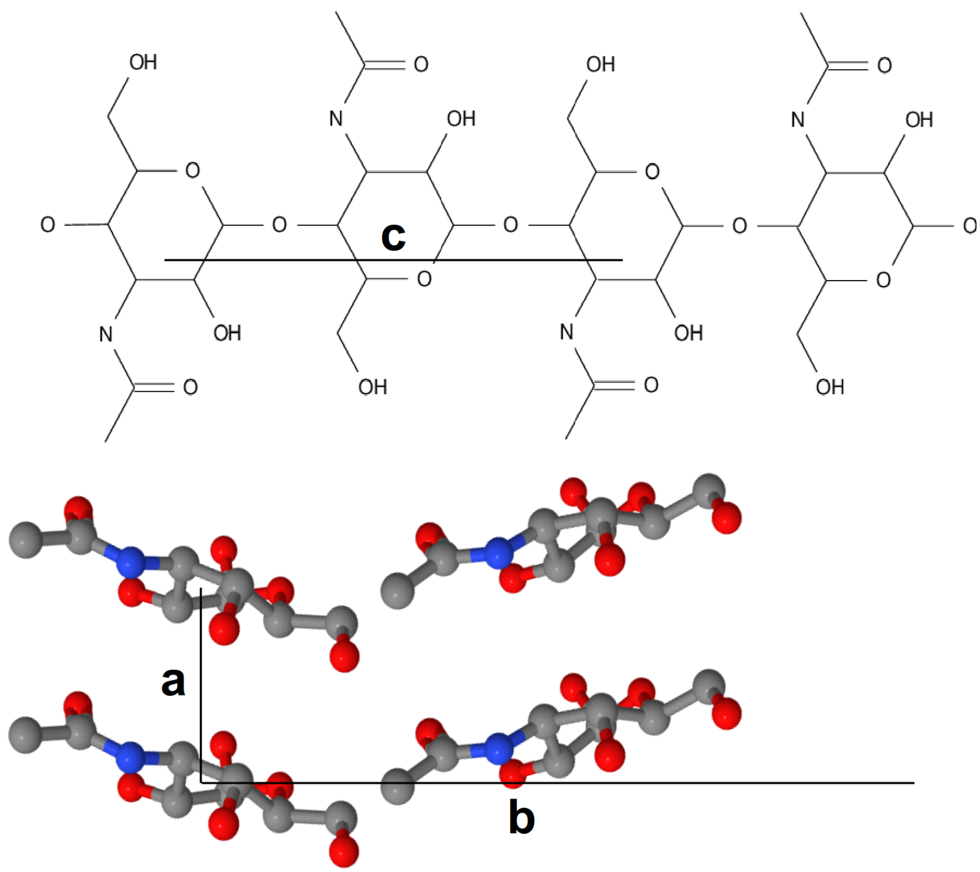

Figure 5. The Crystal Structure of Chitin. The c base vector is in the chain length direction.

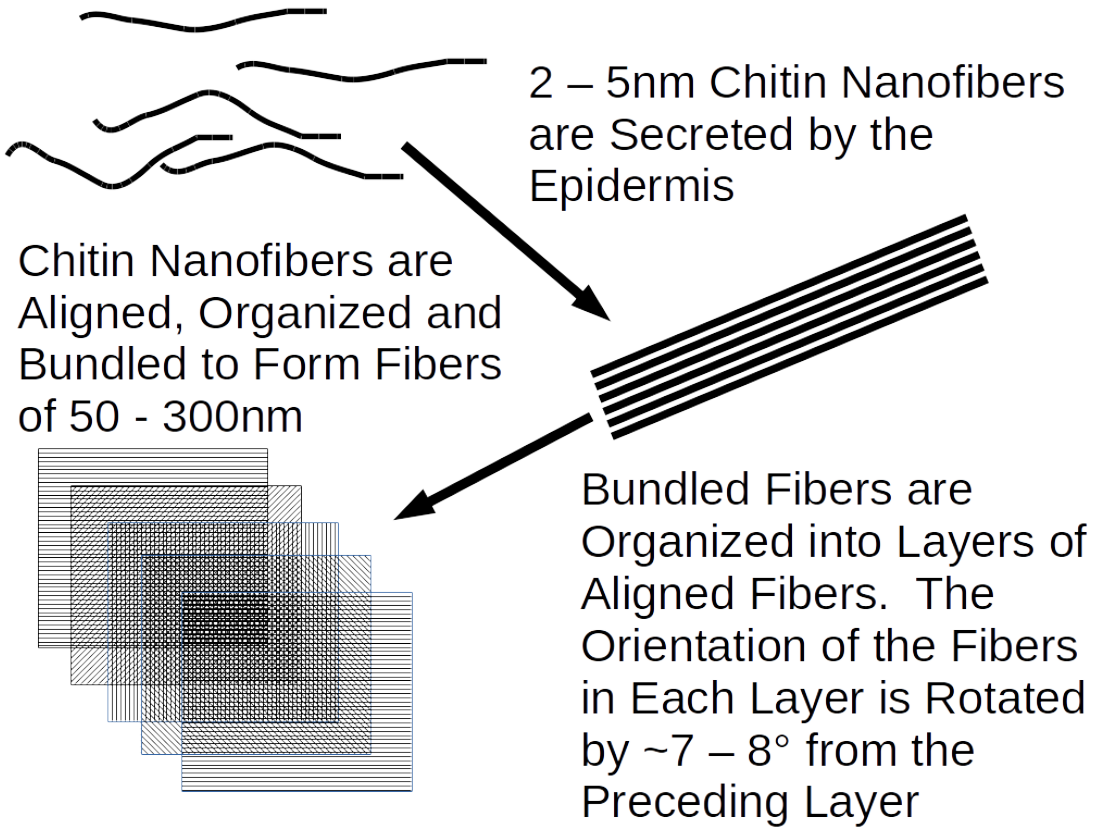

Figure 6. Chitin Fibrils are Bundled into Chitin Fibers. The fibers are organized in to laminar sheets that make up the cuticle.

1.4 Polarization and Methods of Polarization

1.4.1 Random Polarization

Randomly polarized or unpolarized light is light that is composed of electric field elements oriented in multiple, random directions. This is a typical state for light and other electromagnetic fields, and we interact with unpolarized light on a regular basis.

1.4.2 Elliptical Polarization

The general state of polarization is elliptical. Linearly polarized and circularly polarized light are special cases of elliptical polarization. When unpolarized light becomes elliptically polarized, the tip of the electric field vector traces out an elliptical path in the plane perpendicular to the direction of propagation of the light. This elliptically polarized light can be decomposed into two linear polarized waves whose angles of polarization are perpendicular to one another (Figure 7).

The electromagnetic wave equation for this system can be described mathematically using the classical sinusoidal plane wave solution for the electric and magnetic fields:

$$\vec{E}(\vec{r},t) = E * \Re(|\psi|e^{i(kz-\omega t)}) \tag{1.1}$$

and

$$\vec{B}(\vec{r},t) = \hat{z} \times \vec{E}(\vec{r},t) \tag{1.2}$$

and

$$c = \frac{\omega}{k}. \tag{1.3}$$

Here, the electric field is represented by $\vec{E}$, the magnetic field is represented by $\vec{B}$, c is the speed of light, k is the wave number and ω is the angular frequency. The normalized Jones vector is defined as:

$$|\Psi\rangle \equiv \begin{pmatrix} \Psi_x \\ \Psi_y \end{pmatrix} \begin{pmatrix} \cos\theta & e^{i\alpha_x} \\ \sin\theta & e^{i\alpha_y} \end{pmatrix} \tag{1.4}$$

The ellipse traced out by the electric field has a semi-major axis, A, and a semi-minor axis, B, that can be defined by (Figure 8), where

$$A = E\sqrt{\frac{1 + \sqrt{1 - \sin^2 2\theta \sin^2 \beta}}{2}} \tag{1.5}$$

and

$$B = E\sqrt{\frac{1 - \sqrt{1 - \sin^2 2\theta \sin^2 \beta}}{2}} \tag{1.6}$$

and

$$\beta = \alpha_y - \alpha_x \tag{1.7}$$

The orientation of the ellipse in the x – y plane is determined by the angle, ϕ, that the semi-major axis makes with the x – axis and can be calculated by

$$\tan 2\phi = \tan 2\theta \cos \beta. \tag{1.8}$$

The direction the electric field precesses in the x – y plane can be be either clockwise or counterclockwise, left or right handed. If β is negative, the polarization is counterclockwise, or left handed. If β is positive, the polarization is right handed.

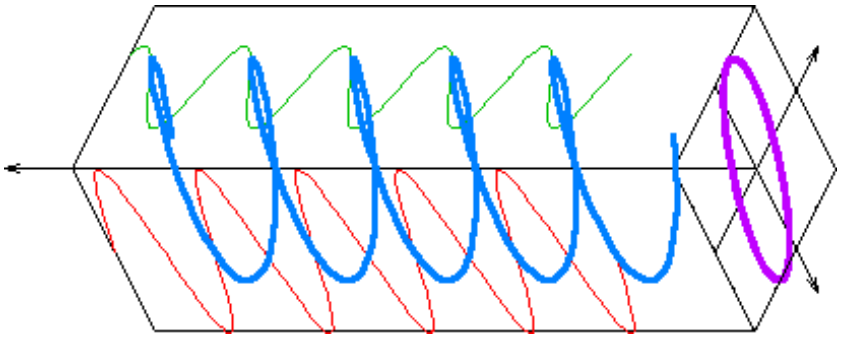

Figure 7. Elliptically Polarized Light. An example of elliptically polarized light as the sum of two component vectors.

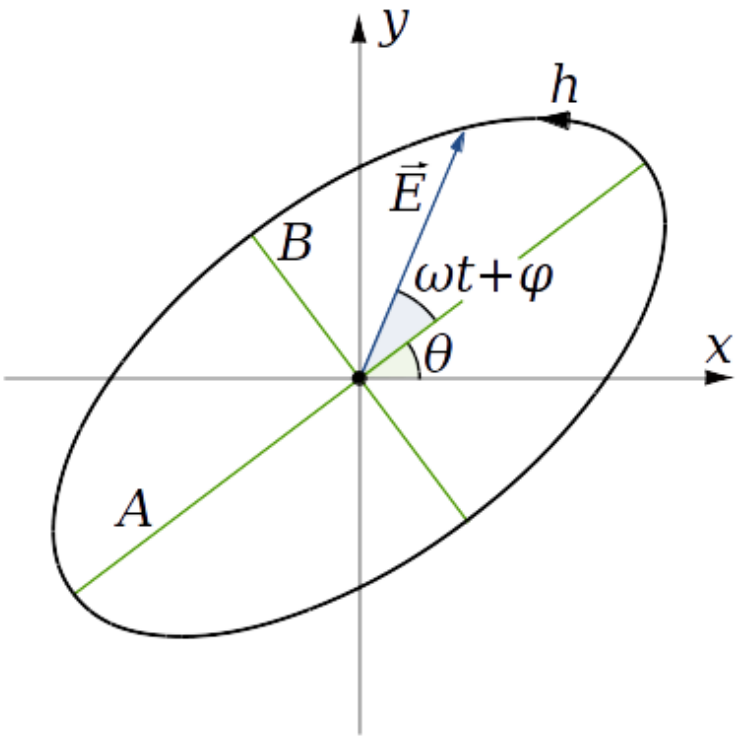

Figure 8. The Ellipse of Polarization. The polarization ellipse shows semi–major and semi–minor axes and angles.

1.4.3 Circular Polarization

Circularly polarized light is a special case of elliptically polarization in which the semi-major axis and the semi-minor axis are equal (Figure 9) and

$$\beta = \pm\frac{\pi}{2} \tag{1.9}$$

and

$$\theta = \frac{\pi}{4} \tag{1.10}$$

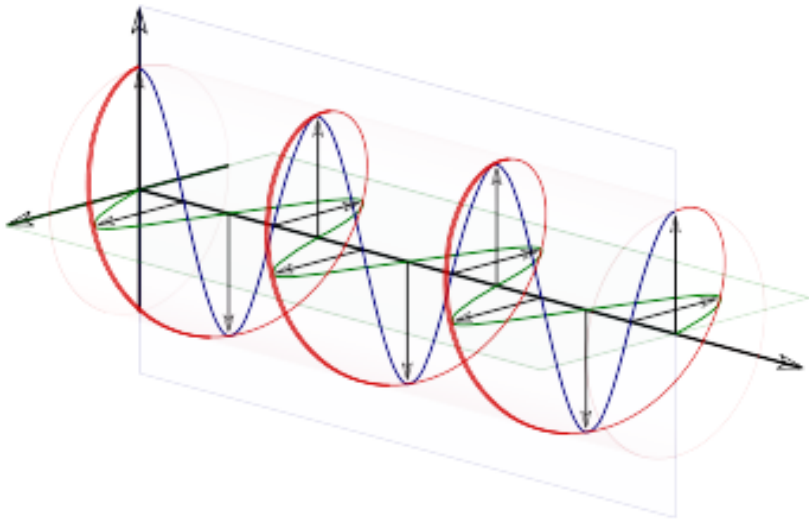

Figure 9. Circularly Polarized Light. An example of circularly polarized light as the sum of two component vectors.

1.4.4 Linear Polarization

Starting from the initial conditions from the case of elliptically polarized light and $\beta = 0$, the ellipse of polarization becomes a line. The semi-major axis, A, traces out the amplitude of the electric field and the semi-minor axis becomes zero. The angle, ϕ, that the semi-major axis makes with the x – axis is equal to θ (Figure 10).

1.4.5 Malus' Law

Light can be polarized in a number of ways. In this case we polarize the light by means of a polarizing filter, a Polariod-type film. This linearly polarized light then has an electric field vector that is oriented in a specific direction (Figure 10).

A simple and effective means to describe polarization and the axis of polarization is to imagine a grid of parallel conducting wires whose diameter is much smaller than their length. If this grid is placed in the path of unpolarized light, the portion of the electric field that has a vector component parallel to the wire grid will excite the electrons in the wires and cause them to move up and down the wires with the frequency of the light. The motion of the electrons causes ohmic heating in the wires which dissipates the energy of the field with components parallel to the wires. The only electric field component that is left is that which is perpendicular to the grid, and this is the axis of polarization.

Malus's Law tells us that if unpolarized light propagating in the **z** direction is shown through a polarizer lying in the x – y plane, it will have intensity defined by

$$I_0 = {E^2}_0 \tag{1.11}$$

If the polarizer has a polarizing axis that is at some angle, θ, from the x-axis, then the electric field (E) will look like:

$$\vec{E_0} = E\cos\theta\hat{x} + E\sin\theta\hat{y} \tag{1.12}$$

The polarized light has only the electric field components that lie in the axis of the polarizer, all others being completely attenuated. If another polarizer is placed in the beam behind the first, with a polarizing axis lying in the +x – axis, only the component along the x – axis will remain.

$$\vec{E_0} = E_0\cos\theta\hat{x} \tag{1.13}$$

and

$$I = {E^2}_0\cos^2\theta = I_0\cos^2\theta \tag{1.14}$$

In a perfect polarizer, if the polarizing axes are parallel, there will be no decrease in intensity. If the polarizing axes are perpendicular, the intensity will be zero.

1.4.6 Polarization by Absorption (Dichroism)

Polarization by dichroism occurs due to an anisotropy of the material that light is transmitted through. Randomly polarized light transmitted through a dichroic material will have the electric field at particular angles of polarization selectively ab-

sorbed. The component being absorbed is completely or partially attenuated, leaving a preferentially polarized light to pass. Dichroism is commonly found in nature and can be observed in the crystal tourmaline.

1.4.7 Polarization by Scattering

Scattering events induce polarization due to small particles acting as dipoles. The dipoles are oscillating at the frequency of the light with which they are interacting. The dipole antennae, that is effectively created, re-radiates a perpendicular to the line of oscillation. This type of polarization is caused by Rayleigh scattering from molecules in the atmosphere.

1.4.8 Polarization by Reflection

When light is reflected from a non-metallic surface at an angle, θ, between zero and 90 degrees, some or all of it becomes linearly polarized. If the angle is Brewster's angle, θ_B, all of the reflected light is polarized. Brewster's angle can be calculated by:

$$\theta_B = \arctan \frac{n_2}{n_1} \tag{1.15}$$

where n_1 is the index of refraction of the initial media of propagation and n_2 is the index of refraction of the media from which the ray is reflected/refracted.

At angles between zero and 90 degrees, other than Brewster's angle, the reflected light is partially polarized. At an incident angle of 90 degrees, the unpolarized incident light is reflected unpolarized. The angle of polarization of reflected light is

perpendicular to the direction of propagation and parallel to the surface from which it is reflected.

1.4.9 Birefringence

The phenomenon associated with birefringence arises due to a material anisotropy. This anisotropy leads to a difference in the index of refraction that is dependent upon directionality of the material. Birefringence is typified by a double image of light transmitted through a birefringent material. This arises from the difference in the indices of refraction; unpolarized light is made up of a combination of many angles of polarization. When light is incident upon a surface, p – polarized light is the component that is parallel to the incident surface and the direction of propagation, while s – polarized component is normal to the direction of propagation and the p – polarized component. S – polarized light "sees" a different index of refraction than p – polarized light. The s – polarized light is perpendicular to the optical axis and is refracted by the ordinary index of refraction, n_o, while the p – polarized light is parallel to the optical axis and is refracted by the extraordinary index of refraction, n_e. At this point two things occur: the transmitted light is broken into two rays of perpendicularly polarized light, and one of the rays is retarded from the other due to the difference in the indices of refraction.

Birefringent materials occur naturally and artificially. Many naturally occurring crystals are birefringent due to an difference in lattice parameter, either in one or two dimensions. Polymeric materials can be made birefringent by subjecting them to a mechanical strain, such as drawing a thermopolymer fiber.

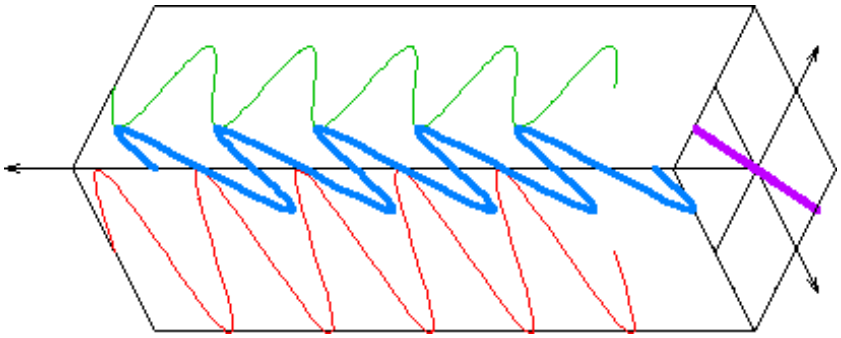

Figure 10. Linearly Polarized Light. An example of linearly polarized light as the sum of two component vectors.

1.5 Overview

So began, one summer day, the investigation into the optical transmittance and absorbance of the wings of cicadas.

The optical properties of wings in turn lead to the questions regarding the overall organization of the chitin that makes up the wing. Questions of organization turn to questions of how chitin is organized and if it can be organized artificially.

The artificial organization of chitin and the ability to manipulate it at the molecular level is the ultimate goal. The ability to tap into this widely available resource would be a boon to the plastics industry in general: a polymer that is tough and versatile and can be biodegraded. The ever looming problem of filling up landfills with discarded bottles, bags, and packaging would no longer be an issue. It would all be degraded by bacterial chitinases, which are prevalent in the soil in which the refuse would be buried.

The biomedical industries would benefit, also. Chitin is a biocompatible polymer. Cell scaffolding produced from a biocompatible polymer that is insoluble in water but is biodegradable would allow for longevity in the body without permanence.

I will start with an excavation, of sorts, by peeling off the outer layers of the cicada to determine how the chitin is arranged in situ. The removal of the extracellular matrix of the cuticle will afford a glimpse into the inner workings of the biologically driven means of biopolymer arrangement. The various cuticle structures can then be quantified through microscopy and computational image analysis to render a better understanding of the workings of the natural world. With this knowledge, it will be possible to go forward with the manipulation of chitin based systems in vitro.

The natural world is profoundly influenced by optical phenomena. These phenomena are manifested in cuticular structures, such as wings. The wing of the cicada is more than just an adaptation to keep it in flight; it could also be a means of optical obscurance that lends a modicum of camouflage, or it could be a means of signaling a mate in an attempt to capitalize on flashy optics. In either case, there is an optical significance to the wing. Unraveling the mystery of the cuticle based optical properties of the wing will open an avenue for the determination of the relevance of synthesized chitin structures.

I will demonstrate a few simple but effective methods of in vitro organization of chitin. Cast films and gels of chitin are a starting place for the further development of fibers and other forms. These forms of organized chitin can be characterized using the same techniques as applied to the cicada.

CHAPTER II

SPECIFIC AIMS

2.1 Aim I

Determine and characterize the patterns of chitin alignment in an insect cuticle Hypothesis: Chitin alignment in cuticle is not the same over the body of the insect. Chitin has a specific function and as this function differs at varying locations on the insect, the degree of alignment will also vary. To test this, it will be necessary to describe a new technique that can remove the extra-cellular matrix and leave behind the in situ oriented and organized chitin. It will also be necessary to describe a means of quantifying the organization and alignment of chitin fibers.

2.2 Aim II

Characterize the liner polarization associated with specific cuticle structures and determine the role that chitin organization plays in this property. Hypothesis: Unpolarized light transmitted through the cicada wing membranes becomes plane polarized. There is anecdotal evidence that fluttering wings of the cicada is accompanied by optical phenomena. It is also known that some arthropods, including some insects, can see polarized light. The polarization of light transmitted through the wing may be involved in the mating cycle or predator/prey interactions. A study of the polarizing effect will be carried out by the use of polarimetry and UV-Vis spectroscopy to determine if this polarization is dependent upon chitin and chitin organization.

2.3 Aim III

Determine underlying rules of chitin nanofiber alignment. Hypothesis: Chitin can be artificially organized by the extrusion of chitin gels. Chitin systems can become valuable tools in biomedical engineering, plastics, and nanoparticle filtering. The organization and alignment of chitin is not well understood. To further the body of knowledge, the basic principles of chitin organization need to be explored. A simple method of chitin gelation will be developed that can render useful morphologies of chitin. These chitin forms can be investigated through polarized microscopy, scanning electron microscopy, and image processing.

CHAPTER III

LITERATURE REVIEW

3.1 Chitin and Arthropod Cuticle

3.1.1 Arthropod Cuticle

Cuticle is the basis for the exoskeleton of arthropods. This exoskeleton is the hard shell that protects the internal, soft organs and morphology of the organism and provides weather proofing and load bearing capability. The cuticle is built on the epidermal layer of cells through the secretion of chitin fibrils and a proteinaceous extracellular matrix (ECM). The ECM is a mix of structural proteins, such as resilin, minerals, lipids and fatty acids [2]. The chitin fibrils are bundled and organized by the proteins in the ECM to form larger fibers, and these fibers are arranged into lamellar sheets that are stacked into a helicoidal, "twisted plywood" pattern called a Bouligand structure[9, 22]. The cuticle is made up of four distinct parts: the epidermis, the endocuticle, the exocuticle, and the epicuticle. As previously mentioned, the epidermis excretes the material of which the cuticle is comprised. The endocuticle and the exocuticle are similar except for the density of material. As cuticle is created by the epidermis, it is moved outward from the organism and compressed and sclerotized [42]. The exocuticle is much denser than the endocuticle, as the endocuticle makes up around 90 volume percent of the total cuticle [14]. The epicuticle is the thin outer layer that promotes weather resistance through a waxy sheath.

The Young's Modulus of insect and arthropod cuticle ranges from 1kPa to 150GPa, making it a versatile bio-composite material [60]. The physical properties of cuticle depend upon the level of mineralization and the amount of sclerotization the cuticle has undergone [26]. The mantis shrimp *Odontodactylus scyllarus* possesses impressive damage and wear tolerance on the specialized cuticle found in a cudgel-like structure. [45]. The dactyl club gets its strength and resilience from a complex composite of hydroxyapatite, calcium carbonate, calcium phosphate, and cuticle[61].

3.1.2 Chitin Morphology and Characterization Techniques

There are many methods and techniques available for chitin characterization. Initially, it was difficult to differentiate between chitin and other polysaccharide biopolymers. The process by which the chitin was extracted with hydrochloric acid would yield inconclusive results due to the production of glucosamine hydrochloride through the indiscriminate conversion of many other nitrogeneous compounds. James Irvine demonstrated in 1909 the use of polarimetry to determine the presence of chitin and the determination that chitin is indeed a uniform molecule found across species and throughout different organs of the same individual organism [30].

It was only a few years later that another technique would be developed to greatly further the understanding of chitin and all other crystalline materials. In 1912 Max von Laue developed the technique of X-Ray Diffraction (XRD) to probe the interatomic distances and periodicity of crystalline structures [21]. Von Laue reasoned that the periodic planes of crystals could be used as a diffraction grating, but seeing that the wavelength of visible light is too long for diffracting in such a short periodicity, he postulated that x-rays could resolve the sub-nanometer distances. The subsequent

development of X-Ray crystallography eventually led to von Laue receiving the Nobel Prize in Physics in 1914.

The first widely accepted structure of chitin was proposed by Meyer and Pankow in 1935, and this structure was further refined by Carlstrom in 1957 through extensive XRD technique refinement for the biopolymer [12,38]. The crystal structure of chitin is orthorhombic. The orthorhombic crystal system is one in which the three base vectors are unequal and mutually orthogonal such that the base vectors $a \neq b \neq c$ and the angles $\alpha = \beta = \gamma = 90$ degrees[29]. The dimensions of a, b, and c reported by Meyer and Pankow are 9.40Å, 10.46Å, and 19.25Å respectively. This was later corrected to a = 4.76Å, b = 10.28Å, and c = 18.85Å by Carlstrom. Currently, the structural lattice parameters have been refined to a = 4.749Å, b = 18.89Å, and c = 10.33Å [53].

The purity and degree of deacetylation of chitin can be determined through the application of x-ray diffraction. Chitin can be deacetylated to become chitosan [27]. As the deacetylation process proceeds and more chitin is transformed to chitosan, the x-ray diffractogram shows a peak broadening and shift as the morphologies of the crystals are blended [65].

Infrared spectroscopy, specifically mid-infrared, measures the fundamental vibrations of molecules. The mid-infrared ranges from 2.5 – 25 μm or 4000 – 400$cm^{-}1$. The infrared region of the spectrum lies between the wavelengths of visible light and microwave radiation. Data from an infrared spectrometer is typically a graph of absorption or transmittance of light through a range of wavelengths. The wavelength is usually reported in distances, such as nanometers or micrometers, or in the form of wave numbers, cm^{-1} . As the light is transmitted through the sample, specific wave-

lengths are absorbed that correspond to the fundamental frequencies of the bonds present in the molecules at hand. This is what makes infrared spectroscopy so convenient for the study of chitin and other polysaccharides, as the bonding in organic molecules is very well defined. A particularly useful form of infrared spectroscopy is Fourier Transform Infrared Spectroscopy (FTIR). An FTIR passes a broad spectrum of infrared light through an interferometer and then through the sample. Computer processing is then used to perform a Fourier transform on the acquired data to to transform the interferogram to a wavelength dependent absorption spectrum. Some advantages of FTIR over conventional infrared spectroscopy are increased through put and better wavelength accuracy. Similar to XRD, FTIR can be used to determine the level of deacetylation in chitin [36].

3.2 Optical Properties of Arthropod Cuticle

3.2.1 Polarization in the Natural World

It has been shown that polarization plays an important role in the optical properties of the natural world. Polarization occurs naturally and is manifested in many ways. The light of the sun is polarized due to scattering from molecules in the atmosphere; light reflected from the leaves of plants and other objects is polarized to some degree [18]. Both of these naturally occurring situations are utilized by organisms as diverse as bees, crickets, bats, and crustaceans to serve as means of navigation [7, 20, 24] . The polarization of light has been shown to influence the selective dining of butterflies, and polarization can be used to train them to preferentially choose shades and colors[35].

Not only do many species have the innate ability to detect polarized light, there is also evidence that mutiple species have the ability to manipulate the polarization

of light. The wing membrane of the dragonfly, *Aeshna cyanea*, has been shown to polarize reflected light [25]. It has been suggested that the polarized light reflected from the wings of some butterflies is implicated in the mating process [56]. The polarized light reflected from the wings of the swordtail butterfly, *Graphium sarpedon*, is the product of specially evolved wing scales, giving rise to the speculation that polarization is an evolutionary benefit to the organism [54].

3.2.2 Structural Color

The color affects of the cuticle structures are due in part to structural coloration. The striking iridescence of the Madagascan sunset moth, *Chrysiridia rhipheus*, is caused by the photonic effects of the layering of the component scales of the wing [62]. The cuticle layers get successively thinner in the exoskeleton from the exterior layer to the innermost layer. This anisotropy of layer thickness has an effect on the reflectivity of the system, prompting structurally induced coloration [11, 55].

3.3 Chitin Formations and Gels

3.3.1 Chitin Extraction

There are two main routes in the extraction of chitin: a chemical route and a biological route. Both routes involve the reclamation of chitin by the processing of waste from crustaceans of other chitin containing organisms. The chemical route is a straight forward one that involves two phases, deproteination and demineralization [44]. The first phase is the deproteination of the cuticle by digestion in an alkali environment. The second phase if the demineralization through the digestion in an acid.

Biological chitin purification involves the use of enzymes to break down the proteins in the cuticle and separate the chitin from the rest of the extracellular matrix. These methods typically involve the fermentation of the cuticle with bacterial strains [1, 32, 33].

3.3.2 Chitin Fibers and Formations

The manipulation of chitin is strangely underdeveloped. Chitin has many properties that would, seemingly, allow for the ease of manipulation even though it is a highly insoluble material. Chitin has been shown to form a cholesteric liquid crystal and exhibit a certain degree of self assembly [5,43]. The formation of chitin fibers and films has been shown through the solution drying of chitin dissolved in hexafluoro – 2 – propanol and LiCl/DMAC[66]. Chitin fibers have been shown to self-assemble across gaps of various length scales and have applications in tissue engineering [51]. Mold patterned chitin microneedles have been developed for use in drug delivery and testing, taking advantage of the biocompatibility and abundance of chitin [31].

3.3.3 Chitin Gel Formations

The formation of chitin gels generally starts with the preparation of chitosan. Chitosan being the water soluble derivative of chitin, is easier to work with in aqueous solutions. Once a chitosan gel is formed, the chitosan is acetylated to become chitin. The factors that affect the chitin gel formation are the solvent and cosolvent conditions and the concentrations of the acetylating agent and the chitosan[39]. The level of acetylation required to form a chitin gel is reported to be greater than 80 % [58]. Chitin hydrogels have also been formed through the use of calcium chloride dihydrate-saturated methanol as a solvent, eliminating the necessity of fluorinated solvents [57].

3.3.4 Extrusion and Fiber Alignment

The orientational alignment of particles of various sizes and shapes is known to be induced by the shear imparted into a material [8]. There are several mechanical means to induce shear into a system. One such manner of shear inducement is through the extrusion of a polymeric material; the shear alignment effect has been described in both melt and solution extruded polymeric material [37].

CHAPTER IV

IN SITU OBSERVATION OF CUTICULAR CHITIN

4.1 Introduction

The alignment and organization mechanism of chitin fibers in the cuticle of arthropods is not well understood. Here, I develop a method for the in situ observation of the chitin fibers in cuticle. The chitin fibers organization is specialized, depending on the morphology and use of the cuticle. Perturbations and defects have an effect on the organization of the chitin. I demonstrate a method for the rudimentary artificial organization of chitin in films. Silica spheres ranging from 250nm to 2μm are used as a perturbation site to form radially symmetric chitin webs. The organization of chitin is quantified by the use of image processing software, ImageJ.

4.2 Chitin Purification

Chitin purification was carried out via a modified method derived from literature [36, 66].

Grind insects/insect parts/shrimp shells to a fine paste. This can be done dry, in ethanol, or under liquid nitrogen. If using liquid nitrogen, wear proper personal protection and perform the operation in the fume hood.

Dry the paste overnight at 70°C; this is sufficient to dry the material. The paste should yield a fine powder. If there are too many large pieces, it will need to be re-ground.

De-mineralize the powder. Mix the powder thoroughly into 1M concentration HCl to de-mineralize the organic matter and dissolve fats and lipids. Fill a 50mL Falcon

tube approximately 1/3 full with loose powder. Fill the Falcon tube to the 50mL mark with the HCl. Mix well and allow to digest overnight at 70°C.

Wash the product to neutralize the pH. Centrifuge the tubes to separate the solid from the liquid. Pour off the supernatant. Refill the tube with reverse osmosis water. Mix thoroughly and re-centrifuge the tubes. Repeat this process 4 to 5 times or until the supernatant is relatively clear and clean.

Remove the protein matrix. Mix the pellet from the last wash step with 1M NaOH to remove the proteins from the chitin. Fill the Falcon tubes to the 50mL mark and mix thoroughly. Allow this to digest overnight at 70°C.

Wash the product to neutralize the pH. Repeat the washing procedure. At this point, the chitin is purified. After the final wash, the purified chitin can be dried in the oven or lyophilized.

Perform proper Quality Assurance Testing. For my purposes, FT-IR will suffice for the characterization of the purified chitin. It can be further tested using X-Ray Diffraction (Figures 11 and 12). Prepared chitin from shrimp shells was compared to chitin from *Drosophila melanogaster*, chitin purchased from Sigma – Aldrich, and a Rakki prepped cicada wing (Figures 13 and 14). Purified chitin was imaged on a Zeiss Auriga scanning electron microscope to see the nanoscale morphology (Figure 15).

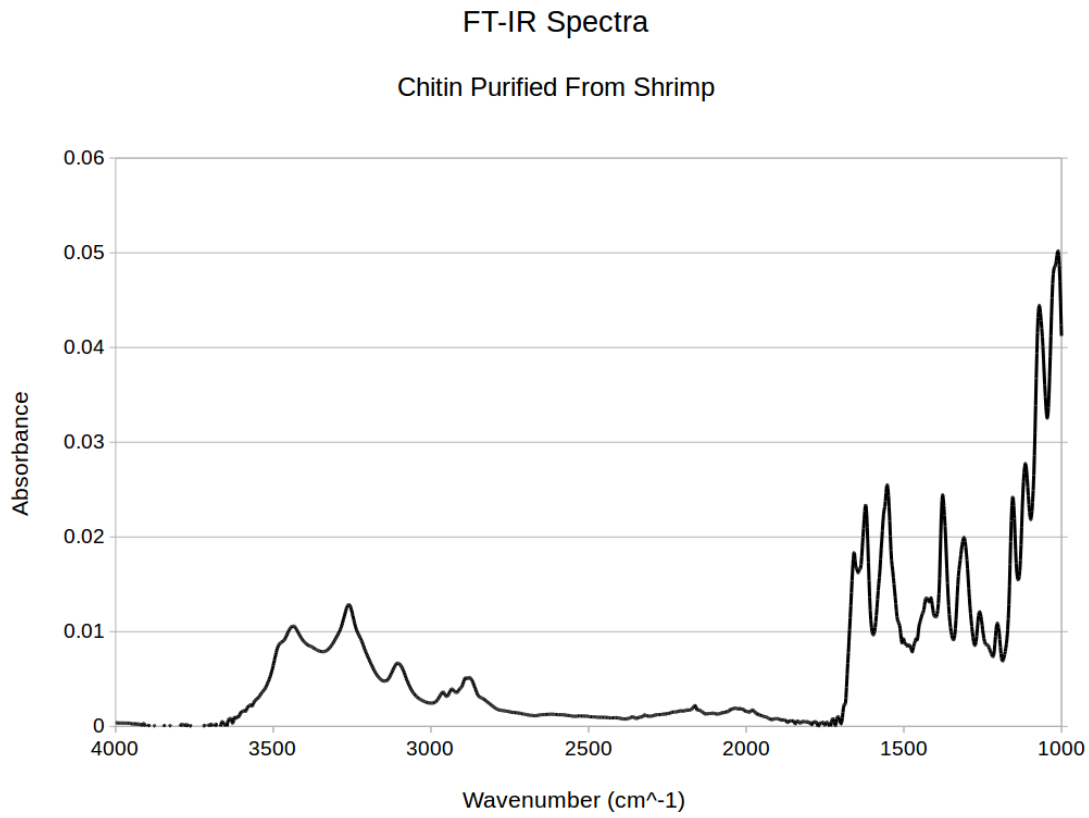

Figure 11. FT-IR Spectra of Chitin Purified from Shrimp Shells. This is the standard form of chitin used in all experiments requiring bulk chitin. Bulk, powdered chitin was used with an Attenuated Total Reflectance (ATR) crystal to produce the spectra.

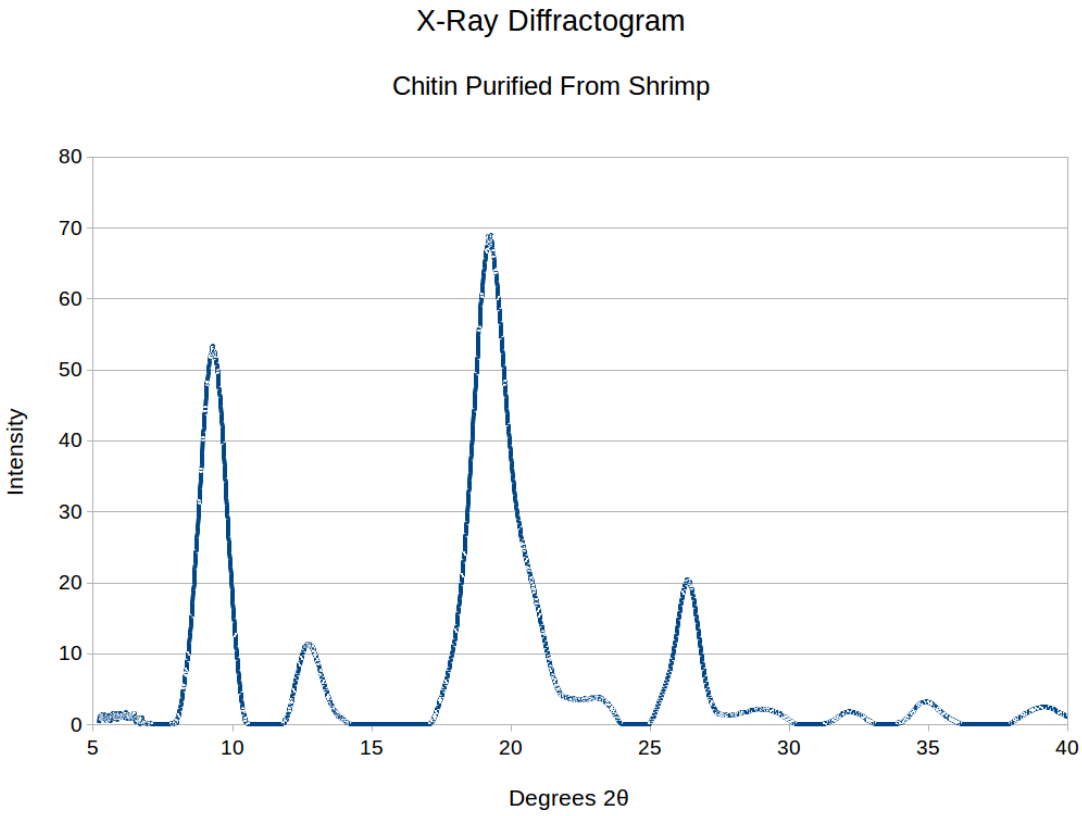

Figure 12. X-Ray Diffractogram of Chitin Purified from Shrimp Shells. Arthropod cuticle contains as much as 30% chitin by weight, making it a readily available source of the material. The X-Ray Diffraction was carried out by mounting ground chitin powder.

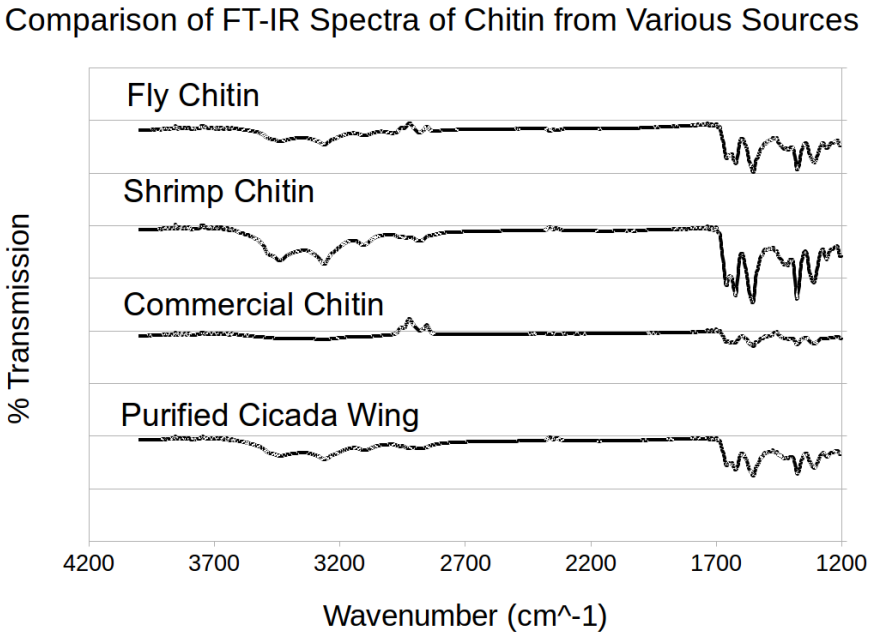

Figure 13. FT-IR Data from Various Chitin Sources. FT-IR data was collected to compare and contrast the quality of chitin obtained from different sources. Chitin was purchased as well as purified from shrimp and fly cuticle. The Purified Cicada Wing is a wing that underwent the removal of the extracellular matrix to leave only the chitin nanostructure behind.

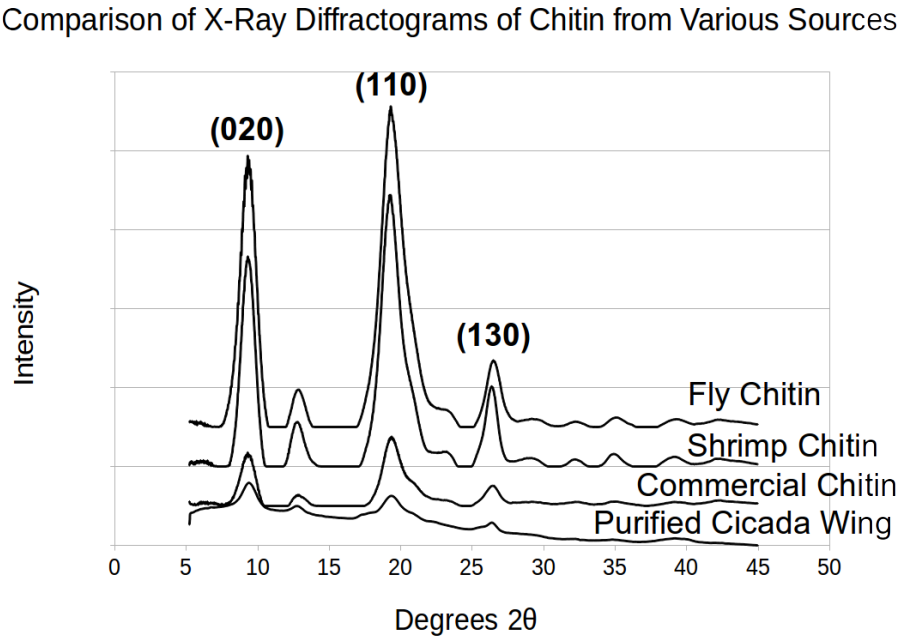

Figure 14. X-Ray Diffraction Data from Various Chitin Sources. X-Ray Diffraction data was collected to compare and contrast the quality of chitin obtained from different sources. Chitin was purchased as well as purified from shrimp and fly cuticle. The Purified Cicada Wing is a wing that underwent the removal of the extracellular matrix to leave only the chitin nanostructure behind.

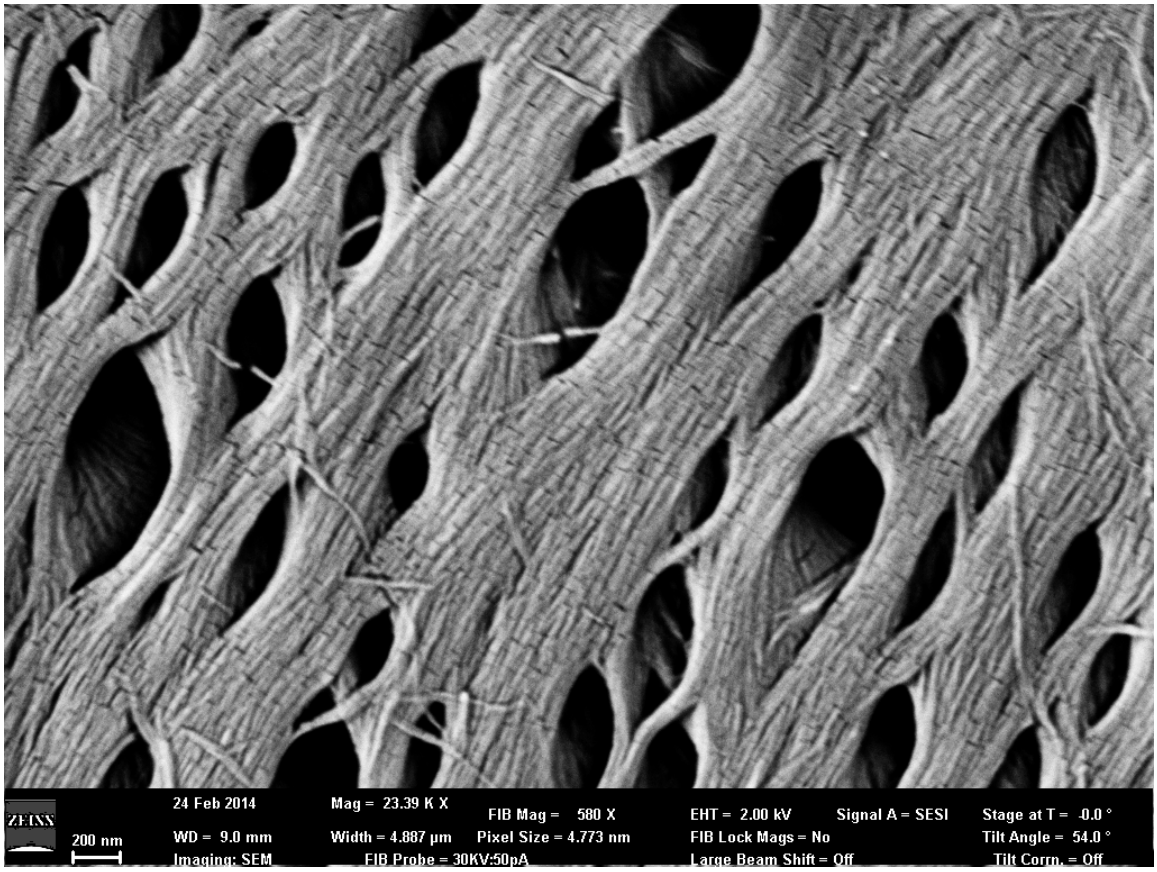

Figure 15. Scanning Electron Micrograph of Purified Shrimp Chitin. After purification, at such magnification, the individual fibers of chitin are visible.

4.3 ImageJ Processing

It has been shown by Simpson, et al, that fiber alignment can be quantified using the "Radial Sums" option of the Oval Profile Plugin as implemented by ImageJ[4]. ImageJ is freely distributed image processing software developed by the National Institute of Health.

Images were analyzed using a Fast Fourier Transform to convert an image from a spatial domain to a frequency domain. This allows common features, such as aligned fibers, to be quantified through the frequency of repetition. A radial sum of the gray value was taken from the center of an oval selection to the oval perimeter. The value reported by the plugin is at a maximum when the radial sum is taken along the direction of the greatest frequency of higher gray values.

The images, as saved from the Scanning Electron Microscope, are 1024 X 768 pixels. Each image was sub-divided to five sections of 250 X 250 pixels. A Fast Fourier Transform (FFT) was performed on each sub-division of the image to render a frequency domain image. An oval selection of radius 50 pixels was then used to select the central region of the FFT image. The oval profile was plotted using a division of n = 360 and "Radial Sums" plotting mode. The sums are reported about a 180 degree section of the oval selection, since the fibers can be approximated as straight.

4.4 Rakki Prep Method

The preparation method, herein known as the "Rakki Prep", is a method of preparing the various sections of the sample in a manner that removes all the extracellular matrix and leaves the chitin unmolested. This method follows similarly with bulk chitin extraction but depends upon careful handling and mounting of the materials.

I used Brood ii cicadas of *M. septendecim*, from the Great Southern Brood of the summer of 2013. I utilized a section from the head, eye, wing, leg, and back in this study of chitin organization.

The "Rakki Prep" is a continuation of the bulk processing of chitin, as described above. Most importantly, the difference in the processing is the care taken in the preparation of the various parts of the cicada. In this preparation, the selected portions of the cicada were carefully dissected and treated to the digestive acid and subsequent base extraction of chitin, removing the lipids, fatty acids, metals, and proteins and leaving the chitin as it is organized in the organism.

This method of treatment is meant to allow a view of the organization of the chitin fibers within the organism. The stripping away of the ECM and leaving of only the chitin can help to answer questions that arise from the challenges of artificial organization.

Five sections of the cicada were prepared via the "Rakki Prep" method: the eye, the head, the leg, the thorax, and the wing. These five sections were selected for their differences in function. As the sections are all made of cuticle, there is an overlap in the function, such as keeping the insides in and the outside out. However, differences can be seen, such as protection, load bearing, flight control surfaces, and sensory organs. Of course, the head and thorax would be in the protection scheme, the leg is load bearing, the wing is flight control, and the eye is a sensory organ.

Scanning electron micrographs were taken on a Zeiss Auriga SEM. The SEM images of the Rakki Prepped sections show a nice detail of the in vivo chitin organization. The back and head sections reveal a close alignment of the fiber structure (Figures 16 and 17). The leg section reveals a less organized alignment of individual fibers

but larger bundling of fibers, leading to an apparent scale up of fiber organization as described in the standard model of chitin and cuticle organization (Figure 18). The eye and wing sections show the least amount of organization within the chitin. The eye structure is comprised of ommatidia covered by protein lenses to make up the compound eye. Once the protein lens is removed, the underlying structure of the ommatidia is revealed (Figure 19). The wing structure reveals a random webbing of chitin fibrils (Figure 20). This could be due to the wing's necessity of biaxial strength due to the stresses of flight. The cicada sections were imaged via SEM and processed with the ImageJ software and Oval Profile plugin. The results of the Radial Sums output are summed up in Table 1. It can be seen that a greater deal of organization and chitin fiber alignment is exhibited in the head and back of the cicada than in any other section investigated. The leg, eye, and wing sections show a lesser degree of chitin fiber alignment (Figures 21, 22, 23, 24, and 25).

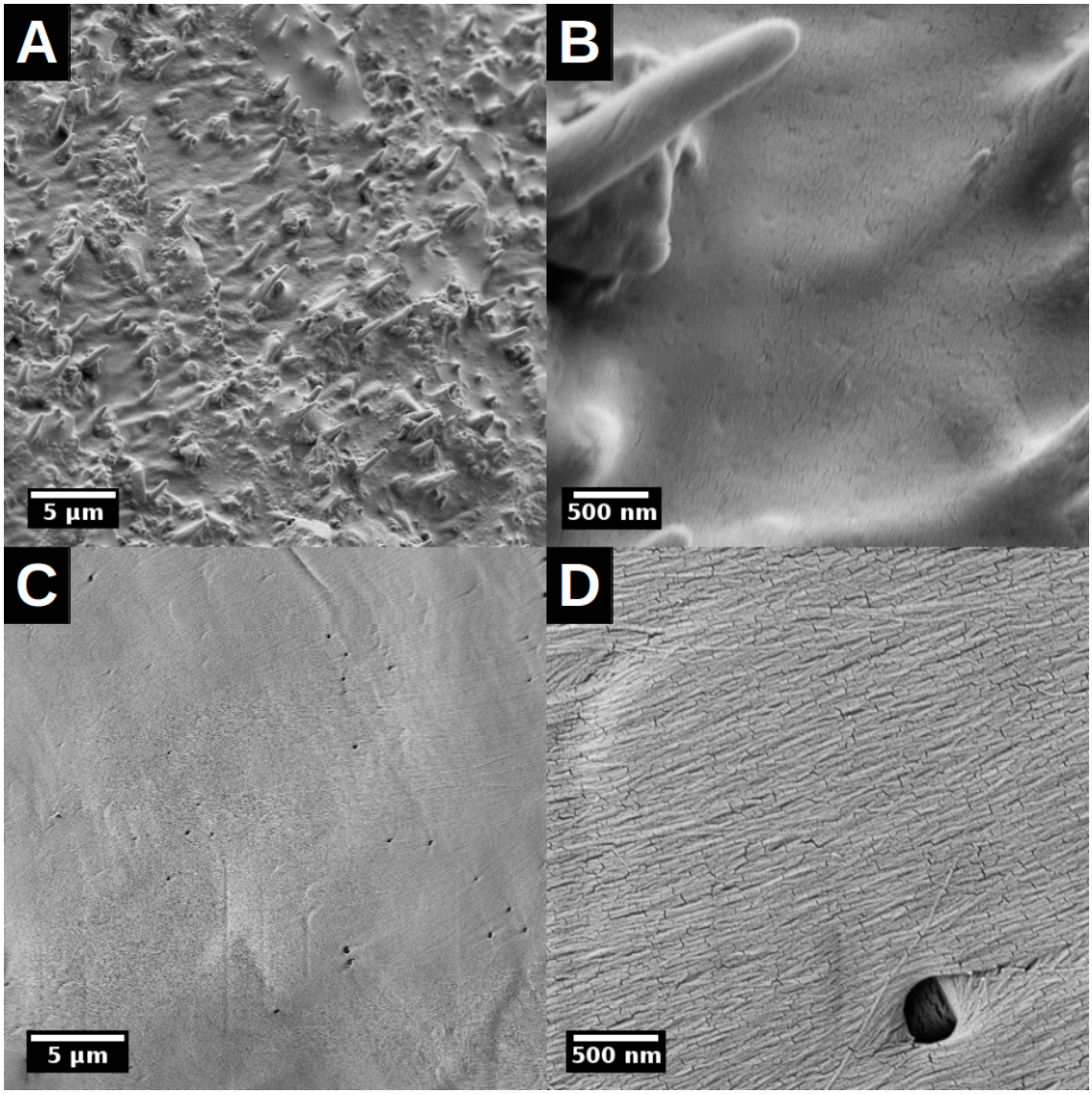

Figure 16. Detailed Image of a Section of the Cicada's Head. A is a low resolution SEM scan of the head, showing surface morphology and topography in situ. B is a higher resolution scan of the same. C is a low resolution scan after the Rakki Prep process. Note surface features have been mostly erased. D is a higher resolution of C; in this image the individual chitin fibers can be seen as they are organized in the cuticle. Sample location is an area of the head between the eyes.

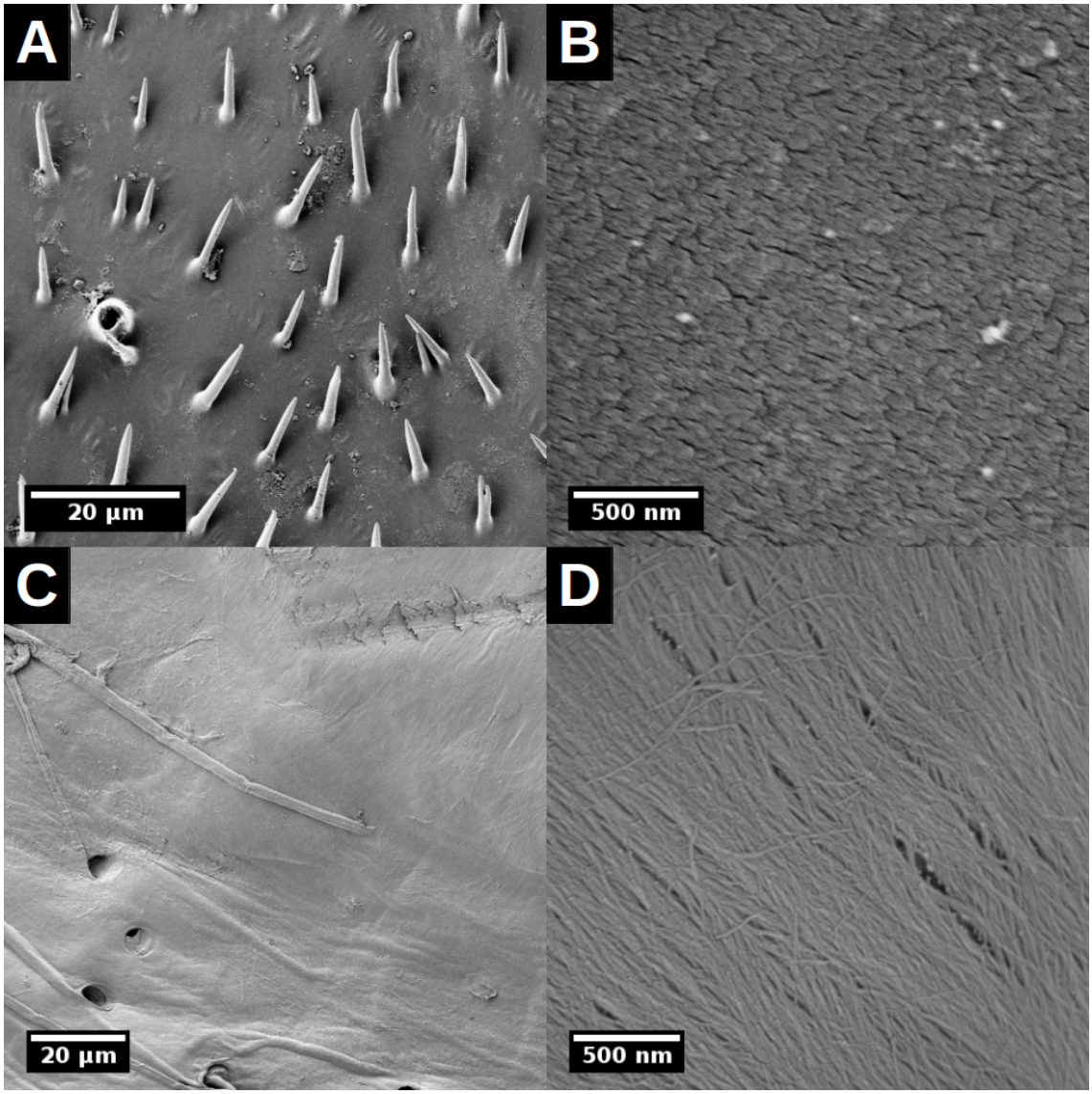

Figure 17. Detailed Image of a Section of the Cicada's Back. A is a low resolution SEM scan of the back, showing surface morphology and topography in situ. B is a higher resolution scan of the same. C is a low resolution scan after the Rakki Prep process. Note surface features have been mostly erased. D is a higher resolution of C; in this image the individual chitin fibers can be seen as they are organized in the cuticle. Sample location is of an area above the wing joint of the dorsal thorax.

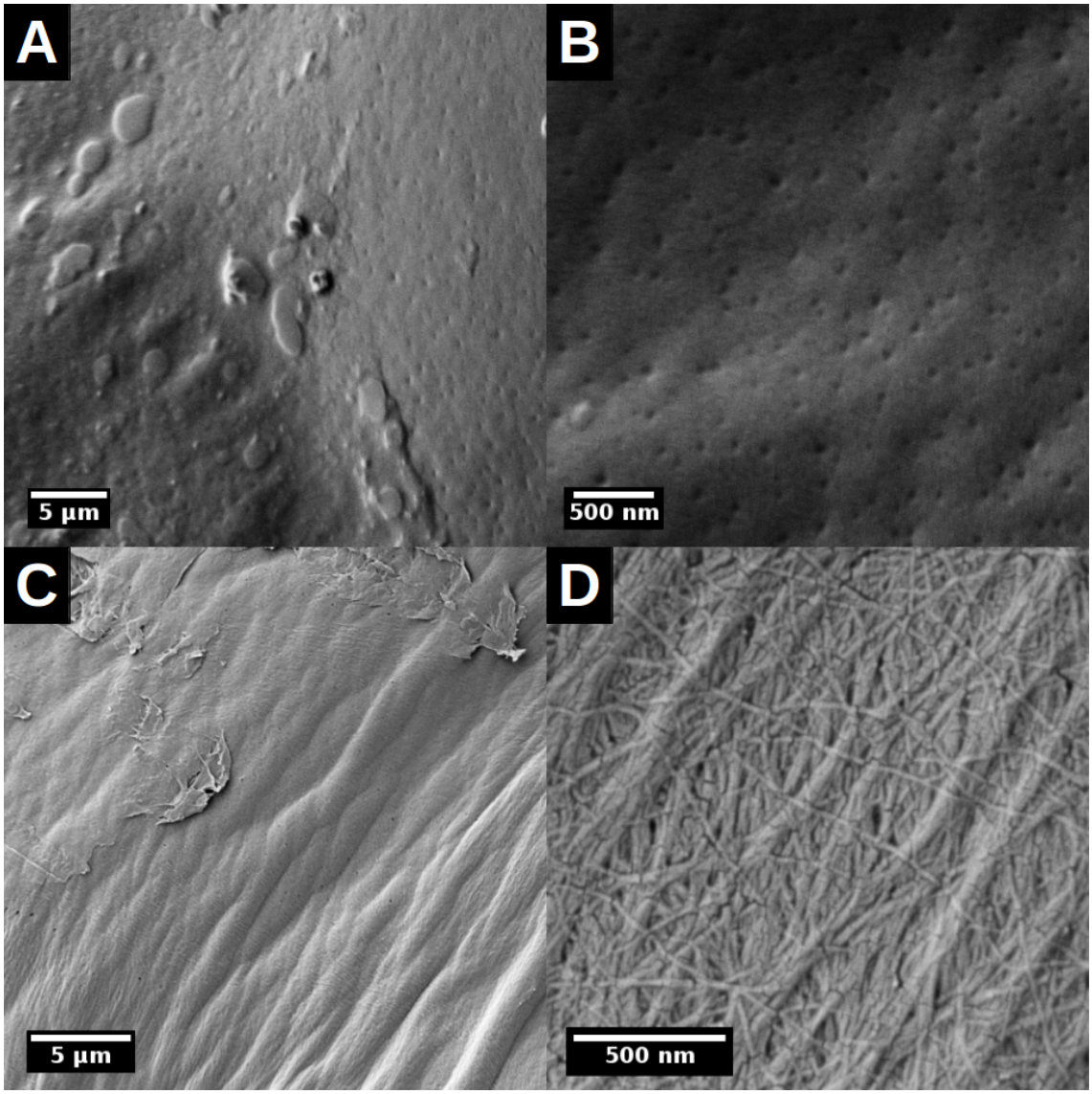

Figure 18. Detailed Image of a Section of the Cicada's Leg. A is a low resolution SEM scan of the leg, showing surface morphology and topography in situ. B is a higher resolution scan of the same. C is a low resolution scan after the Rakki Prep process. Note surface features have been mostly erased. D is a higher resolution of C; in this image the individual chitin fibers can be seen as they are organized in the cuticle. The sample location is of a central area of the tibia.

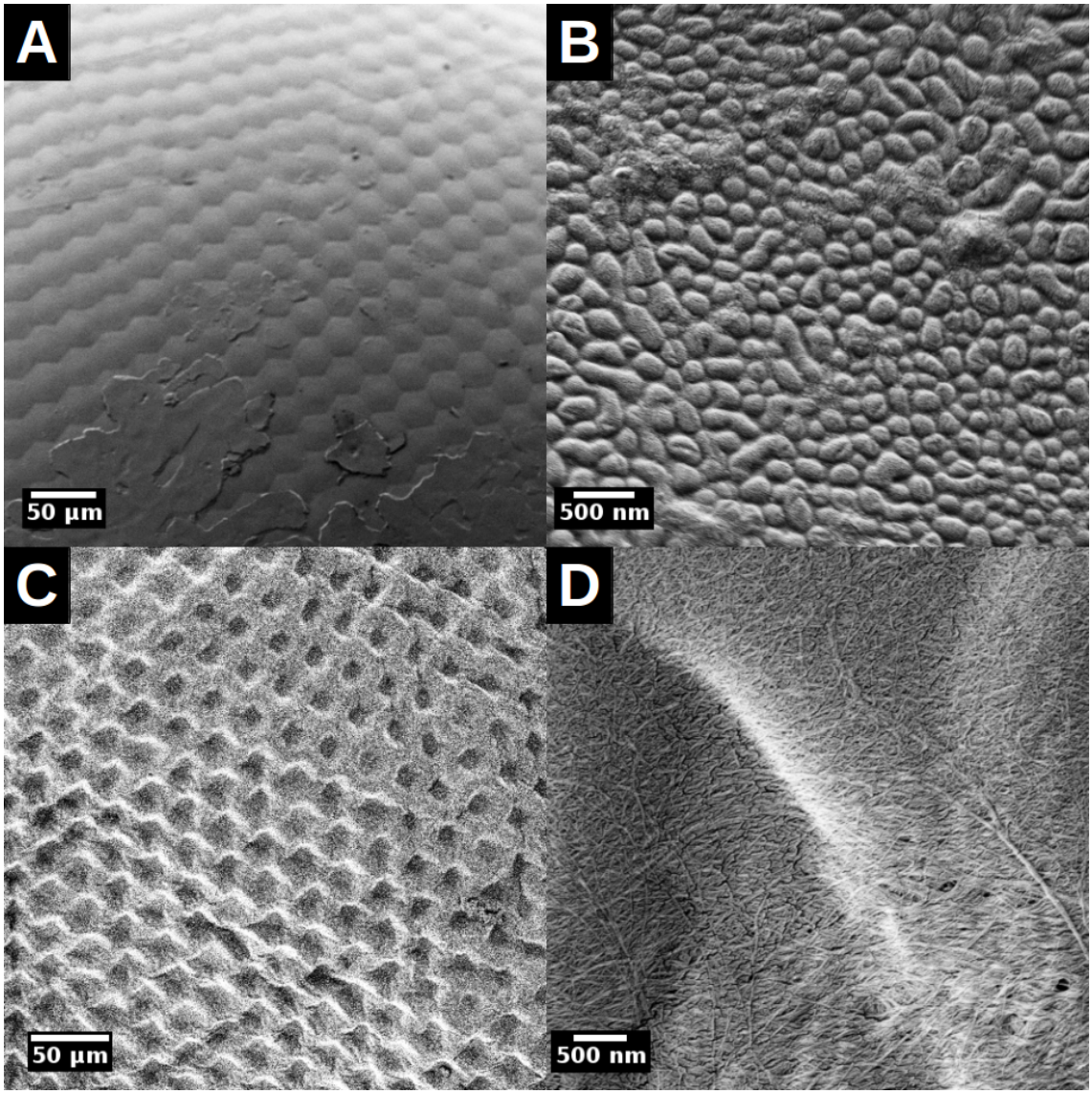

Figure 19. Detailed Image of a Section of the Cicada's Eye. A is a low resolution SEM scan of the eye, showing surface morphology and topography in situ. B is a higher resolution scan of the same. C is a low resolution scan after the Rakki Prep process. Note surface features have been mostly erased. D is a higher resolution of C; in this image the individual chitin fibers can be seen as they are organized in the cuticle. The sample area is of an area at the center of the eye.

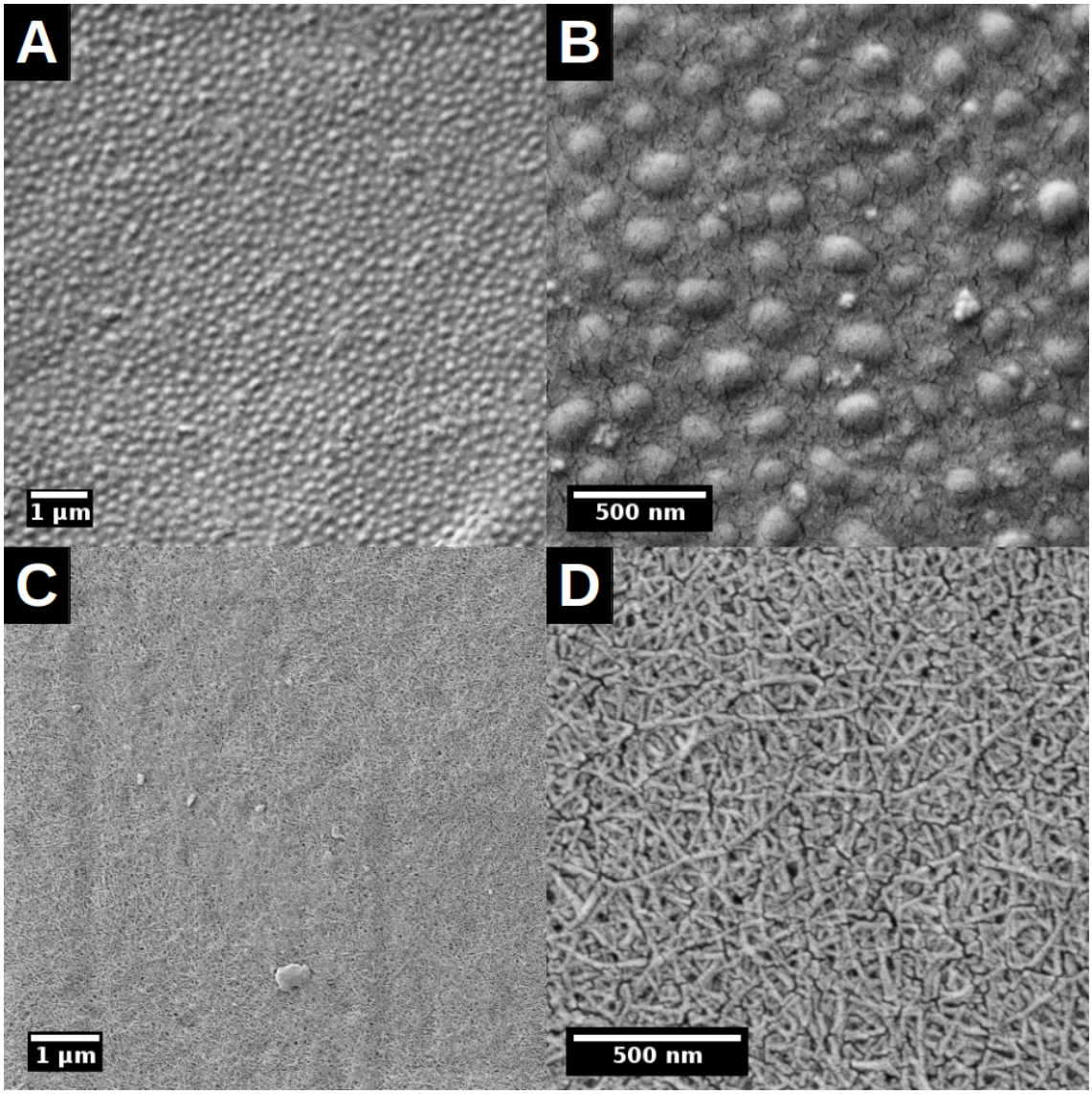

Figure 20. Detailed Image of a Section of the Cicada's Wing. A is a low resolution SEM scan of the wing, showing surface morphology and topography in situ. B is a higher resolution scan of the same. C is a low resolution scan after the Rakki Prep process. Note surface features have been mostly erased. D is a higher resolution of C; in this image the individual chitin fibers can be seen as they are organized in the cuticle.The sample area is delimited by the first major branch of the Media vein where it divides into the Media Anterior and Media Posterior.

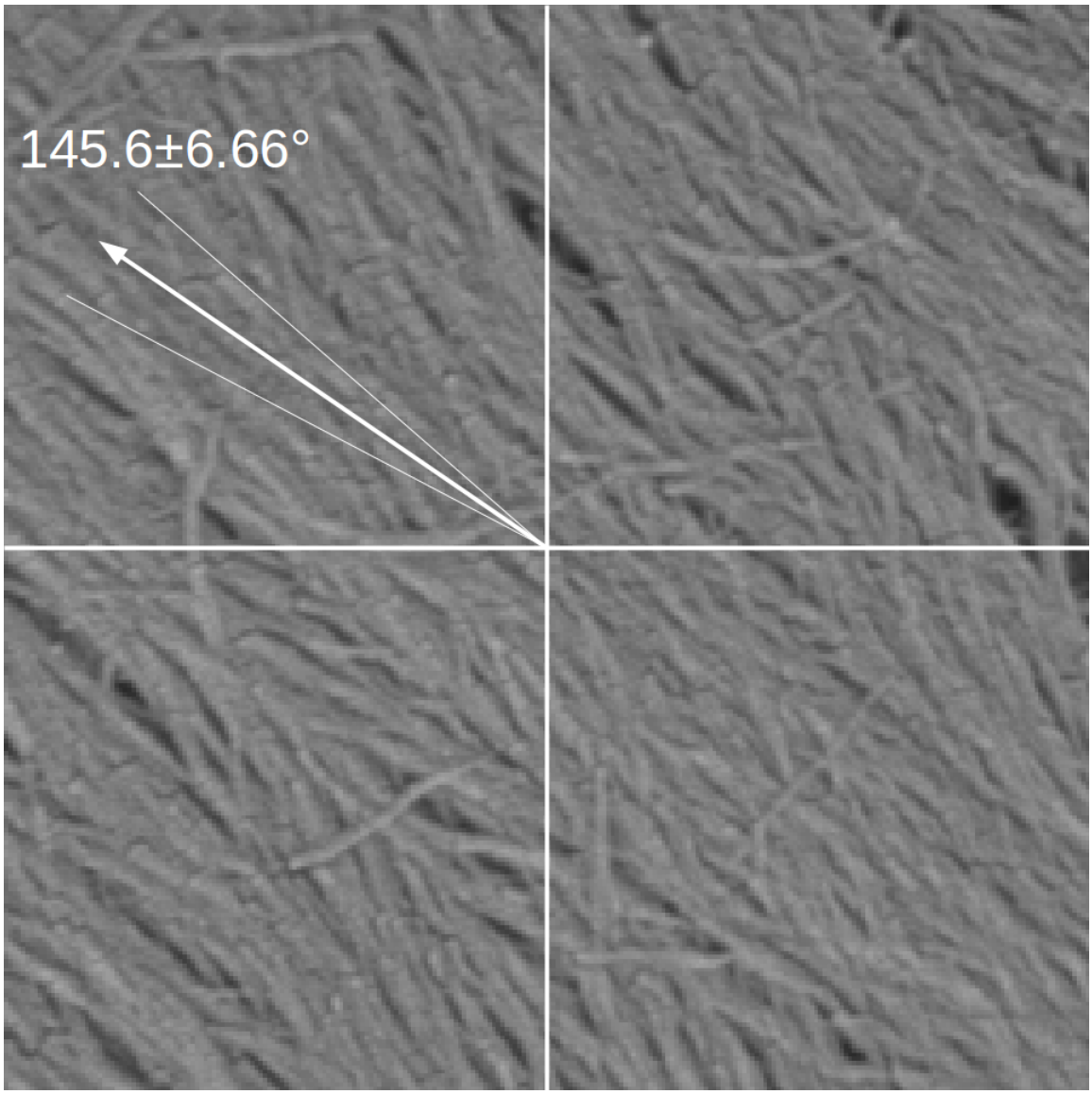

Figure 21. Directionality of the Thorax. Image detailing the directionality of the organization of chitin fibers in the cuticle of the cicada's back. Low standard deviation of the angle suggests a highly organized motif. Error is reported to one standard deviation.

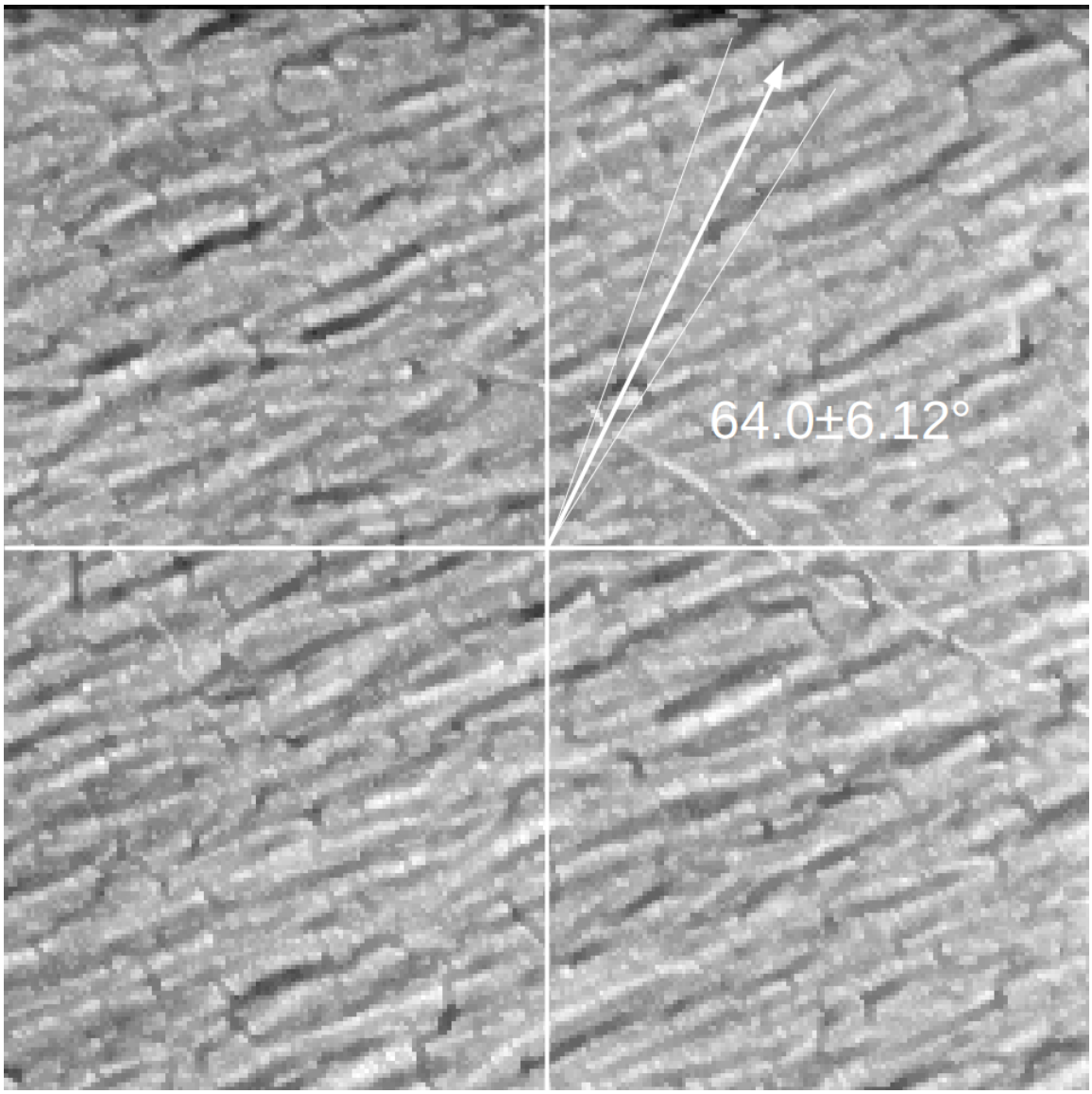

Figure 22. Directionality of the Head. Again, low standard deviation of the average angle indicates a high level or uniformity. Error is reported to one standard deviation.

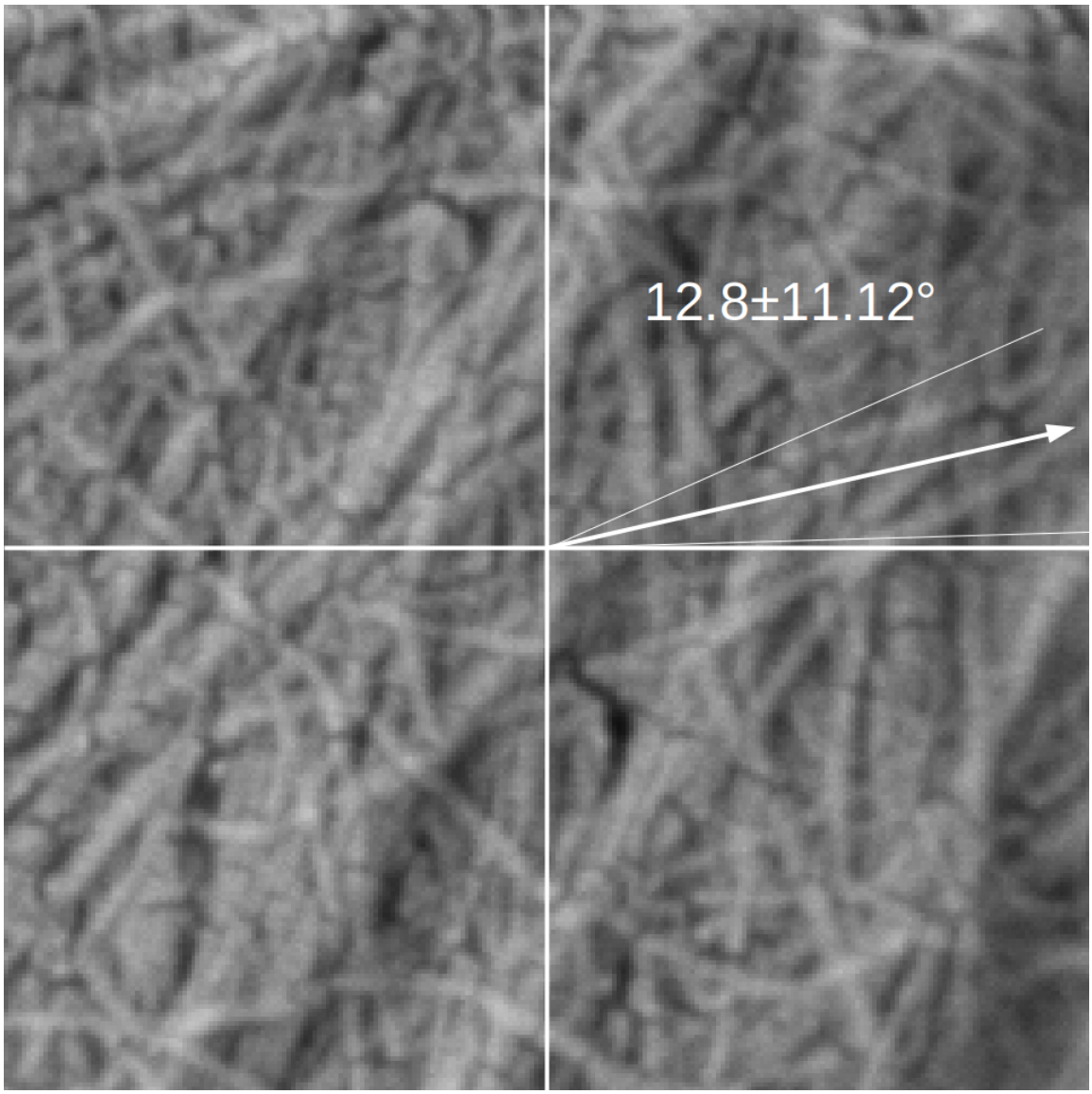

Figure 23. Low Directionality of the Leg. The leg section of the cicada indicates a decline in the uniformity of the directionality of the chitin fibers. This can be seen in the image and the larger standard deviation corroborates this. Error is reported to one standard deviation.

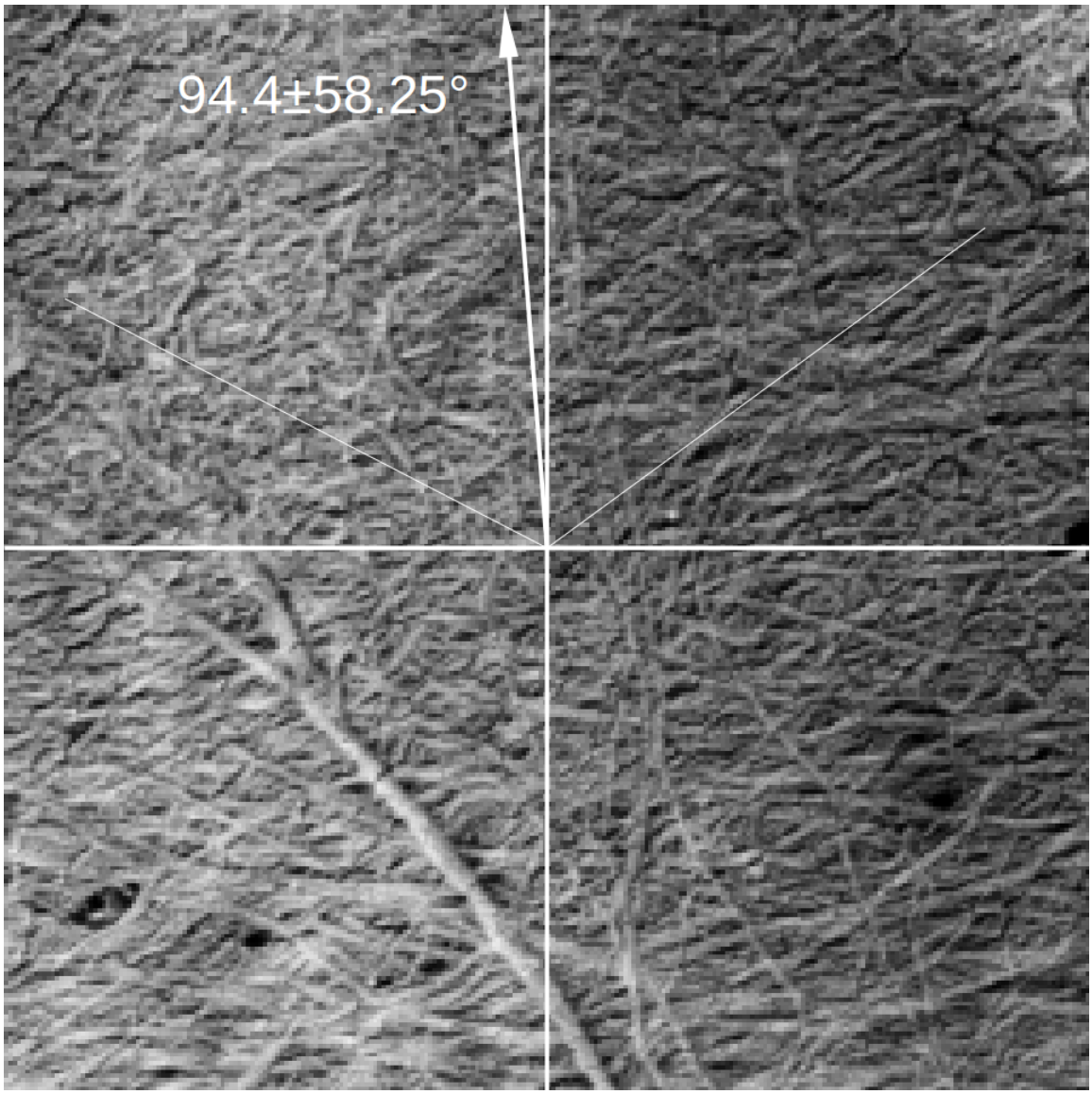

Figure 24. Low Directionality of the Eye. The eye shows a great deal of confusion and entanglement of the chitin fibers. Note the large standard deviation of the average angle. Error is reported to one standard deviation.

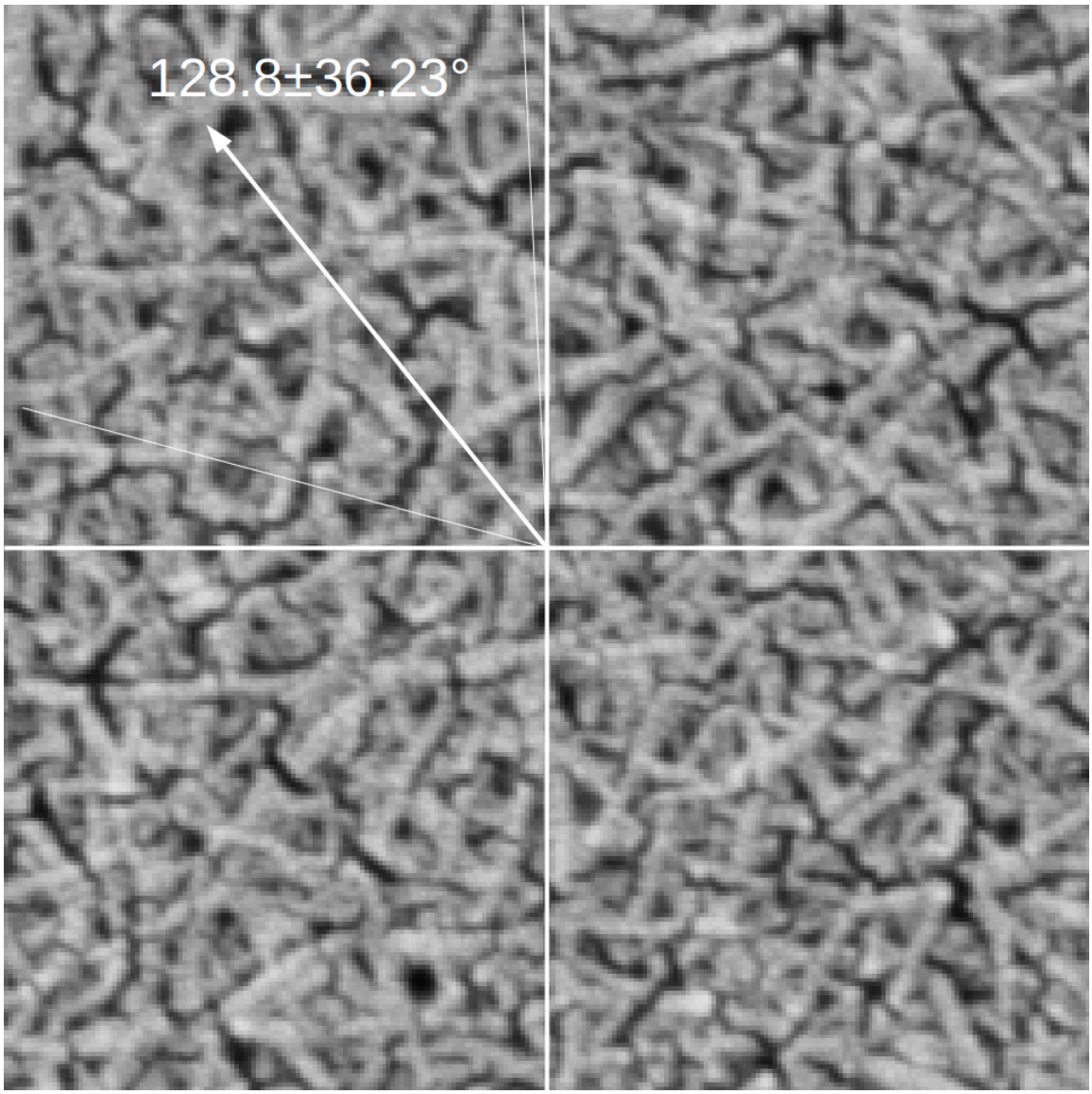

Figure 25. The most Random Assemblage of Fibers seen is the Wing. The high/low difference in the radial sums is the lowest of all measurement. Error is reported to one standard deviation.

Table 1. Radial Sums Output of Body Parts. The "Mean High Angle" is the major angle in which the bulk of the fibers are aligning. The "Difference" is the disparity between the Max and Min Radial Sums. A greater difference indicates a greater degree of alignment.

	Mean High Angle	**First Standard Deviation**	**Max Radial Sums**	**Min Radial Sums**	**Difference**
Wing	128.8	36.23	4046.87	3835.05	211.82
Eye	94.4	58.25	3844.77	3597.33	247.44
Leg	12.8	11.12	4193.00	3733.98	459.02
Head	64	6.12	3716.57	3031.45	685.12
Back	145.6	6.66	4020.96	3170.71	850.26

4.5 Chitin Film Perturbation

The chitin webs were developed as a means to probe the inducement of the organization of chitin, artificially. The hypothesis being that the introduction of a point defect will initiate a strain and from this strain, alignment will arise. The point defect I introduced came in the form of silica spheres of differing sizes, ranging from 250nm to 2μm. The overarching idea for the strain induced alignment comes from the drying of the HFIP solvent as the film covers the sphere.

Chitin may be cast into a film by the dissolution of it into a fluorinated solvent such as hexafluoro – 2 – propanol (HFIP). The chitin/HFIP solution was simply allowed to wet a surface, and as the solvent evaporates, the chitin is left behind. The chitin film, being insoluble in most other solvents, could then be washed with deionized (DI) water and ethanol. The films formed in such a manner created a randomly oriented web of chitin fibers lying along the substrate (Figure 26). The fibers can be oriented by the introduction of imperfections on the substrate surface (Figure 27 and 28). Fiber alignment is generally perpendicular to the edge of the imperfection and is anchored to the surface and imperfection, which in this case is a contaminant on the silicon substrate. The silicon substrate is merely washed with ethanol and distilled water prior to use, leaving the native oxide layer intact. This system can be exploited to preferentially align and organize the chitin fibers.

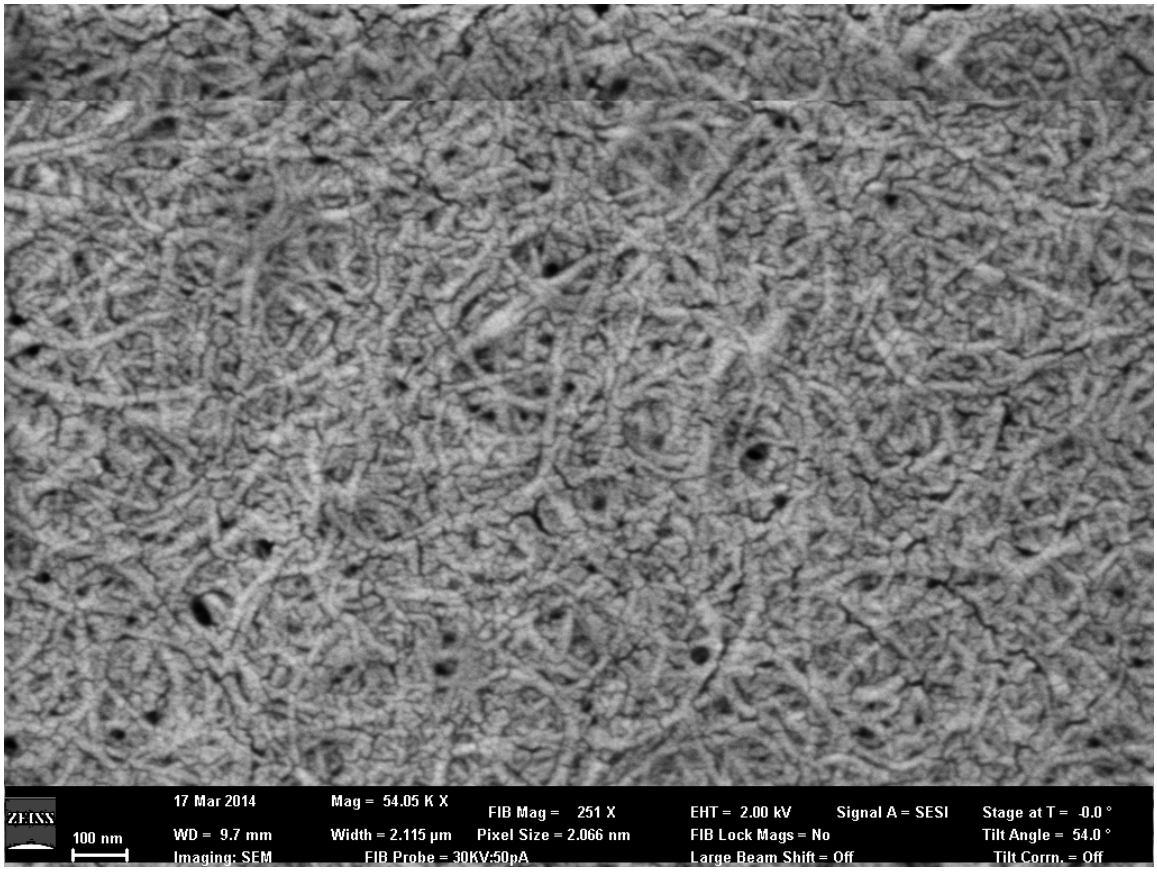

Figure 26. Chitin Films. Chitin dissolved in hexafluoroisopropanol (HFIP) cast as a film on a silicon substrate to produce a mat of chitin once the HFIP evaporates. These films are solvent resistant. The fibers are randomly oriented in the case of the films.

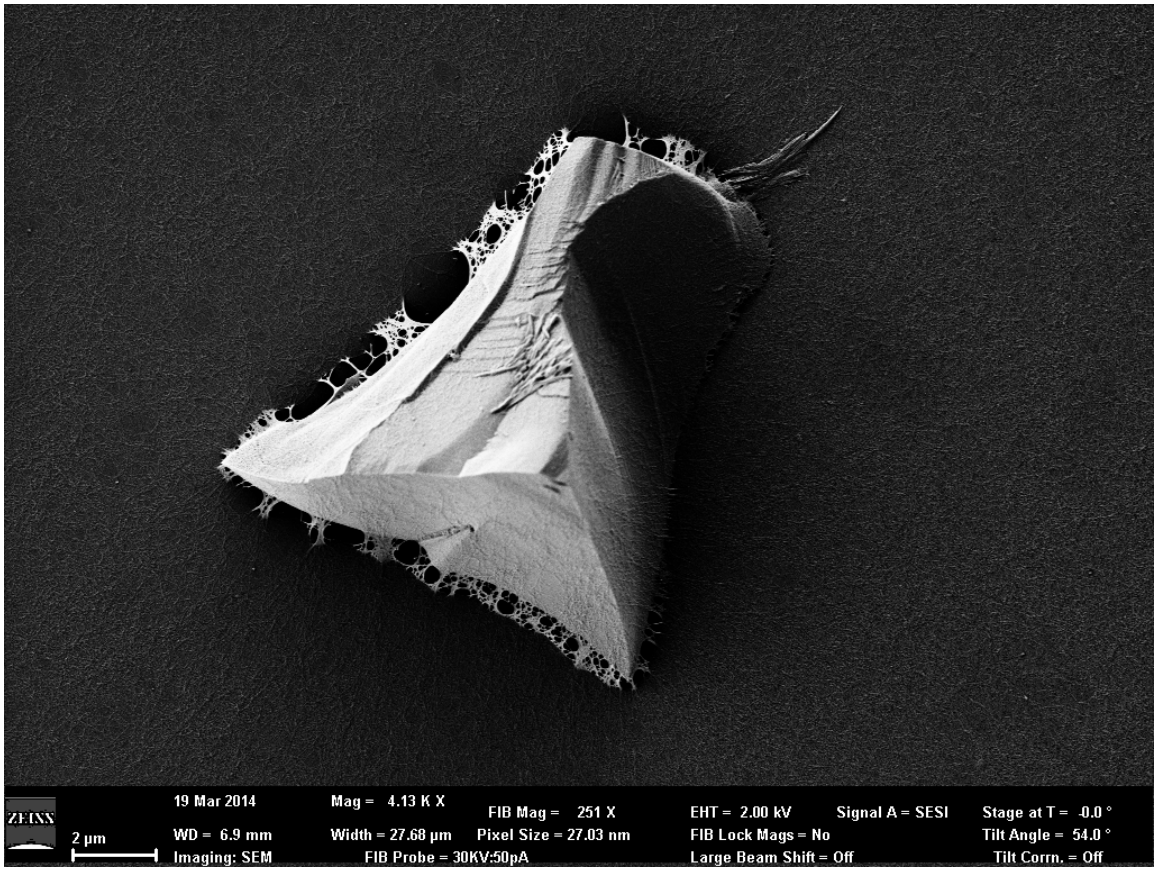

Figure 27. Chitin Film Cast on a Silicon Surface with an Imperfection. In this case a chip of silicon wafer contaminant.

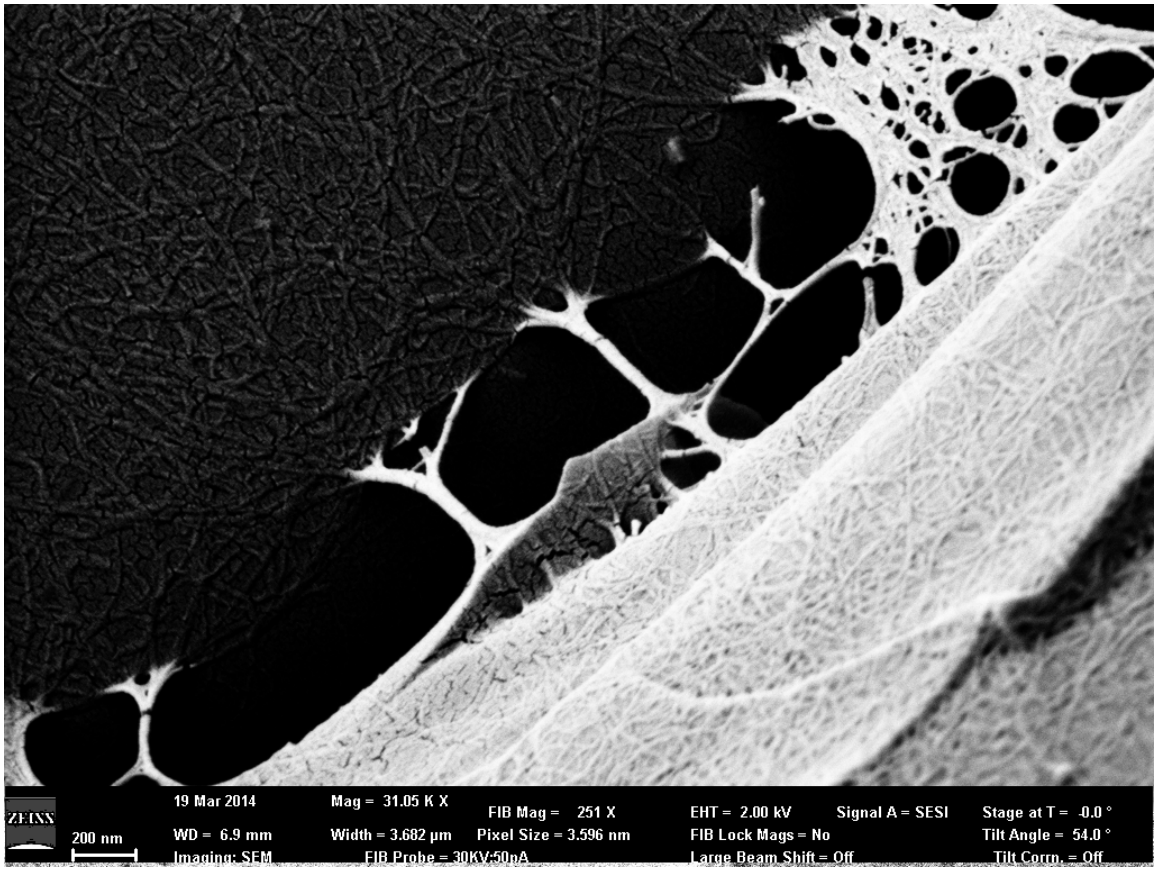

Figure 28. Close-Up of the Silicon Imperfection on the Silicon Surface. The chitin aligns in a direction normal to the direction of the edge of the contaminant, anchored to the surface and the contaminant.

Chitin was dissolved into HFIP at a ratio of 0.1mg of chitin to each milliliter of HFIP. The solution was sonicated for ten minutes to ensure dissolution of the chitin. To the Chitin/HFIP solution 0.5mg of silica beads were added. Four diameter sizes of beads were used: 250nm, 500nm, 1μm, and 2μm. The bead suspension was sonicated for ten minutes. Silicon wafer pieces were cut into 15mm by 15mm sections and cleaned with DI water and ethanol. The Si wafer pieces were dried using compressed, dry nitrogen. Working quickly, 100μL of each suspension was pipetted onto the surface of a silicon wafer square. The HFIP was allowed to evaporate and was washed with DI water and ethanol. Once dry, the squares could be sputter coated and imaged via SEM.

The chitin films deposited with the various sized beads show a tendency toward a radial symmetry. The chitin prefers to radiate outward from the edge of the bead form in an umbrella-like or circus tent-like structure. The bead size that leads to the most complete tenting appears to be the 1μm beads (Figure 31). The web formation occurs when the beads settle on to the substrate, while immersed in chitin dissolved in HFIP. The HFIP is exceedingly volatile and is readily evaporated in ambient conditions. As the solvent is driven off, the chitin condenses around the beads already on the substrate. Each bead serves as a nucleating sight for chitin and solvent as the solvent evaporates. At some point, the chitin:HFIP ratio becomes unstable and the chitin drops out of solution, leaving chitin webs draped over silica beads (Figure 34).

There is an apparent selection process occurring as the diameter of the bead is varied. As the beads were cleaned in the same manner and the chitin/HFIP solution came from the same stock solution, there is an obvious differentiation in the selection of bundles that span the gap between the bead and the substrate. Figure 29 shows a

bundling of fibers crossing the 250nm bead that tend to resemble the disorder of the background of the chitin nanofiber network while the 500nm and 2μm beads (Figures 30 and 32) demonstrate a much more selective population of bundles spanning the gap. The 1μm beads (Figure 31) show a more dramatic tent-like structure. As a size comparison, the beads of the various sizes were imaged at the same magnification to demonstrate the differences of scale involved (Figure 33).

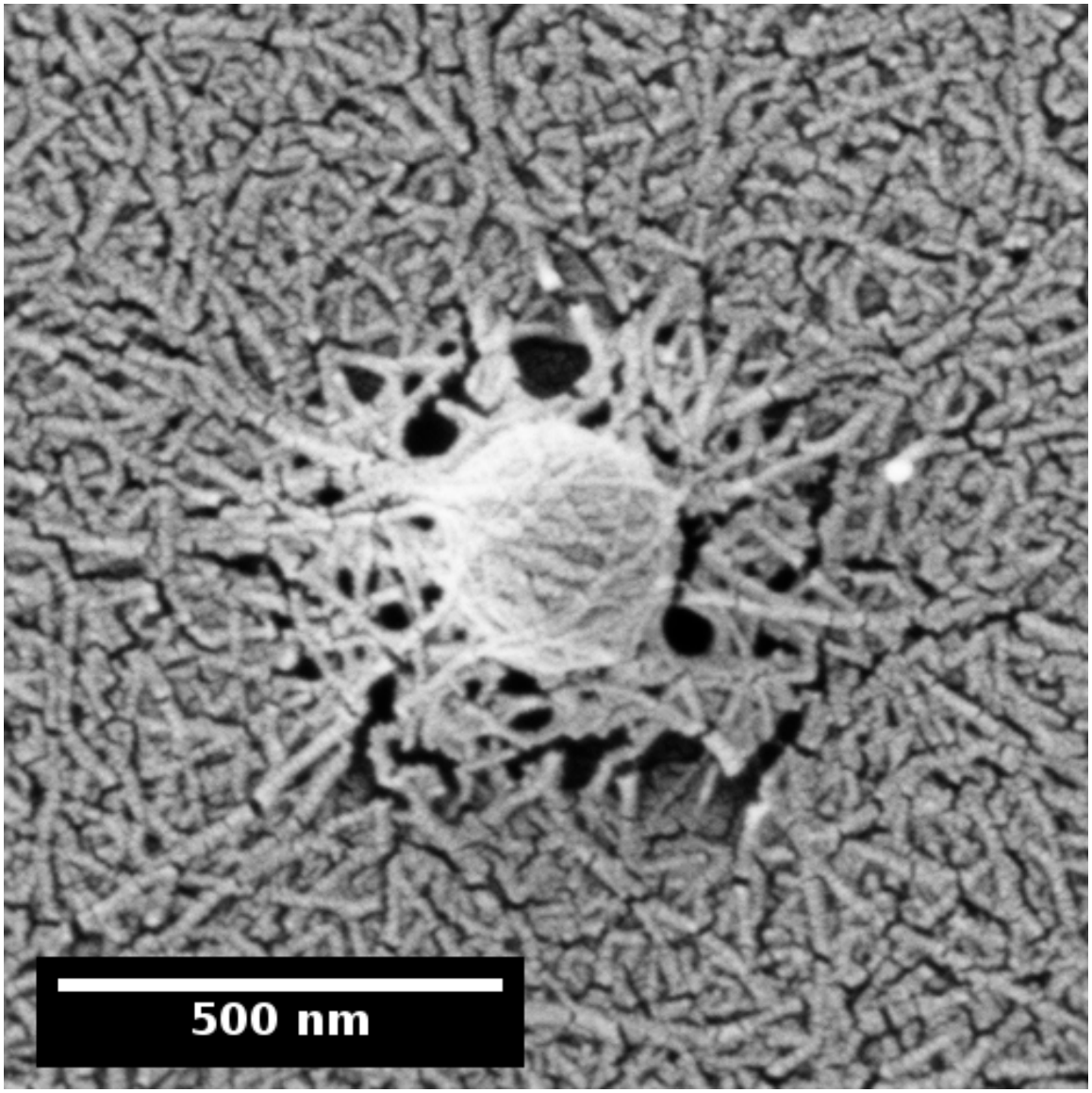

Figure 29. This 250nm Silica Bead was Deposited with Chitin in HFIP. The perturbation of the chitin film leads to radial alignment that is dependent upon stress induced by the height of the bead.

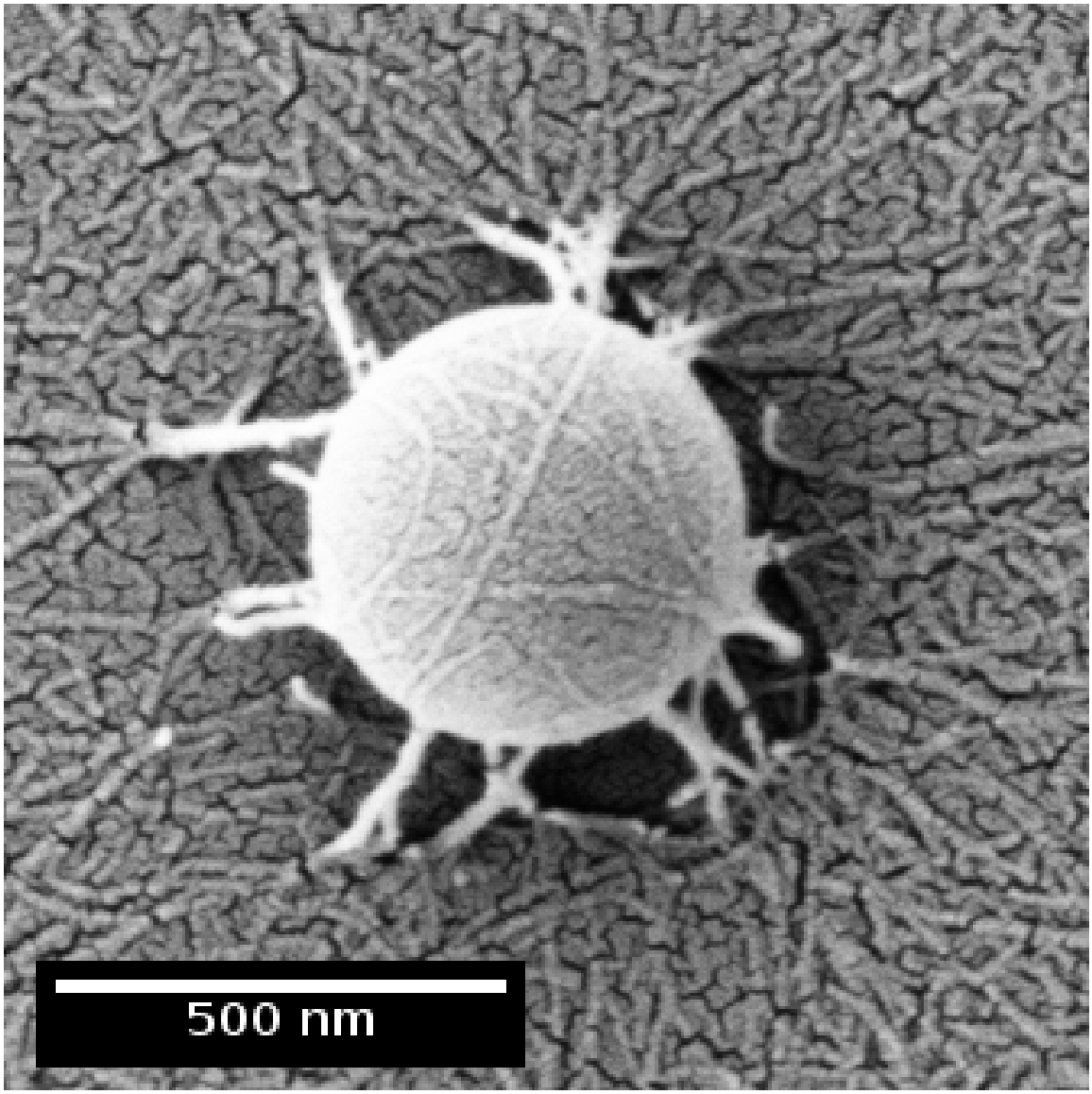

Figure 30. This 500nm Silica Bead was Deposited with Chitin in HFIP. The perturbation of the chitin film leads to radial alignment that is dependent upon stress induced by the height of the bead.

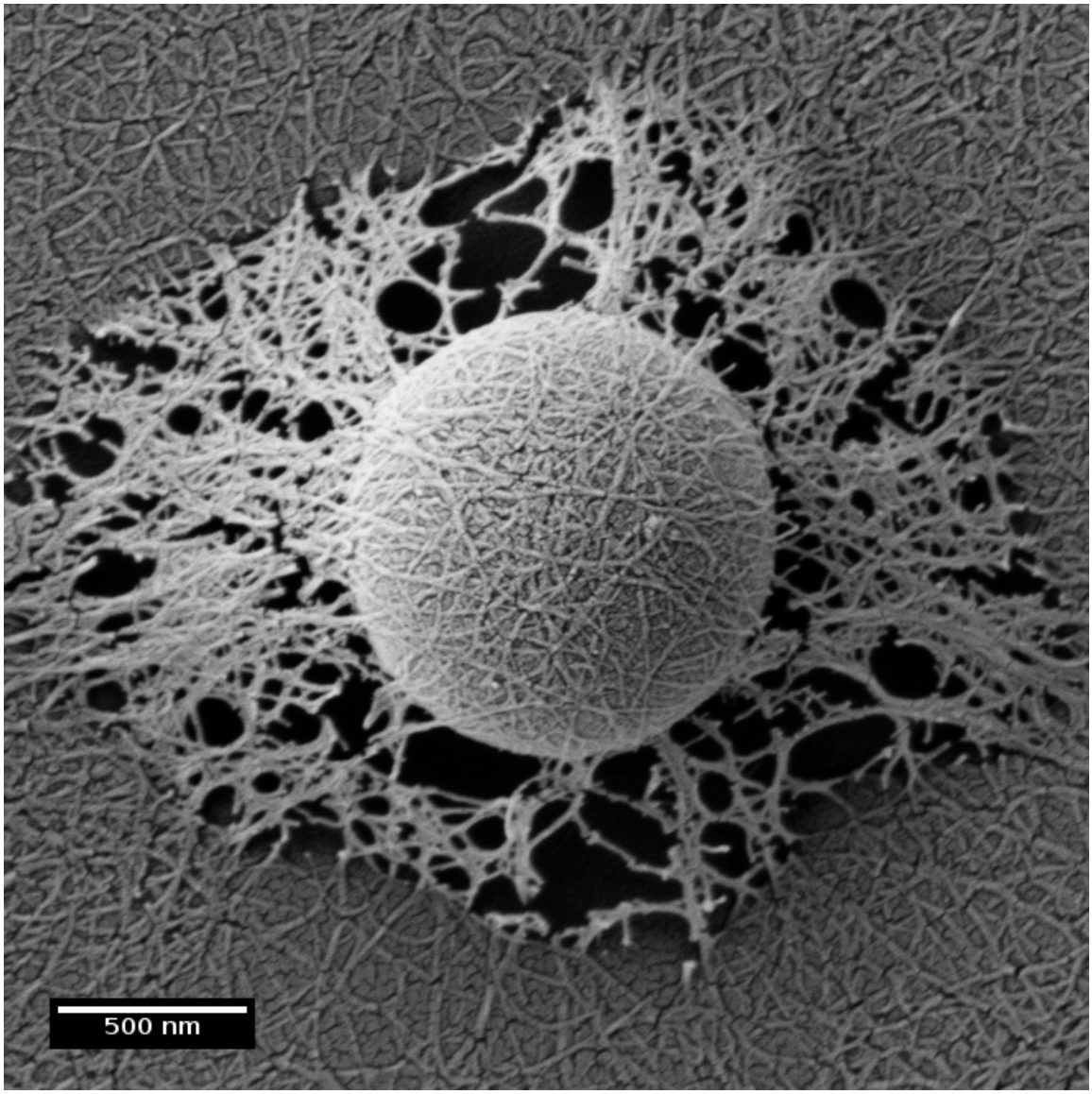

Figure 31. This 1μm Silica Bead was Deposited with Chitin in HFIP. The perturbation of the chitin film leads to radial alignment that is dependent upon stress induced by the height of the bead.

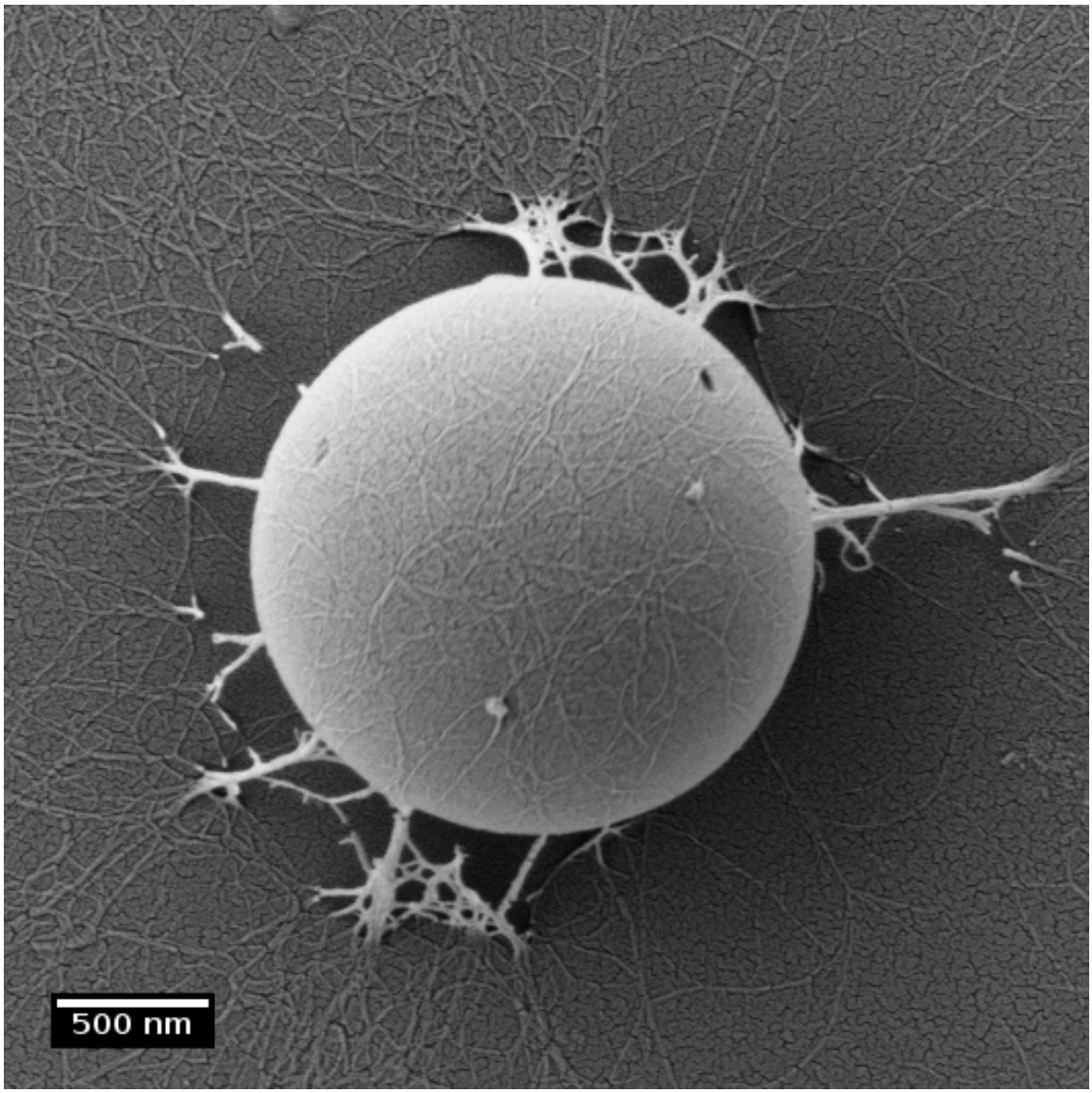

Figure 32. This 2μm Silica Bead was Deposited with Chitin in HFIP. The perturbation of the chitin film leads to radial alignment that is dependent upon stress induced by the height of the bead.

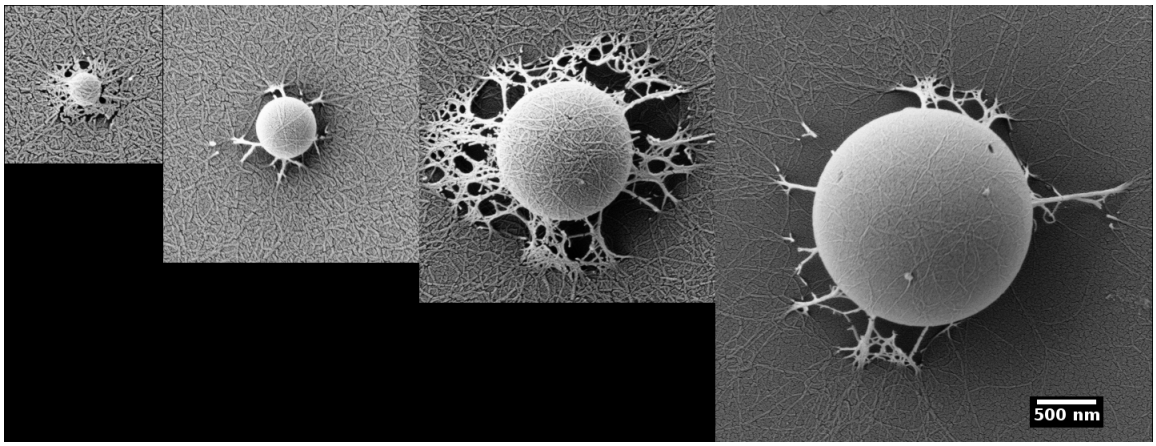

Figure 33. Side by Side Comparison of Bead Size. As a visual size comparison, images of beads viewed at the same magnification are laid side by side to see the scales involved. From left to right: 250nm silica bead, 500nm silica bead, 1μm silica bead, and 2μm silica bead.

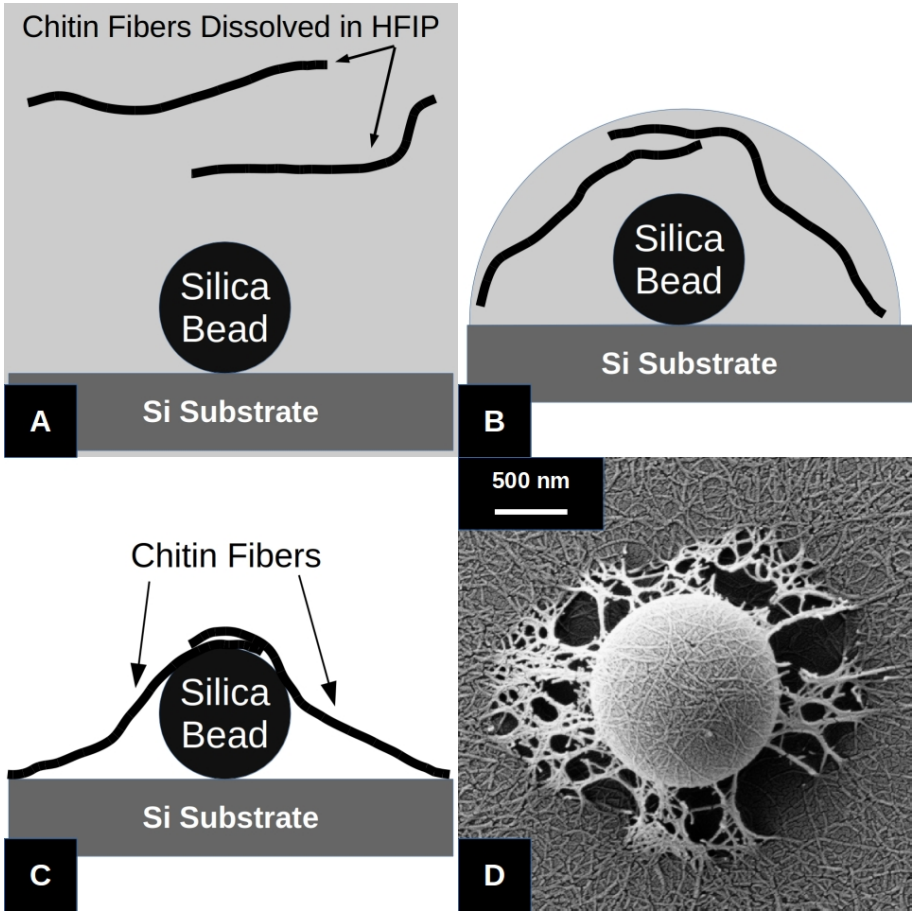

Figure 34. Chitin Web Formation. Schematic diagram of the formation of chitin webs about their bead perturbations. The chitin is dissolved in HFIP with the beads in suspension. The beads settle to the substrate, A. As the solvent evaporates, pockets of HFIP and chitin congregate about the beads, B. The solvent evaporates off, leaving the chitin fibers draped over a bead, C and D.

Table 2 shows the data values of a series of webs made from 1μm silica spheres. In this case, I preselected the high and low angle values due to the radial alignment of the nanofibers. The data was taken from areas on the web at 0, 90, 180, and 270 degree from the center of the sphere due to the necessity for a square image area to be processed. The area to be used as the background standard was taken from an area where there was no bead located (Figure 35). The perturbation of the beads is seen to fall off rather quickly, leaving a randomly oriented background on the silicon substrate.

Table 2. The Radial Dependence of High and Low Angle about Beads. The high angle/low angle differences are shown here. The measurements were taken at 0, 90, 180, 270 degrees around the bead to show a radial dependence upon the direction of the fiber orientation.

	Background	**0 Degrees**	**90 Degrees**	**180 Degrees**	**270 Degrees**
	632.3	790.4	1003.2	841.0	865.3
	406.7	707.7	597.6	576.6	559.2
	482.3	396.2	636.8	526.4	476.2
Mean	507.1	631.4	745.9	648.0	633.6
Std Dev	114.8	207.9	223.7	169.0	204.9

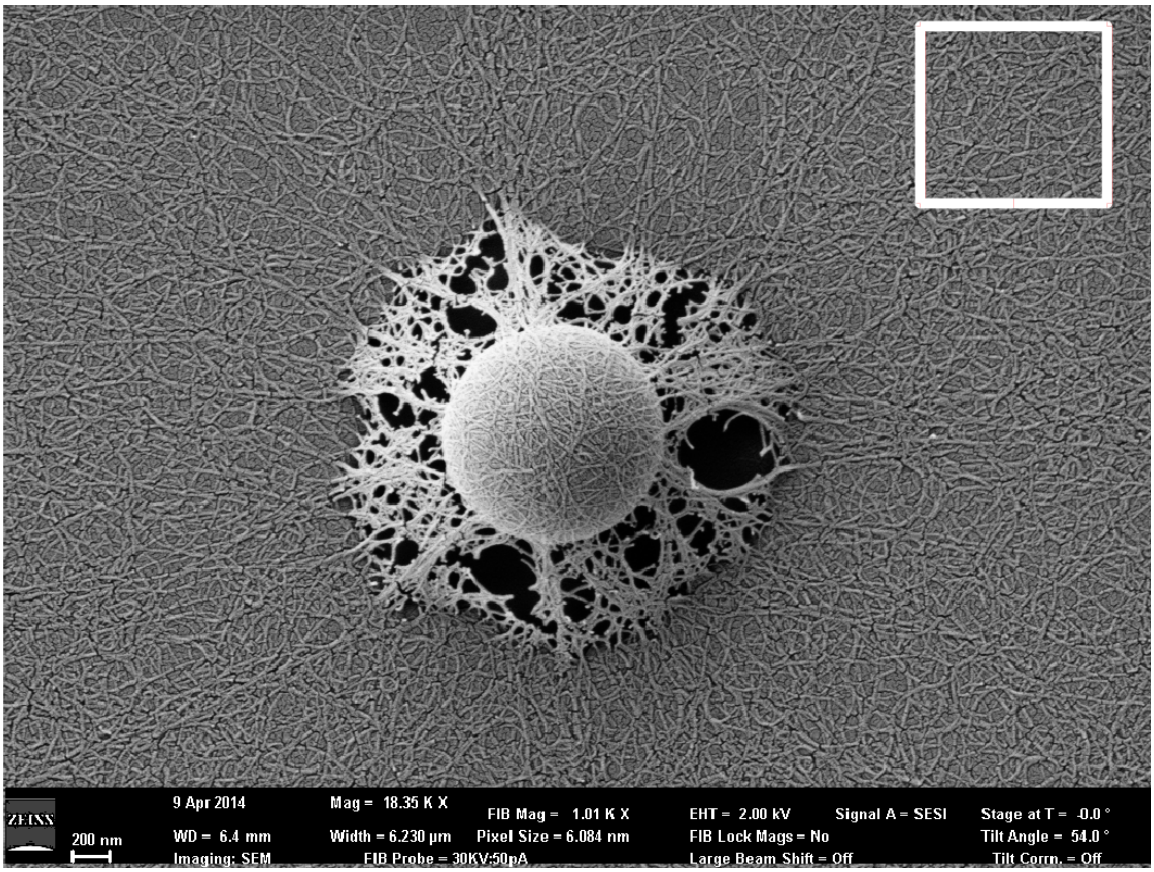

Figure 35. White Square Indicates area of Background Measurement.

4.6 Nanofiber Measurements

The Rakki Prep Method also allows the direct measurement of bundles of chitin nanofibers in situ. These measurements taken from the dissected and prepared sections of the cicada can then be compared to the tendency of the nanofibers to bundle when films of chitin are perturbed (Table 3). The bundle diameter does not show a great difference among the differing sections of insect cuticle. There is, however, a noticeable difference in bundle width among the fibers bundled due to perturbation.

Table 3. Nanofiber Bundle Measurements. The removal of the extracellular matrix allows in situ measurement of nanofiber bundles as they are organized in the insect cuticle. This can be compared to the bundling of fibers observed through the perturbation of chitin films using nanometer diameter beads.

	Average	σ	**2** σ
Head	23.86	4.87	9.74
Eye	19.68	1.94	3.88
Thorax	25.40	5.38	10.75
Leg	14.54	4.56	9.13
Wing	22.60	3.75	7.51
250nm Bead	13.90	2.33	4.66
500nm Bead	27.28	9.74	19.47
1μm Bead	15.51	3.66	7.31
2μm Bead	48.96	7.88	15.76

4.7 Discussion

The development of the Rakki Prep method for the visualization of in situ chitin organization will allow for the further study of chitin based structures in the natural world. The evolutionary development of chitin and the structures that it underlies has had a significant jump on contemporary engineering. The ability to visualize the morphology of the myriad of specialized structures utilized by the natural world can open up interesting new dimensions in practical engineering and problem solving.

The quantification of the alignment of chitin via the ImageJ Oval Profile plugin allows for a practical metric in the design and implementation of chitin based systems. The difficulty in working with chitin is the lack of solubility in common solvents and the difficulty associated with making it chemically active. The notion that it can be aligned simply by the proper placement of a perturbation may allow the design and implementation of simple chitin based systems.

CHAPTER V

CHITIN LINEAR POLARIZERS

5.1 Introduction

In this section, I will show that unpolarized, visible light transmitted through the clear membranes of cicada wings becomes polarized. To accomplish this, it will be necessary for me to have a means of polarizing the light to be transmitted through the wing membrane, focusing on a discreet spatial area of the membrane, rotating the membrane about the optical axis, and quantifying the intensity of the light transmitted through the membrane.

I will also compare the polarized light of the cicada wing to the optical phenomena of birefringence. Birefringence arises due to the anisotropy of the index of refraction in a material. Typical birefringent materials are solid state crystals with an anisotropic lattice constant and polymers under mechanical strain. The American Association of Textile Chemists and Colorist (AATCC) have a standard method (Standard Method 20-2007) for the determination of birefringence.

5.2 Cicada Wings and Chitin Films and Fibers

Cicadas were collected locally during the summer of 2013, which coincided with the emergence of the Brood ii cicada. Cicadas were abundant and easily collected. The wings were removed and stored frozen. For use, the wings were dehydrated in methanol and cleaned via sonication. The cicada wings were mounted on glass slides to facilitate transport and mounting in the microscope. The use of the glass slide also aids in the mounting the wing as flat as possible. Scanning electron micrographs

of the wing show the surface morphology and the layering that is endemic to the cuticle formation (Figure 36 A). A set of wings also received the Rakki Preparation. In this manner of preparation, the wing was stripped of minerals, lipids, and fatty acids by digestion in 1M hydrochloric acid (HCL). The proteinaceous extracellular matrix (ECM) was then removed via digestion in 1M sodium hydroxide (NaOH). This preparation technique leaves behind the chitin fibers as they are organized and oriented in vivo (Figure 36 C).

Cast chitin films were created by dissolving chitin in hexafluoroisopropanol (HFIP) at a ratio of 10mg per mL. The films were cast onto a glass microscope slide and the HFIP allowed to evaporate in ambient. The resulting film is a randomly assembled mass of chitin fibrils lying on the glass surface (Figure 36 D).

Chitin fibers were formed by extruding chitin dissolved in HFIP under acetone. A volume of 100μL was drawn into a syringe with a tuberculin needle. The needle tip was immersed in acetone and the plunger was depressed fully, in a quick, steady fashion. As the solution was extruded, the HFIP was rapidly diffused from the solution, forming a filament of chitin as the more solution is forced out. As the HFIP was diffused from the solution into the acetone, the chitin fibers entangled, as they are insoluble in acetone. The fibers are thin and filamentous and are optically clear. Once formed, the fibers were transferred to purified water to remove the acetone or dried, depending upon future use. In the case of polarizing microscopy, the fibers were dried over night at 70°C. Fibrils show alignment under scanning electron microscopy in the extruded fiber (Figure 36 B).

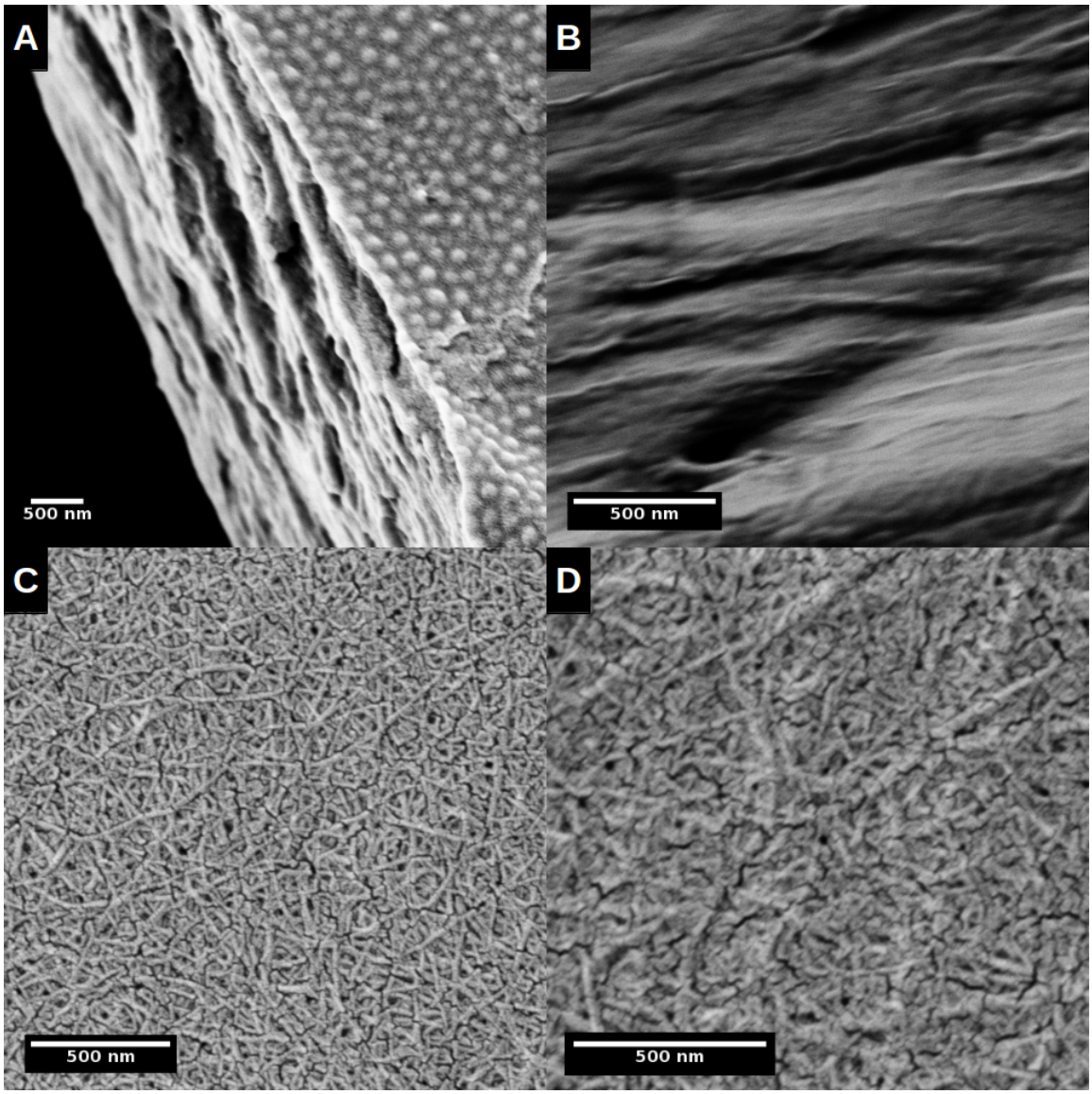

Figure 36. A Comparison of Wings, Fibers, and Films. SEM images of a cross-section of a M. septendecim wing, A, an extruded chitin fiber, B, an M. septendecim wing after being Rakki Prepped, C, and a cast film of chitin, D.

5.3 Broad Spectrum Polarimetry

UV – Vis data was collected on a Varian Cary 6000i unit. Initial data was collected by placing a fixed wing in the light path of the UV – Vis and placing a polarizing film (Thor Labs) over it and varying the film by forty-five degree angles (Figure 37). This creates a polarizer/analyzer pair with the wings and polarizing films. If the wing does act as a polarizer, this method will indicate so by a change in the percent transmission as the angle changes. Data collection was taken over a range of 400 – 800 nanometers of wavelength of light. This method served as a first approximation to determine if there were any polarizing effect. The spectroscopic data shows a change in the percent transmission of the light passed through the wing membrane as the angle of the polarizing film was varied between 0, 45, and 90 degrees (Figure 38). The change in the percent transmission over the 400nm wavelength range suggests that there is a polarizing effect due to the wing.

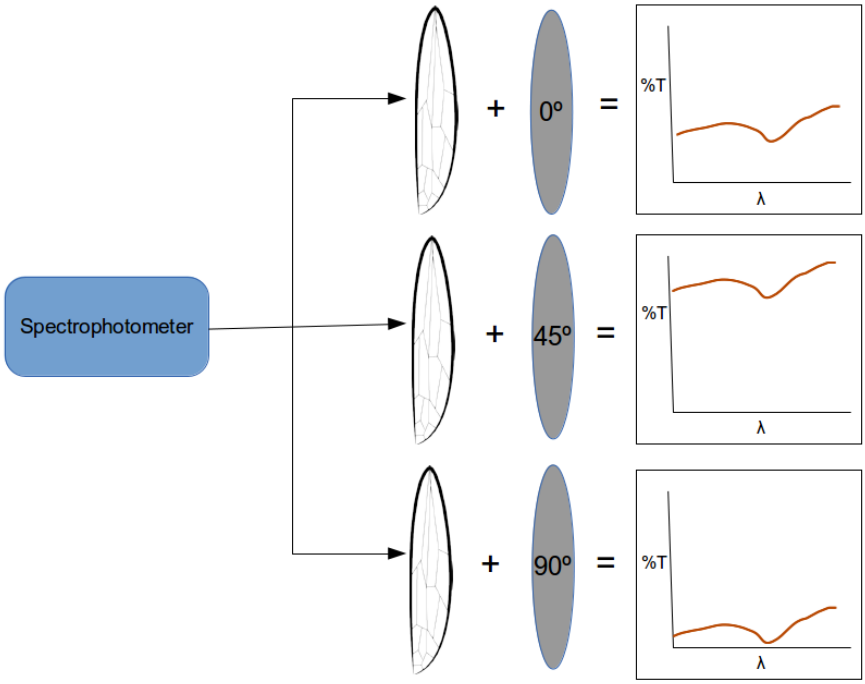

Figure 37. Schematic Diagram of the Spectroscopy Setup. The wings are fixed and the polarizing films are rotated through 0, 45, and 90 degree angles. The change in percent transmission indicates the effect of polarization.

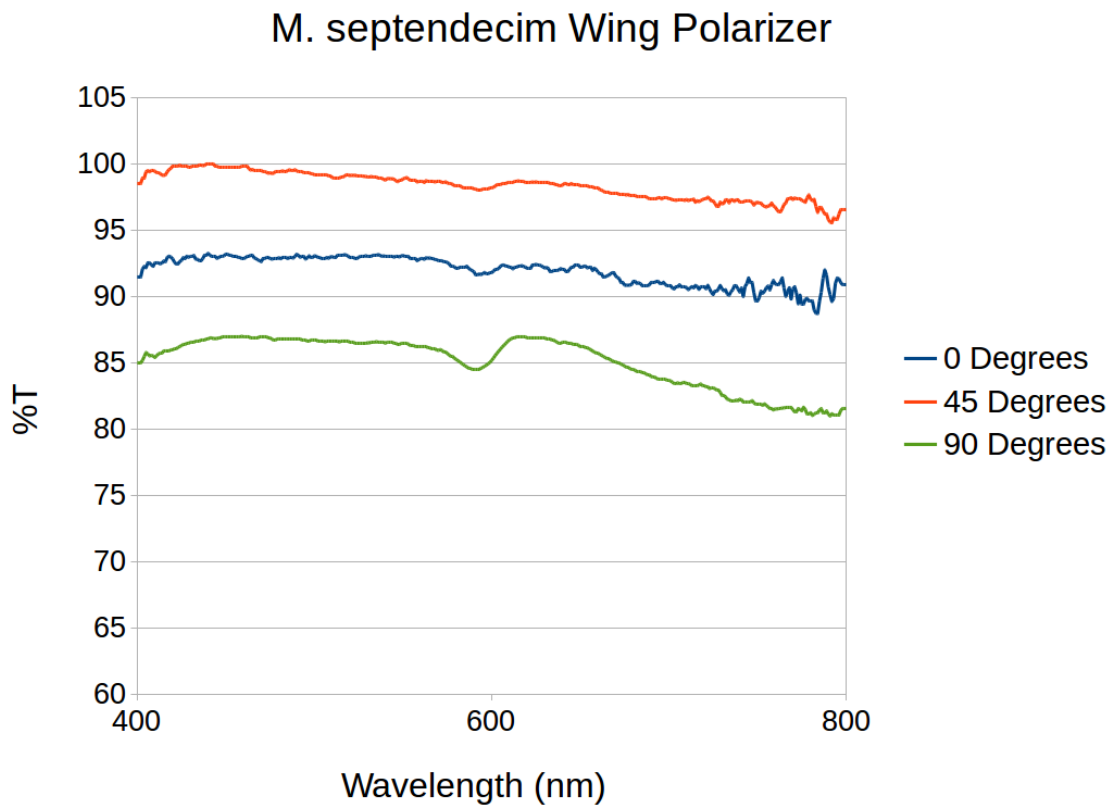

Figure 38. UV – Vis Spectroscopy Data. UV – Vis spectra of the percent transmission of light through the wing/polarizer pair. The percent transmission is seen to change as the angle of the polarizer is changed. Data was collected from 400 – 800 nanometers

5.4 Polarizing Microscopy

The polarization experiment was carried out on a Omax polarizing light microscope. This microscope has a polarized light source that passes light through a rotating stage. The stage rotates about the optical axis of the microscope and can be rotated 360 degrees. There is a cross polarizer the is located between the objective lens and the eyepiece lenses. The light source polarizer is fixed and the cross polarizer can be rotated 90 degrees. Samples were rotated through 180 degrees and images were captured every ten degrees.

The membrane section of the wing analyzed for this experiment consisted of the central field of the wing, delimited by the first major branch of the Media vein where it divides into the Media Anterior and Media Posterior (Figure 39). The data collected with the polarizing microscope further supports the idea that wing membranes of the M. septendecim polarize transmitted light.

Wings were mounted on glass slides to produce a sample that is flat. The membrane was analyzed at three locations: a spot toward the distal end, a central spot, and a spot towards the marginal end (Figure 39). Micrographs were recorded using a 40X objective for each section at ten degree intervals, from 0 – 180 degrees. The micrographs were then analyzed using ImageJ software (NIH). A circular area of 50 square pixels was selected about the axis of rotation and the average pixel value was calculated. The average pixel value was then plotted with respect to the angle at which it occurred. The raw data was treated with a baseline correction and normalized to a fit on a scale between zero and one. The normalization process allows for a less cumbersome comparison with Malus' Law. This data was then graphically analyzed by contrasting it to a graph of Malus' Law and correlating it to a fit. The

treated data from the individual spots on the wing show a differing angle of polarization across the wing membrane (Figures 40, 41, and 42). The data compiled from three wings and three spots on each wing was aligned by the maximum of the angle of polarization and averaged to show a statistically significant correlation with Malus' Law (Figure 43). The Rakki Prepped wing shows no dependence, thus not obeying Malus' Law (Figure 44). On the other hand, the analysis of the extruded chitin gel fiber shows a correlation to a dependence, which suggests birefringence (Figure 45). The idea of birefringence is supported by analyzing the extruded chitin fiber using Standard Method 20-2007 of the AATCC. The cast chitin film shows neither polarization nor birefringence and does not correlate with either Malus' Law or AATCC Standard Method 20-2007 (Figure 46).

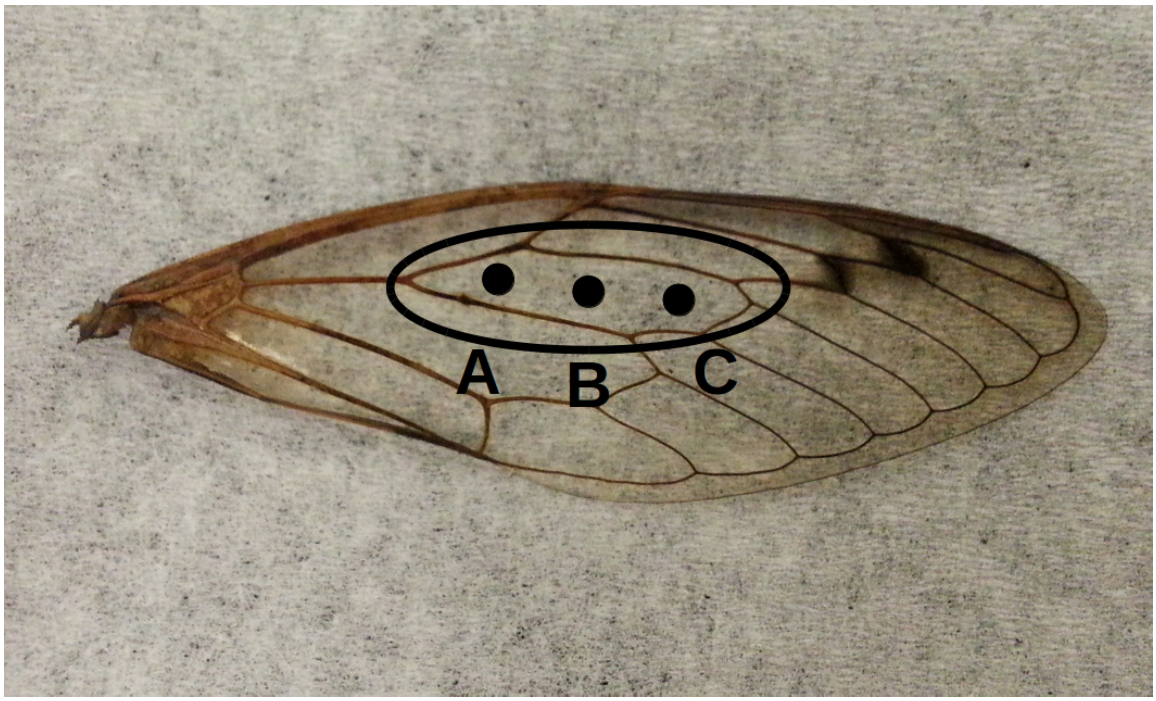

Figure 39. Forewing of *M. septendecim*. Circled area denotes the area of measurement: a central field of the wing, delimited by the first major branch of the Media vein where it divides into the Media Anterior and Media Posterior. Measurements were made at three areas of the membrane: A, B, and C (indicated by black spots).

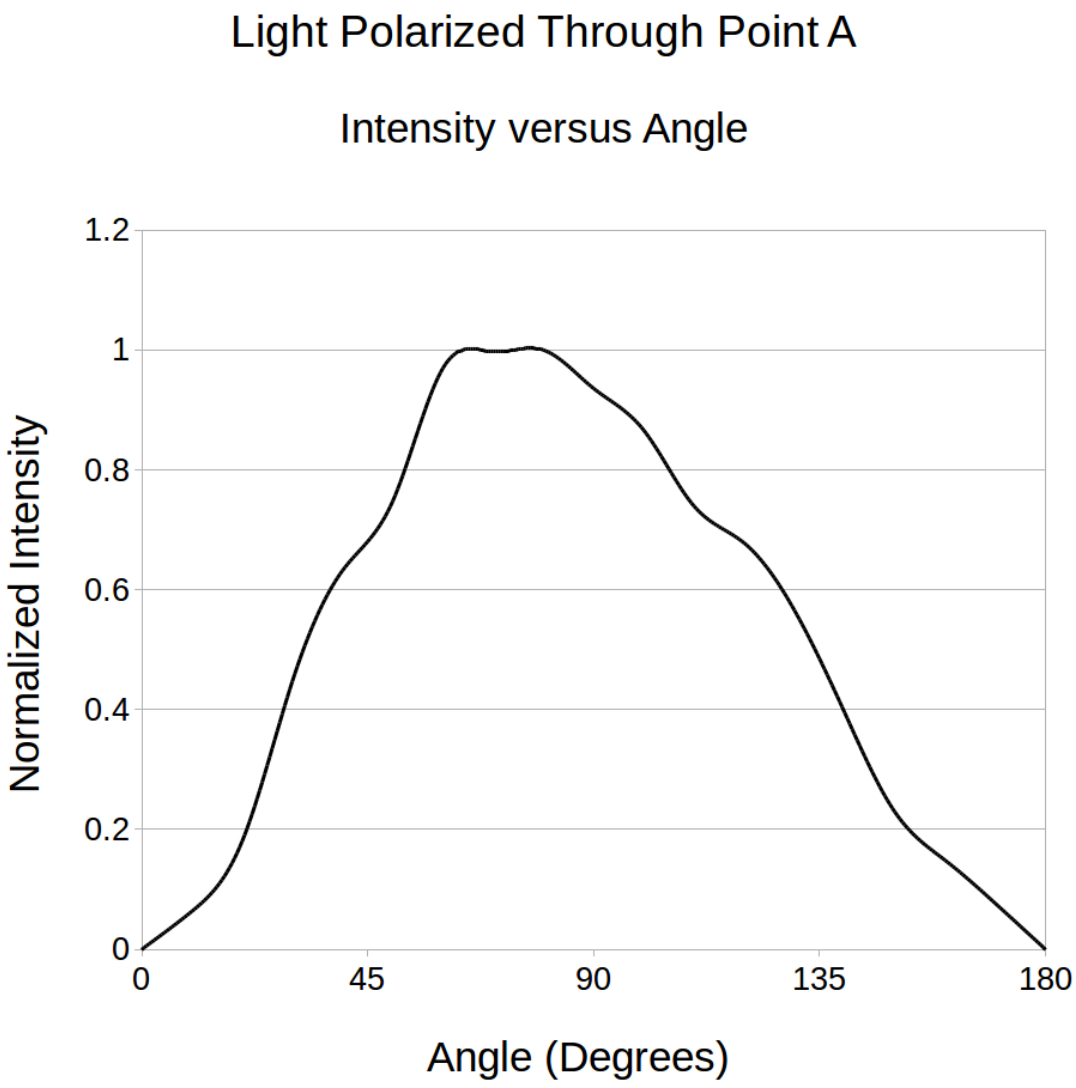

Figure 40. Polarization Data from Spot A. Polarized light transmitted through the wing creates a polarizer/analyzer pair. The graph shows a change in intensity as the microscope stage rotates through 180 degrees.

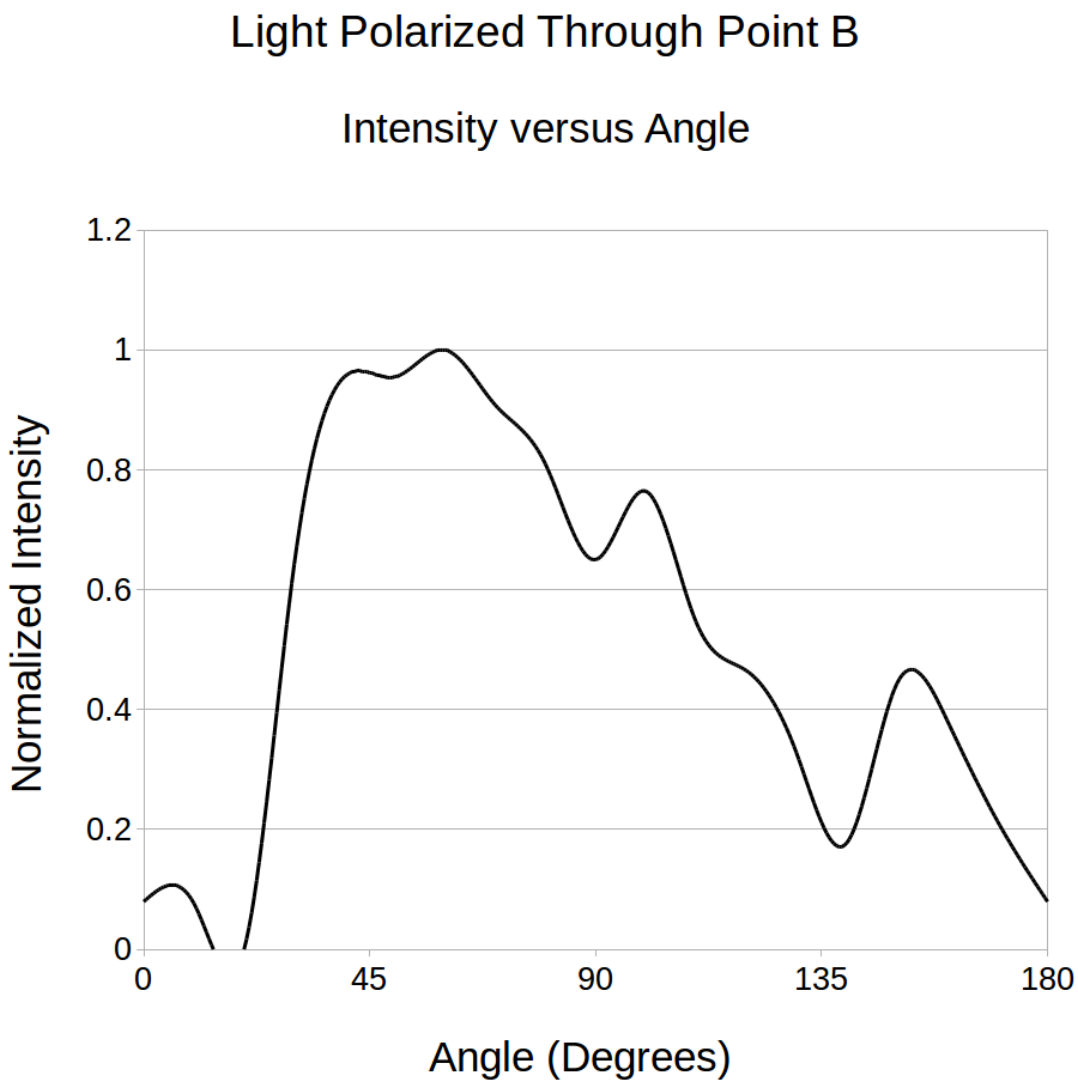

Figure 41. Polarization Data from Spot B. Polarized light transmitted through the wing creates a polarizer/analyzer pair. The graph shows a change in intensity as the microscope stage rotates through 180 degrees.

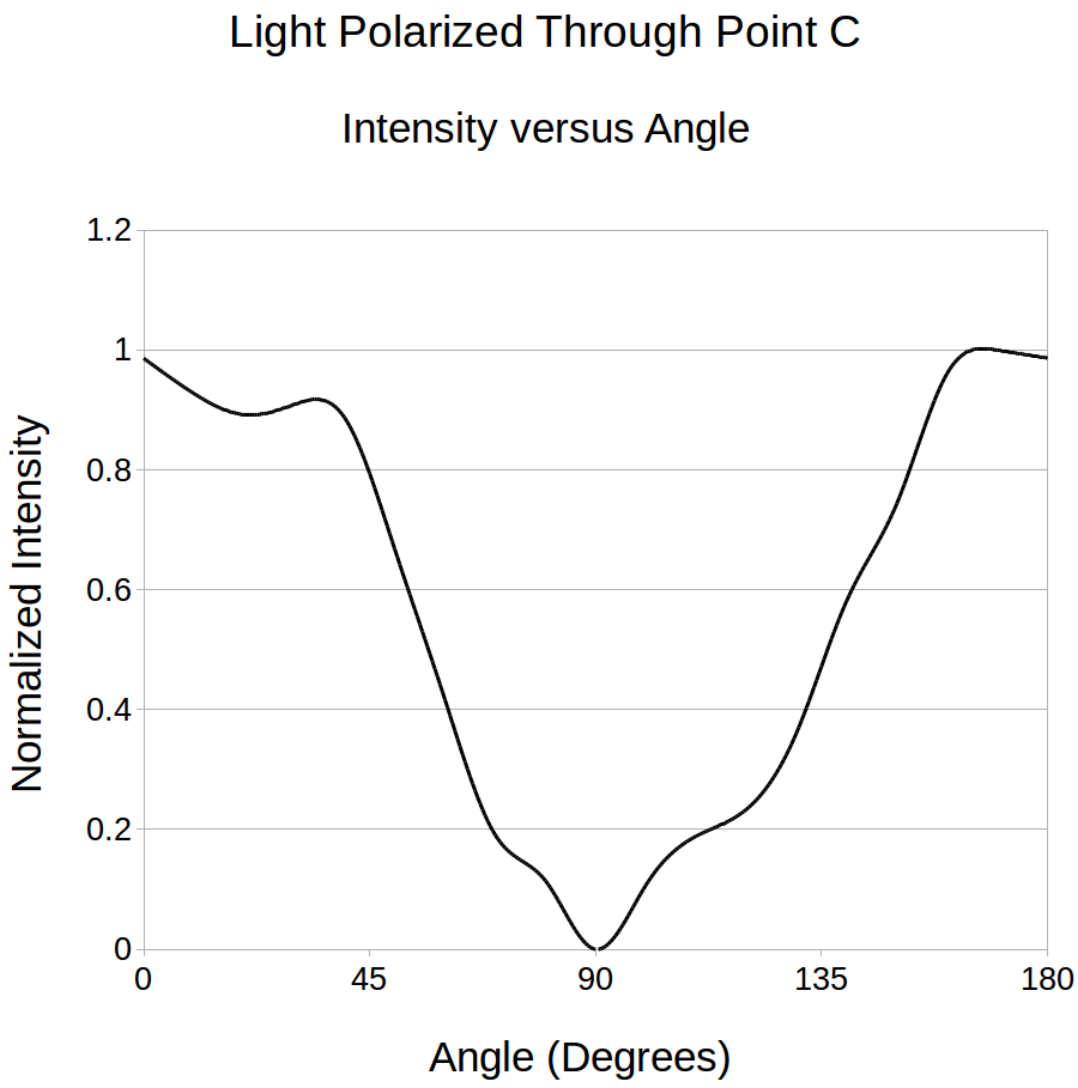

Figure 42. Polarization Data from Spot C. Polarized light transmitted through the wing creates a polarizer/analyzer pair. The graph shows a change in intensity as the microscope stage rotates through 180 degrees.

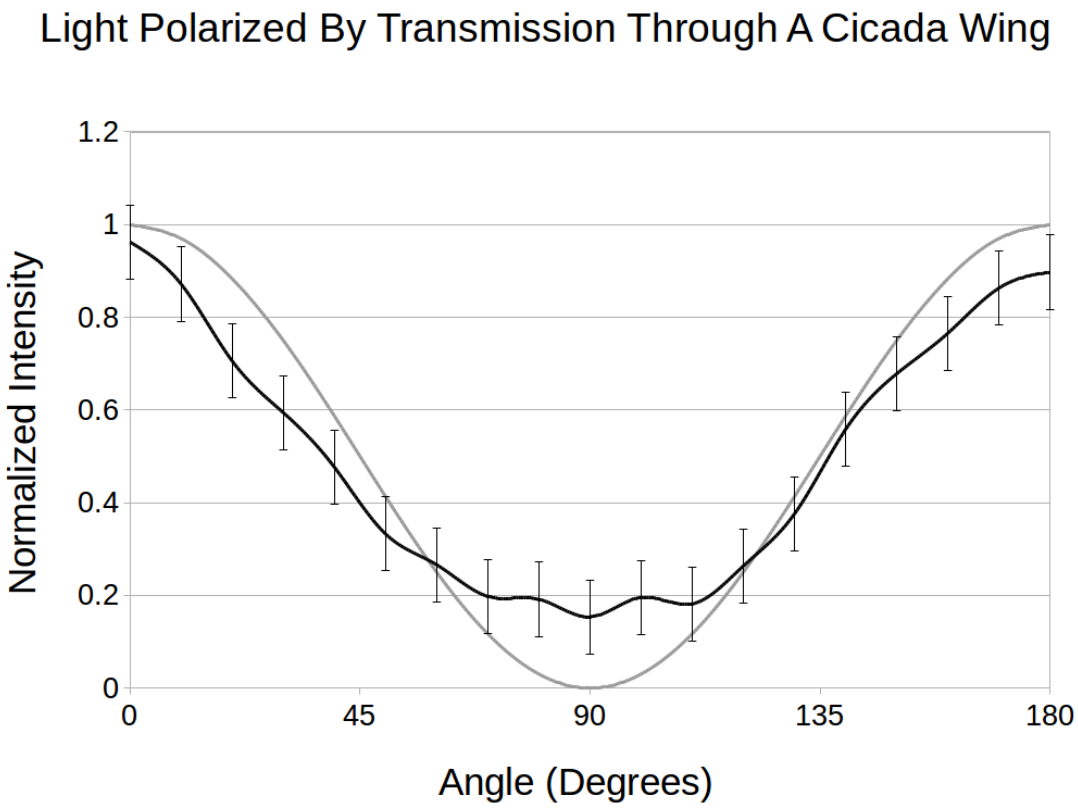

Figure 43. Polarization of the Wing. Light transmitted through the wing membrane of *M. septendecim* shows a close fit to Malus' Law and a $\cos^2(\theta)$ dependence. Light gray line represents an idealized Malus' Law.

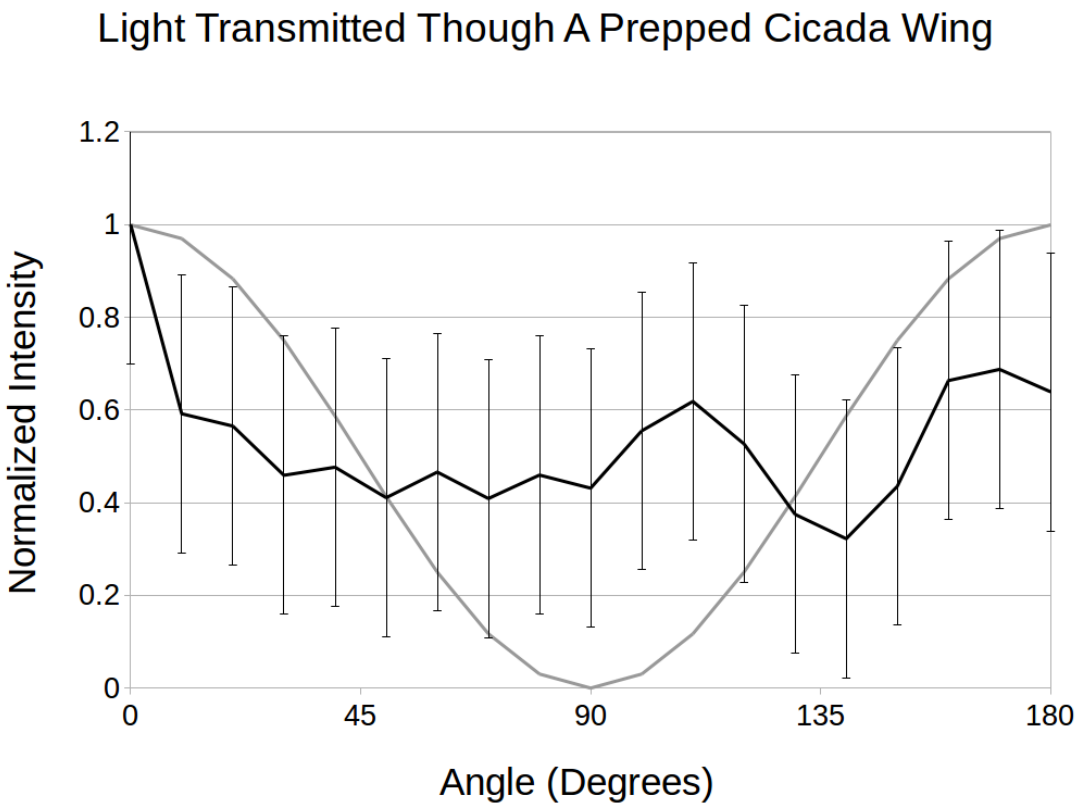

Figure 44. Polarization of the Prepped Wing. The light transmitted through the prepped cicada wing shows no correlation to Malus' Law. The removal of the extracellular matrix has left the wing devoid of the ability to polarize transmitted light.

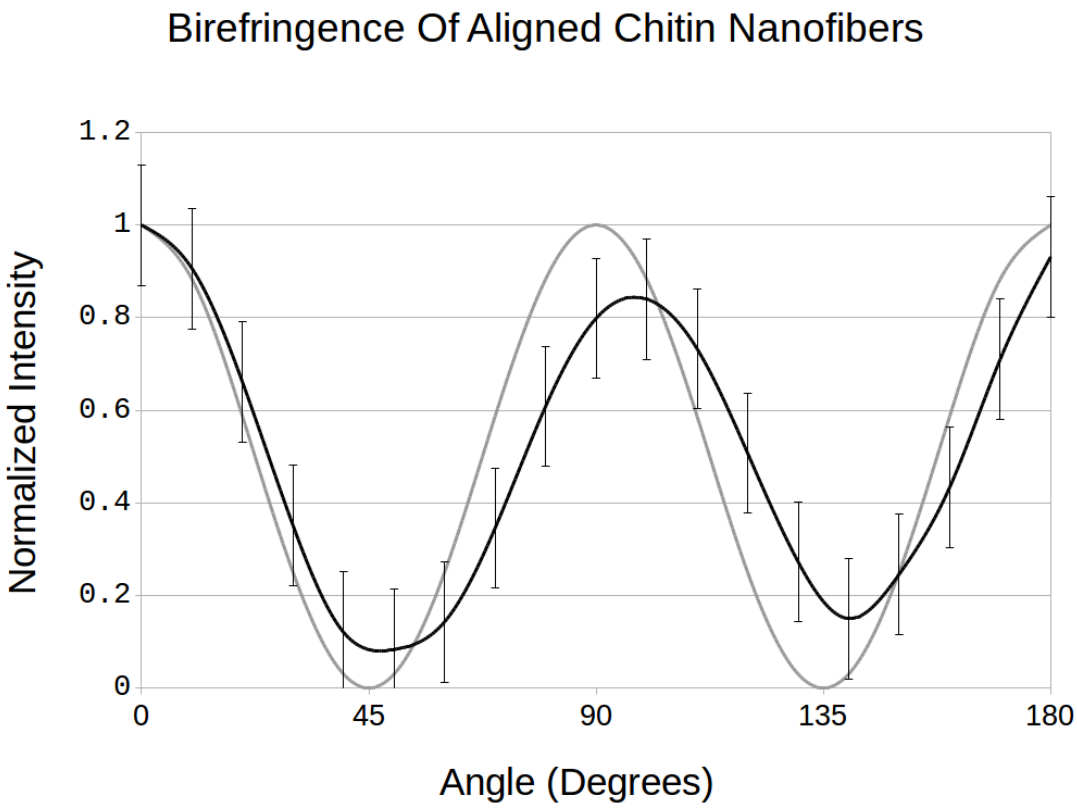

Figure 45. Birefringence of Aligned Chitin Nanofibers. The aligned chitin nanofibers formation shows a distinct $\cos^2(2\theta)$ dependence which is attributed to birefringence. The birefringence is attributed to an anisotropic index of refraction stemming from nanofiber alignment. Light gray line is showing idealized birefringence.

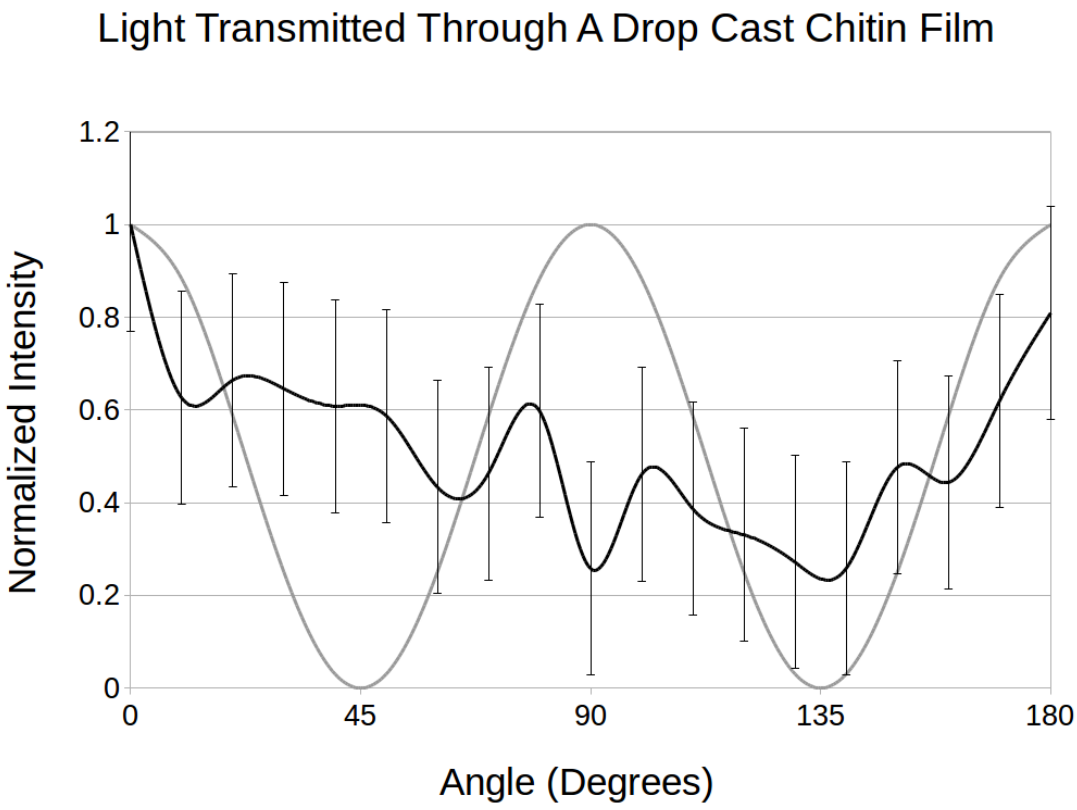

Figure 46. Correlation of the Drop Cast Chitin Film. The Drop Cast Chitin Film has a random assemblage of nanofibers. This randomness shows neither polarization nor birefringence of transmitted light.

5.5 Discussion

The data gathered strongly supports the hypothesis that the wing membrane of the the cicada *M. septendecim* polarizes transmitted light. The mechanism of this polarization by the wing membrane is most likely due to dichroism, or selective absorption through the multiple layers of the cuticle. The standard model of the cuticle shows that it is composed of multiple layer of aligned chitin embedded in a matrix of proteins that serve to create a rigid composite material, much akin to modern fiber glass. The polarization does not arise from the chitin alone, as the Rakki Prepped wing shows no correlation to Malus' Law or birefringence. This dichroic effect may arise from the anisotropic nature of the organized insect cuticle.

Also, the angle of polarization is not consistent across the membrane. It has been shown that insects, and some of the predators that prey upon them, have the ability to "see" polarized light. If a wing inherently polarizes transmitted light it may be seen as a disadvantage to wave a polarized flag. It may have become evolutionarily advantageous to rotate the angle of polarization across membranes to reduce the overall target visibility to predation.

CHAPTER VI

CHITIN GEL FORMATIONS

6.1 Introduction

This section details the creation and processing of Chitin Gels, Chitin Gelatinous Blobs, and Chitin Gelatinous Fibers, each of these features being distinct in nature but emanating from a common source. The former of the three entities, the Chitin Gel, is the basis of the latter two. A Chitin Gel is defined as a random assemblage of chitin nanofibers; which are randomly oriented and consist mostly of water. A Chitin Blob is a Chitin Gel formation that has been slowly extruded. A Chitiin Gelatinous Fiber is a Chitin Gel formation that has been rapidly extruded, forming a long, continuous fiber or a short, staple fiber.

The Chitin Gel, in its basic form, is the most versatile; as it has the ability and flexibility to be processed into many shapes and useful forms. The uses of these are varied and can be seen in exempla, but not limited to: tissue scaffolding, filtering material for nanoparticles, support scaffolding of nano-textured surfaces and structures, biodegradable plastics, and so on. The Chitin Gel is flexible, optically clear, and predominantly water, making it a hydrogel.

The Chitin Gelatinous Blobs and Chitin Gelatinous Fibers share the basic form of the Chitin Gel but differ in the morphology of the final product. Where the Chitin Gel in its purest form is a random tangle of chitin polymers, the Chitin Gelatinous Blob and Chitin Gelatinous Fiber exhibit a degree of chitin polymer orientation. This orientation is imparted due to the action of their creation. The creation of these

entities is through an extrusion process. Fortunately, there are in place standard methods for the determination of the polymer alignment in extruded fibers. The American Association of Textile Chemists and Colorists have a Standard Method 20-2007 that addresses the qualitative analysis of the birefringence of an extruded fiber. The birefringence is an important aspect of extruded polymer fibers as it is an indication of the alignment of the polymer that comprises the fiber. The birefringence arises from anisotropy of the index of refraction of the material. A material with a constant index of refraction will refract light the same, no matter the orientation of the light to the material. A material with an anisotropic index of refraction will have in one direction an ordinary index of refraction (n_o), usually in the direction of the optical axis, and perpendicular to that, an extraordinary index of refraction (n_e). Plane polarized light with a polarization vector not parallel to either index of refraction passing through a material with an anisotropic index of refraction will be spit into two components, a fast wave and slow wave. The slow wave will be retarded from the fast wave by a fractional wavelength. The fast and slow waves will be orthogonal to one another. If another polarizer, the analyzer, is placed after the material with a polarization vector perpendicular to the initial plane polarized light, the vector components of the fast and slow waves will be summed in a single plane polarization. The intensity of the resulting lignt is dependent uponthe summation of the components of the incoming light and and the polarization angle of the analyzer.

Typically when a light is analyzed with crossed polarizers, all that is visible is a dark field. If another polarizer is inserted between the crossed polarizers, the angle of polarization is changed from perpendicular to the angle of the inserted polarizer, at an intensity cost. In similar fashion, when a material with an anisotropic index

of refraction is placed between crossed polarizers, the splitting of the fast and slow waves creates a new polarization state and the material becomes visible through the analyzer as a bright image in a dark field.

The anisotropic nature of the index of refraction is a consequence of the morphology of the material. In the case of polymeric materials, it is due to the alignment of the polymers comprising the material. I can use the birefringence of the material to give an indication of whether or not the underlying polymers are aligned. If I look at the fibers using crossed polarizers and see a bright image on a dark field, birefringence is indicated.

6.2 Chitin Purification

For the preparation of Chitin Gels, Gelatinous Blobs, and Gelatinous Fibers, a preparation of purified chitin must be obtained by a modification of processes derived from literature [36, 66]. In order to obtain the purified chitin, several steps must be accomplished. These steps include the de-mineralization of the parent cuticle, the removal of the fatty acids and lipids, and the deproteinization of the chitin.

There are several sources for obtaining of chitin. These sources are any chitin producing organism which include the arthropods (crustaceans, insects, and arachnids), mollusks (cephalopods and gastropods), and fungi (yeast). In the case of arthropods, the chitin is predominantly manifested in the tough exoskeleton that makes up the rigid, outer structure of the organism. This is predominantly where my chitin store originated.

The first step was to properly clean the organism, or sample of organisms, from which the chitin is to be extracted. Once the organisms were cleaned, they were

lyophilized and finally pulverized. The pulverized material affords much more surface area for the subsequent extraction steps.

The de-mineralization and the removal of fatty acids and lipids was accomplished in the same step. To accomplish this, the pulverized material was immersed in and thoroughly soaked for a period of 24 hours in a 1M concentration of HCl at a temperature of 65 – 75 Degrees Celsius. Agitation may be employed to expedite this step but is not necessary.

After the mixture has thoroughly soaked for a period of 24 hours, the liquid must be removed from the solid. The solid being the desirable part, the mixture was centrifuged, in swing buckets, for a period of 20 minutes at 3500 revolutions per minute. Washing was accomplished by pouring off the supernatant and replacing the liquid with reverse osmosis water. The mixture was then shaken to mix it well, and the centrifugation was repeated at the aforementioned parameters. After each centrifugation, the liquid was discarded and the solid portion retained. The washing was repeated at least six times. After the last washing, the pH was checked using a pH meter. The pH should be that of reverse osmosis water.

At this point, the centrifugation step was repeated and the water discarded. The water was replaced with a 1M solution of NaOH. This step removes proteinaceous material from the chitin. The solution was allowed to normalize and thoroughly soak for 24 hours at a temperature of 65 – 75 Degrees Celsius. After this period of soaking is complete, the before mentioned washing steps were repeated until the final product exhibits a neutral pH.

The processed and cleaned chitin could then be dried. It is stable in a dried, powdery form. This chitin could be further processed to a finer powder by means of

mortar and pestle or left coarse. Coarse material may result in easier handling as the finer powder tends to charge in plastic weigh boats. The chitin was then characterized using Fourier Transform Infrared Spectroscopy and X-Ray Diffraction as a means to verify purity.

6.3 ImageJ Processing

The Oval Profile plugin, authored by Bill O'Connell, is required to perform the quantification action in ImageJ [4]. The Oval Profile plugin can be used to determine the overall direction of fiber alignment and the magnitude to which the fibers are aligned. The area to be analyzed is processed with a Fast Fourier Transform (FFT) before the Oval Profile plugin is applied. The region on which these operations are to be performed are first selected and bound by an oval area selection of the FFT. The plugin is then compiled and run. The Oval Profile plugin divides up the oval area selection into n equal angled radii, emanating from the center of the oval to the oval edge. The plugin then performs the selected operation. The "Radial Sums" operation plots the sum of the gray scale value over the n angles. A more aligned fiber system will have a greater disparity between the sums along the n radii around the oval than the edges and background. The edges and background being darker than the fibers, the low sections of the "Radial Sums" plot will be lower and high sections will be higher as compared to a less oriented fiber system, as the plot is summed over dark and light pixels. A simple experiment to demonstrate the efficacy of the Oval Profile plugin is to perform the operation on a test system of known, well aligned lines.

Three images were created with a black background (the gray value of black is 0): vertical white lines, horizontal white lines, and a cross hatch of vertical and horizontal white lines (Figures 47, 48, 49 and 50). The vertical lines are known to run straight

from 0 to 180 degrees at a regular interval. The horizontal lines are known to run straight from 90 to 270 degrees at a regular interval. The cross hatch image is a combination of the vertical and horizontal lines. From each image, three square sections of 252 by 252 pixels were selected randomly. On each square section, a fast Fourier transform (FFT) was performed and a central circular selection was made on the FFT. The circular selection radius was set at 50 pixels. The Oval Profile plots performed on each of the three selections of the images were averaged to compute the high and low differences. Results are summed up in Table 4. The vertical and horizontal line images show a high value angle that is roughly in accordance with the angle of the line orientation and a low value angle that is roughly ninety degrees offset from the high value angle. This is reiterated in the graphic data generated by the plugin (Figures 51, 52, 53 and 54). The vertical image graph shows peaks at the 0 and 180 angles and a minima at 90 degrees while the horizontal image graph shows a peak about 90 degrees and minima at 0 and 180 degrees(Figures 51 and 52). This is to be expected as the images are a 90 degree rotation of one another. The cross hatched image graph shows peaks at 0, 90, and 180 degrees and minima at angles of about 45 and 135 degrees (Figure 53). Again, this is not surprising as the lines are strongly correlated to a vertical and horizontal alignment. The graph of the random image shows many peaks related to several different lines that were randomly drawn on the black background (Figure 54).

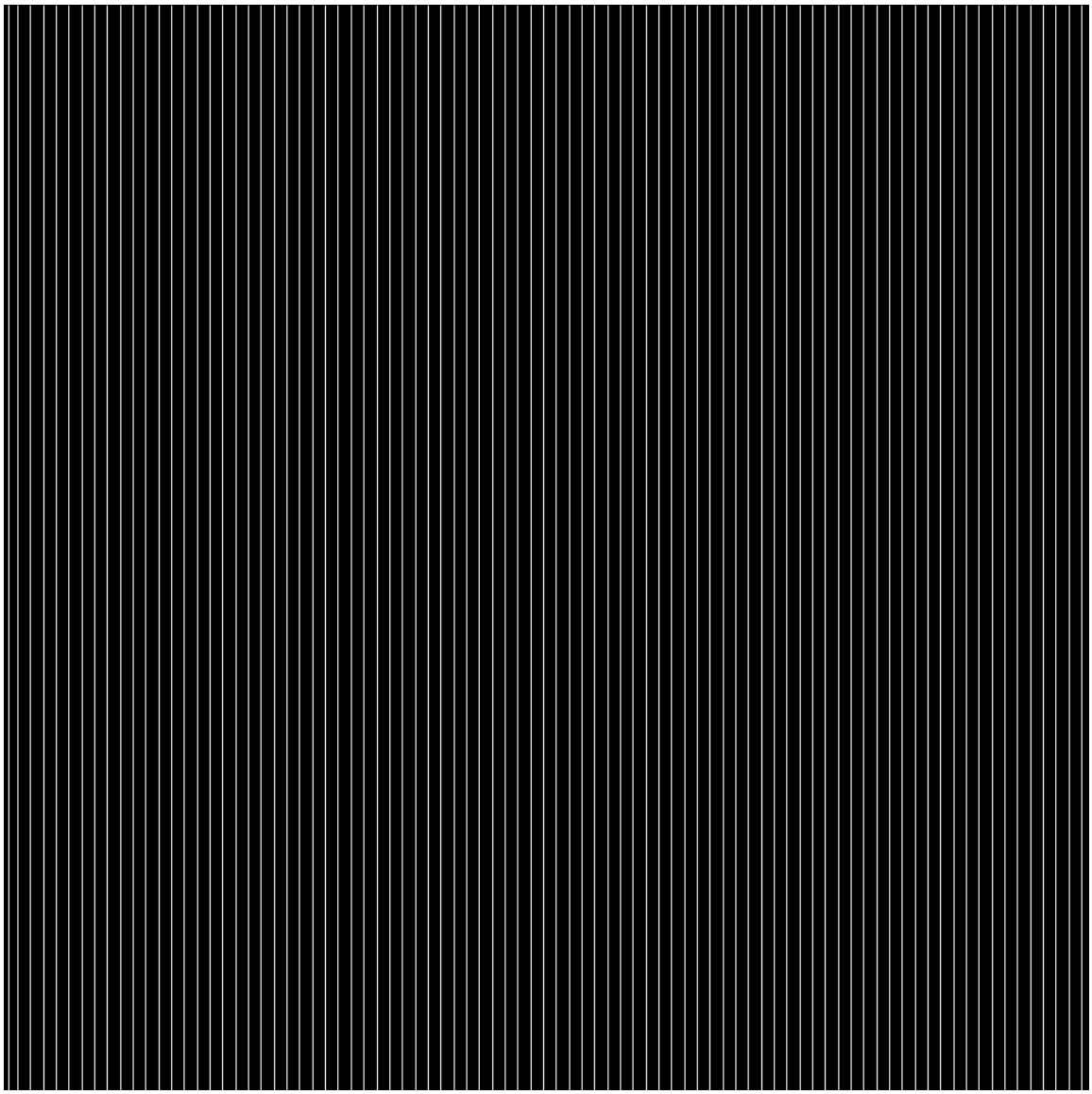

Figure 47. Vertical Lines. To test the efficacy of the Oval Profile plugin, test patterns were created. This is Test Pattern A; a vertical test pattern.

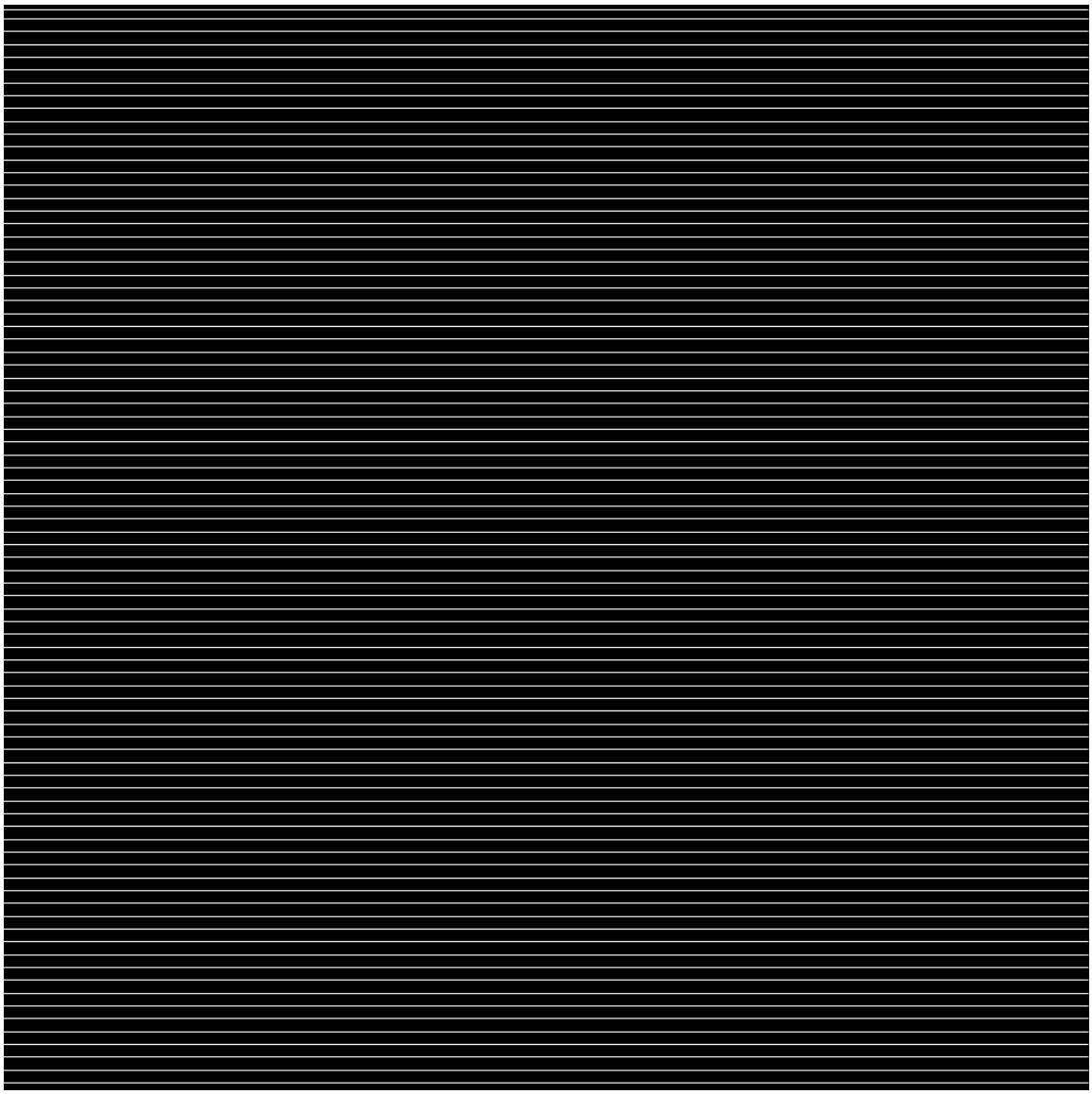

Figure 48. Horizontal Lines. To test the efficacy of the Oval Profile plugin, test patterns were created. This is Test Pattern B; a horizontal test pattern.

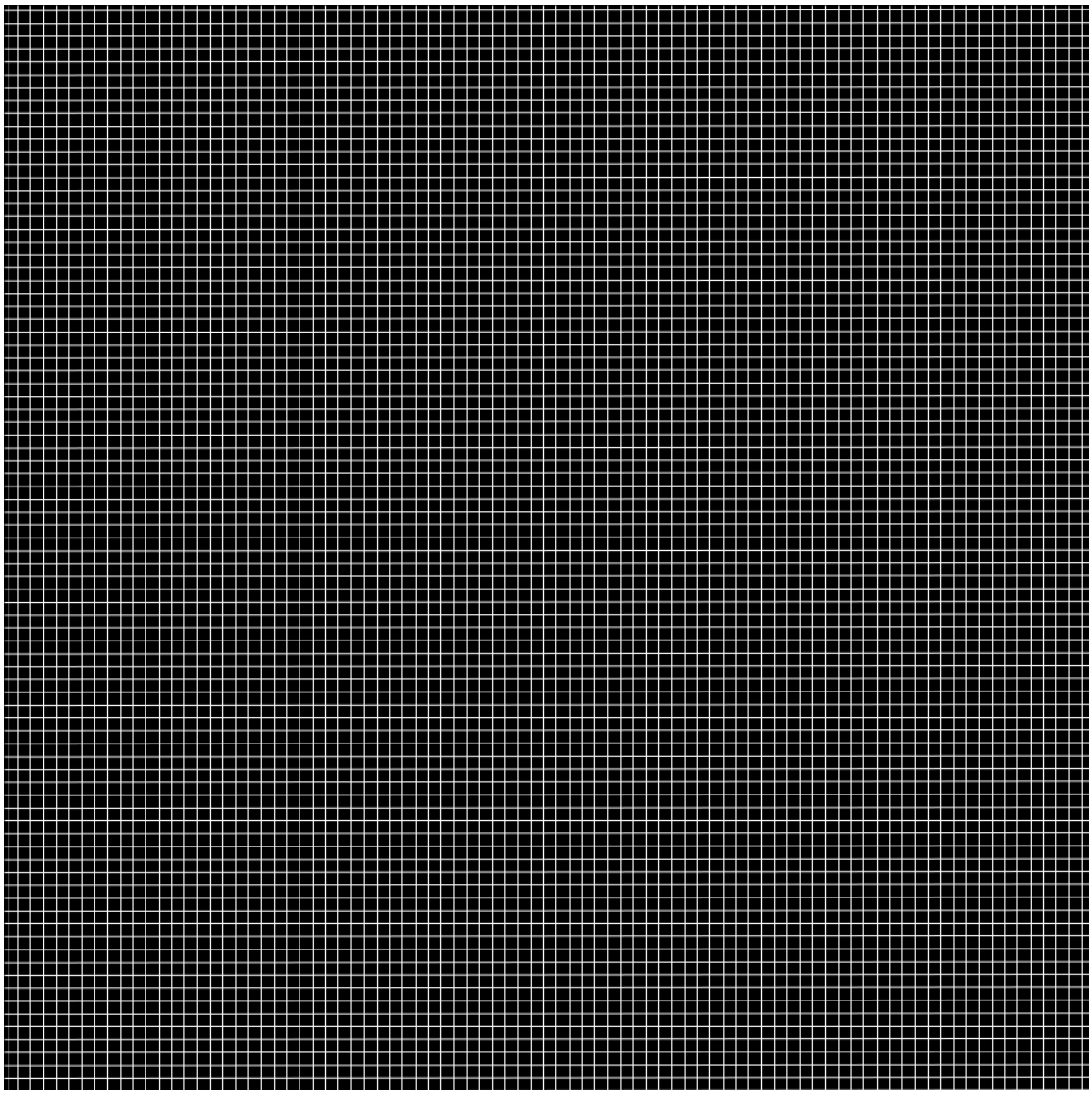

Figure 49. Cross – Hatched Lines. To test the efficacy of the Oval Profile plugin, test patterns were created. This is Test Pattern C; a cross-hatched test pattern and is a combination of Test Patterns A and B.

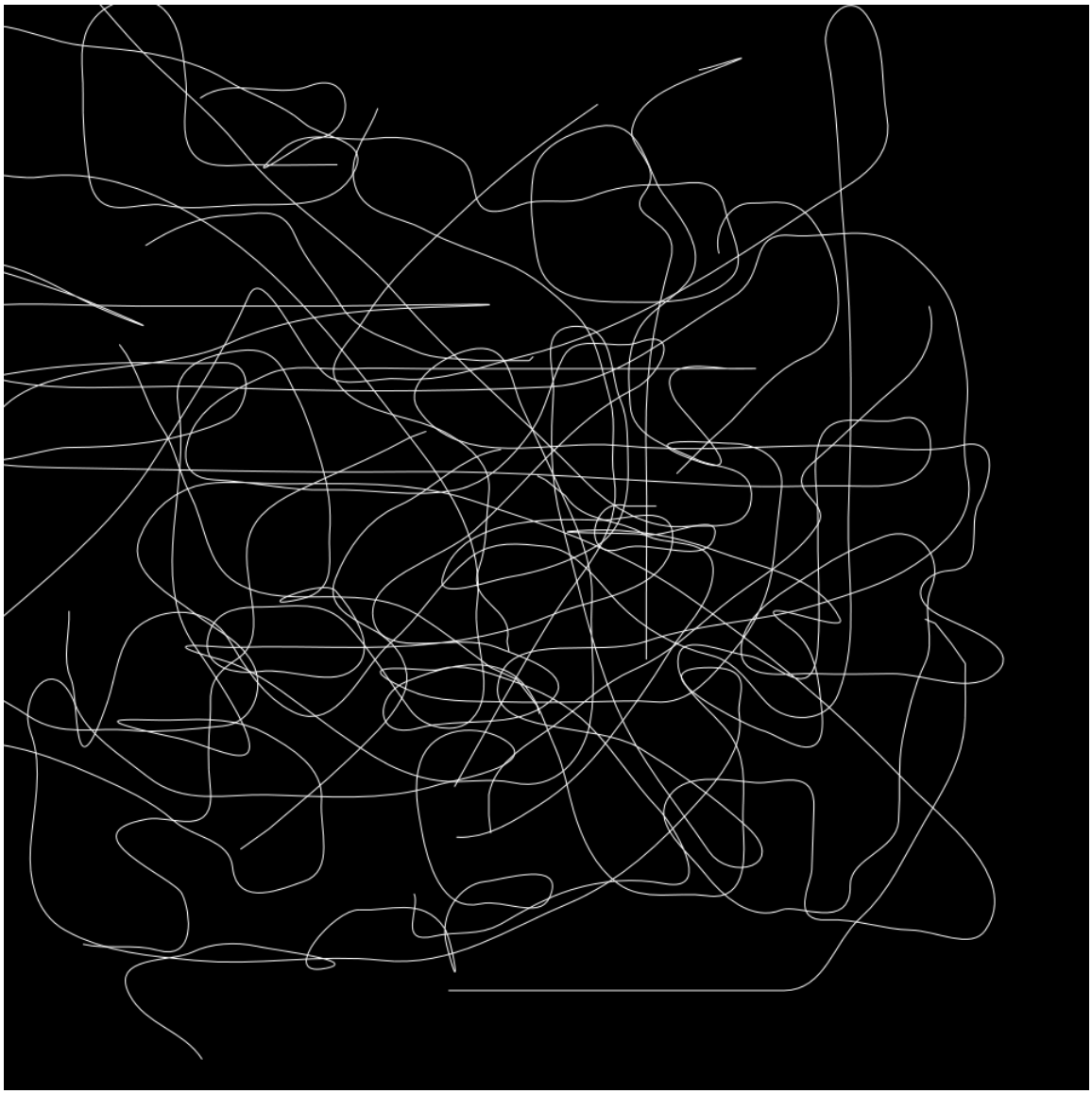

Figure 50. Random Lines. To test the efficacy of the Oval Profile plugin, test patterns were created. This is Test Pattern D; a random test pattern.

Table 4. Image Processing of Test Images. The outcome of the implementation of the Oval Profile plugin as applied to the images of contrived lines. In this set of images, the zero/360 degree angle is at 12 o'clock. The High Angle is the angle associated with greater gray value and the Low Angle is the angle associated with least gray value. High Angle is abbreviated as HA and Low Angle is abbreviated as LA.

	High Angle	**HA Value**	**HA Std-Dev**	**Low Angle**	**LA Value**	**LA Std-Dev**	**Difference**
Vertical	180.0	5184.0	25.8	82.0	4150.2	33.5	1033.8
Horizontal	93.0	5155.2	105.7	8.0	4318.2	169.1	837.0
Cross – Hatch	92.0	3761.9	200.9	45.0	2417.1	394.0	1344.8
Random	269.0	4872.3	116.9	14.0	4110.2	131.8	762.0

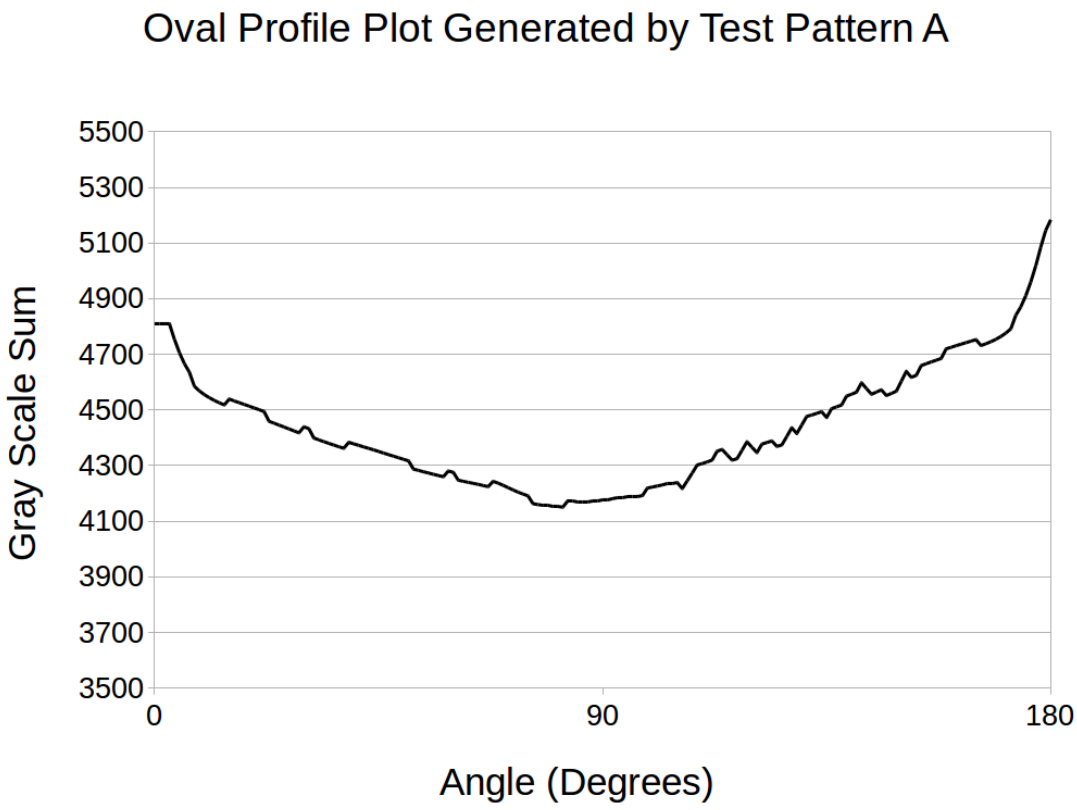

Figure 51. Plot of the Vertical Lines. The Oval Profile plot generated for Test Pattern A shows a maximum at zero and 180 degrees. The line orientation for Test Pattern A has been experimentally set up such that the lines are oriented in the zero – 180 degree direction. Line width is 1 pixel and line separation is 11 pixels.

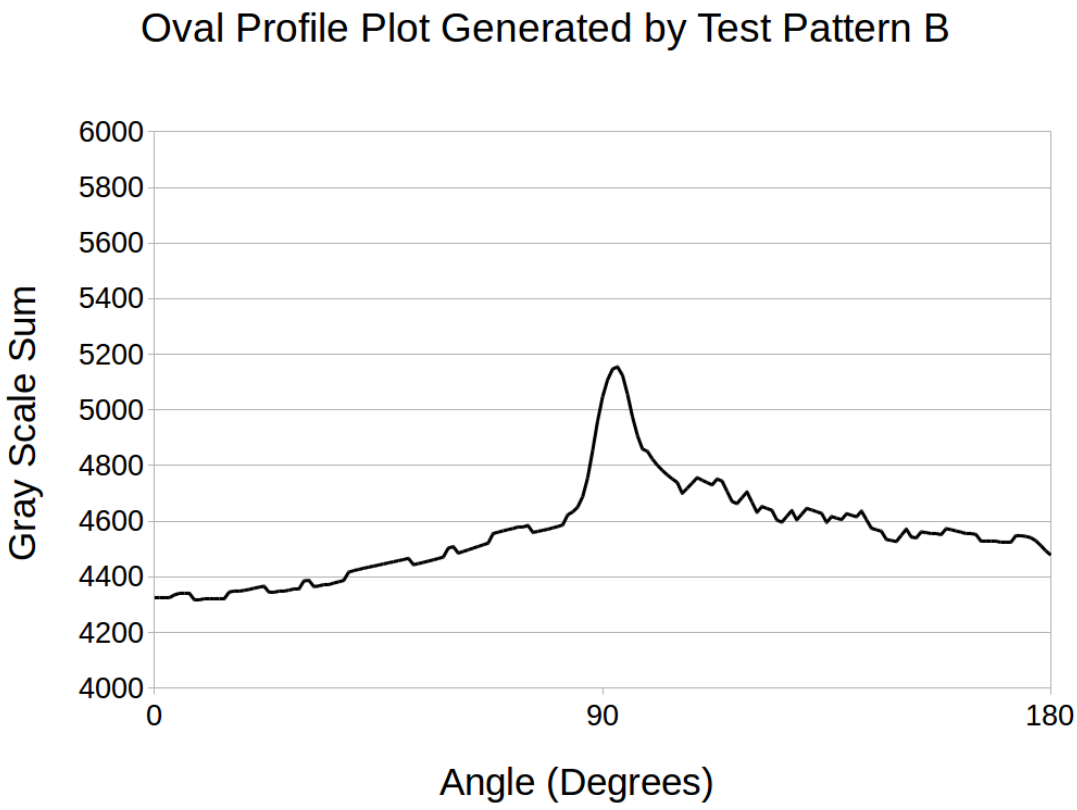

Figure 52. Plot of the Horizontal Lines. The Oval Profile plot generated for Test Pattern B shows a maximum at 90 degrees. The line orientation for Test Pattern A has been experimentally set up such that the lines are oriented in the 90 – 270 degree direction. Line width is 1 pixel and line separation is 11 pixels.

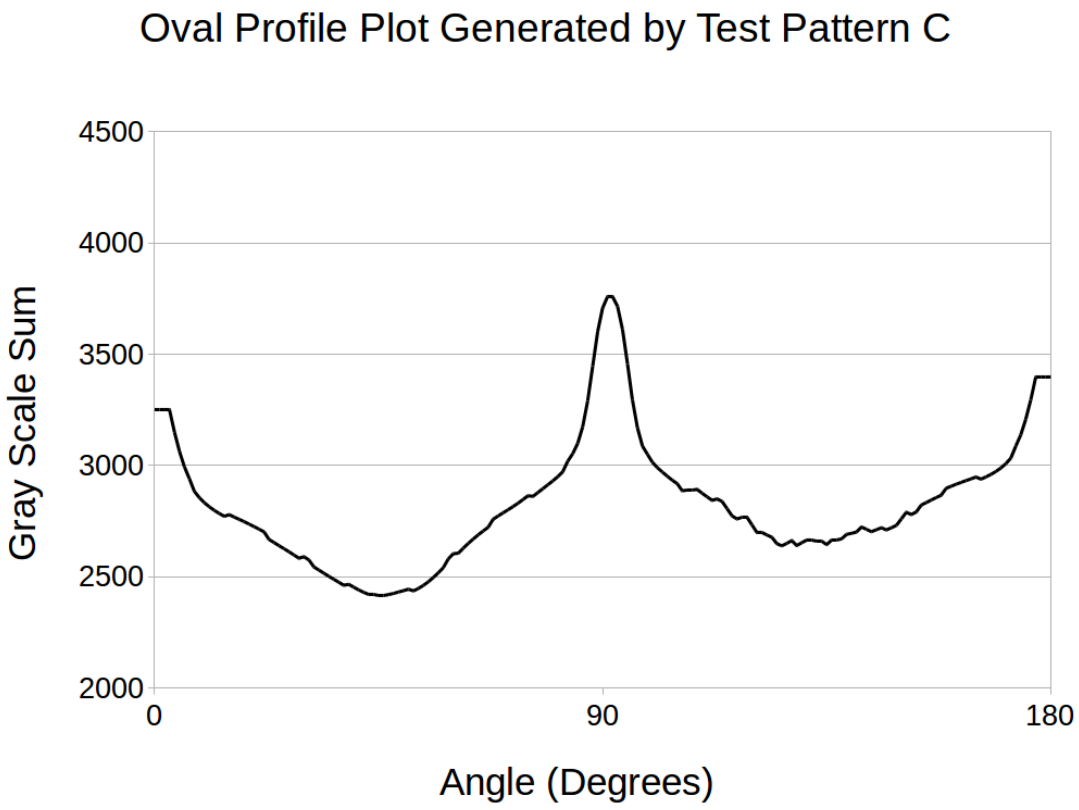

Figure 53. Plot of the Cross – Hatched Lines. The Oval Profile plot of Test Pattern C shows peaks at zero, 90, and 180 degrees. The cross-hatched test pattern is a combination of Test Patterns A and B. Line width is 1 pixel and line separation is 11 pixels.

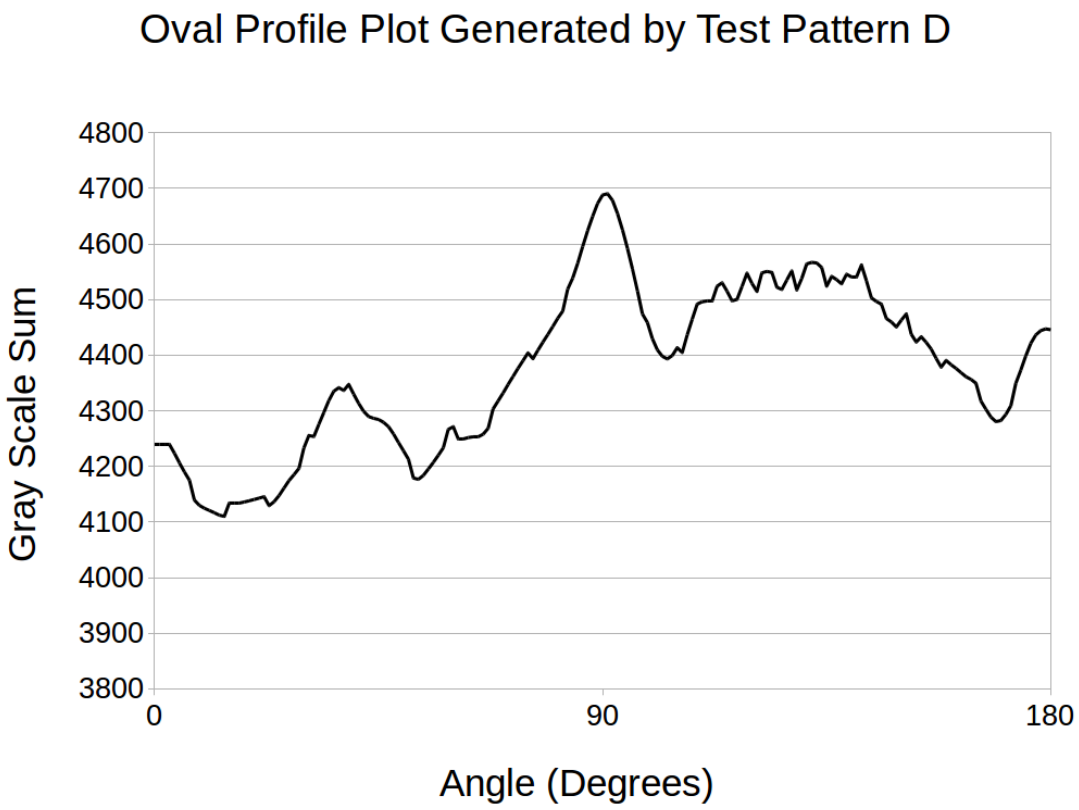

Figure 54. Plot of the Random Lines. The Oval Profile Plot of Test Pattern D shows a random assemblage of peaks, corresponding to the random nature of Test Pattern D. Line width is 1 pixel.

6.4 Chitin Gels

Once the chitin has been purified to an acceptable degree, it may be utilized in the formation of Chitin Gels (CG's). Chitin is rather insoluble in most solvents. The acetylGlucosamine repeat units are bound together with a covalently bound 1 – 4 glycosidic bond, the breaking of which would change the fundamental nature of the molecule. The N-acetylGlucosamine chains are hydrogen bound together to form fibers. This hydrogen bonding can be broken to render individual chains. Hexafluoro-2-propanol (HFIP), $(CF_3)_2CHOH$, is a highly polar solvent used as a means of breaking the hydrogen bonds. HFIP is miscible in water, which is important in the formation and processing of Chitin Gels.

Chitin can be easily dissolved in HFIP in concentrations up to 10 mg/mL, via sonication, with little effort. Once the chitin has been fully dissolved, the solution should appear optically clear.

The addition of even the smallest amounts of water initiates the gelation process. Gelation has been observed with the introduction of 10% water by volume. The process is a sol-gel system where the chitin/HFIP solution (sol) is driven to a gel state by the extraction of HFIP to the water. As HFIP is extracted from the chitin system, entanglement is encouraged through the insolubility of chitin in water. Successive washings of the gel in water remove remaining HFIP. The HFIP may be further removed by heating the gels in an oven to thermally drive off the solvent. Place the gel in a closed vessel filled with water. Bring the water/gel system to equilibrium at a temperature of 50 – 60°C, which is about the boiling temperature of HFIP at 58.2°C. The gel can be created in forms to control shape and macro scale morphology, cast into films and membranes, or dried to create chitin aerogels.

The formation of a membrane is simply an extension of the formation of the basic gel. The membrane can be formed "free standing" or contained within a mold. Free standing membranes are formed by the deposition of the chitin/HFIP sol onto a glass cover slip placed inside a petri dish, a volume of 100μL has been found to yield a membrane approximately 15mm in diameter. Once the sol has stabilized on the glass, carefully pipette water around the periphery of the sol. This immediately gels the edge and prevents the sol from splattering or otherwise deforming. Once the edge has gelled, slowly fill the petri dish with water. This will gel the remaining sol. Allow the membrane to equilibrate solvents, then remove and exchange the water for fresh water. Wash the membrane multiple times to remove as much HFIP as possible. The membranes may also be formed in a mold with little deviation from this procedure. The membranes are mechanically stable but may be backed with a mesh grid to improve mechanical performance.

6.5 Extruded Chitin Forms

The Chitin Gelatinous Blob (CGB) is an extruded form of a Chitin Gel, demonstrating a higher degree of organization. As the chitin/HFIP complex is a thixotropic non-Newtonian fluid, the introduction of shear thinning changes the viscosity. This shear thinning is imparted by the act of extruding the solution, under water, from a pipette tip. The shear thinning is caused by shear stresses that arise from the fluid flowing through the orifice at the pipette tip. As a fluid flows over a surface, there is an interaction zone in which the motion of the fluid is slowed from the velocity of

the main body of the fluid, u(y), to zero, at the surface interface. This shear stress is denoted as:

$$\tau(y) = \mu \frac{\partial u}{\partial y} \tag{6.1}$$

Where u is the initial velocity above the interaction zone and μ is the viscosity of the fluid. This equation is a first approximation, as the viscosity of a non-Newtonian fluid is dynamic; as long as pressure on the pipette and temperature are kept uniform, this approximation is valid.

By modification of the conditions of formation of the CGB, filamentous fibers can be formed. The formation of Chitin Gelatinous Fibers (CGF) is achieved through the increasing of the shear stress to allow for more alignment through shear thinning. This is achieved by decreasing the nozzle size of the extruder and increasing the pressure. The extruder used in the case of the CGB is a 200μL pipette tip. The nozzle size is decreased by extruding from a tuberculin needle. The extrusion event is a swift and steady single push of the plunger.

The extrusion of CG's has been performed under various conditions pertaining to the liquid into which the CG's are being extruded. The CGF's have been extruded into water, ethanol, isopropanol, and acetone. The CGF's extruded into acetone produced the longest, most continuous fibers. CGF's extruded in water, ethanol, and propanol produce shorter, less continuous fibers.

Chitin fiber alignment can be quantified through the use of polarization microscopy and image processing software, such as ImageJ.

A standard method of determining the qualitative degree of constituent polymer alignment in an extruded fiber is by the use of birefringence, as detailed in the American Association of Textile Colorists and Chemists (AATCC) Technical Manual, Standard Method 20-2007 and elsewhere [16, 63]. Briefly, a fiber is analyzed under a polarizing microscope at multiple angles of orientation of the sample fiber to the polarizer. At 0, 45, and 90 degree intervals, the fiber is imaged with the analyzer both at zero degrees and ninety degrees to the polarizer. This effectively shows a bright field and a dark field image of the fiber at forty-five degree intervals. If the fiber appears bright in the dark field image, birefringence is indicated, indicating an alignment in the constituent polymer.

I mounted CGF's on microscope slides for analysis with the polarizing microscope. Analysis was conducted in the manner of AATCC Standard Method 20-2007 and also as a study of intensity versus angle with only the polarizer, leaving the analyzer set to zero.

In the case of AATCC SM 20-2007, birefringence was indicated (Figure 55). The observation of birefringence of the CGF lends strong support to the idea of shear alignment of the chitin polymers through extrusion. Otherwise, rotating the sample through 360 degrees and taking an image every ten degrees shows the change in intensity of the transmitted light as the angle is changed (Figures 56 and 57).

Image processing via ImageJ and the Oval Profile plugin shows a strong correlation between the directionality of the chitin polymer and the long axis of the fiber (Figure 58). Five areas of 300 square pixels were randomly selected on the image to be processed for chitin alignment. The results were averaged to find the average angle of fiber alignment; the tabulated results for the five areas are shown in Table 5.

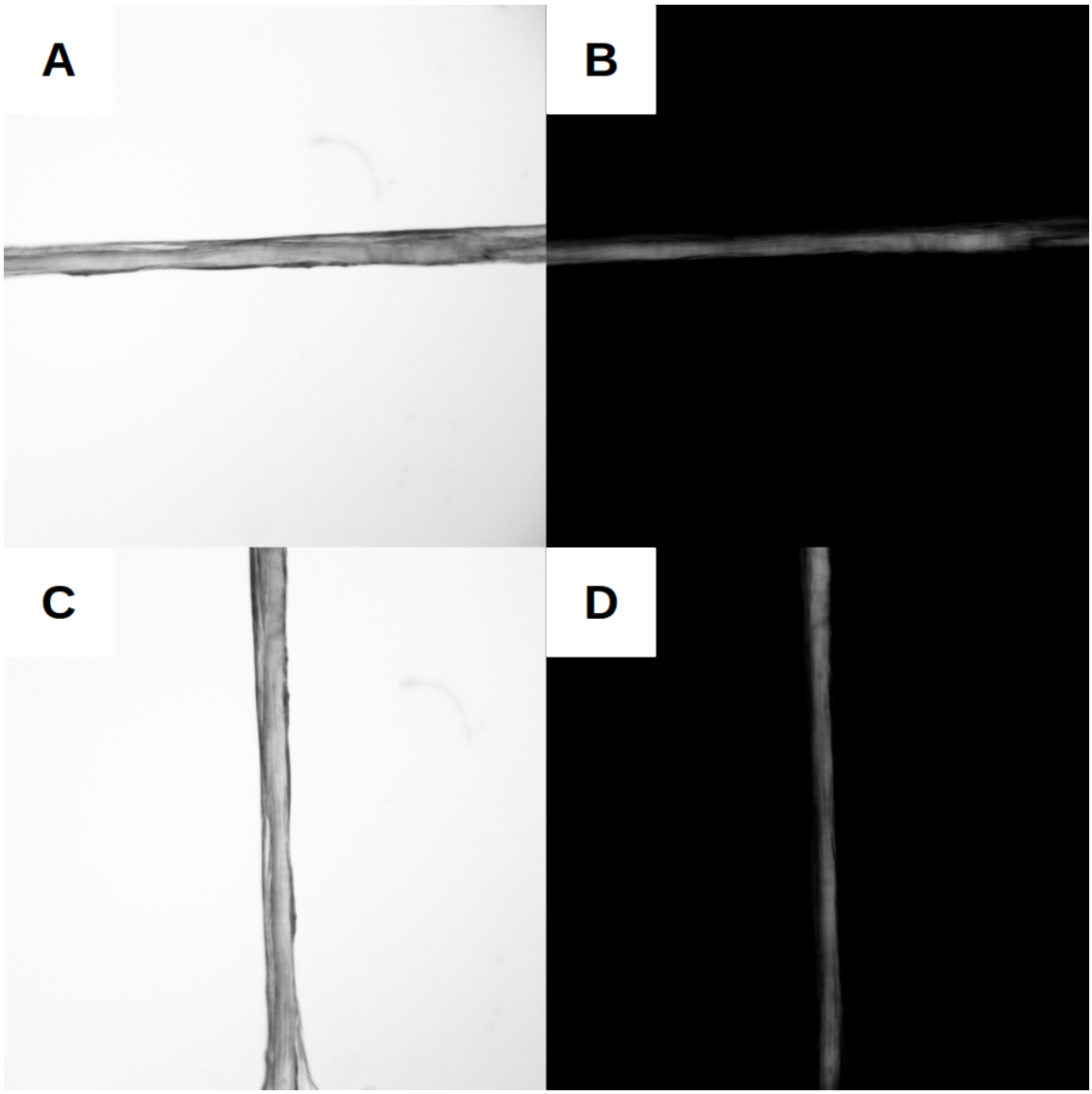

Figure 55. Birefringence of Gelled Chitin Fibers. Images of the chitin gelatinous fiber as taken by the polarizing microscope. A shows the horizontal image of the fiber in bright field. B shows the same fiber with the polarizers crossed to render a dark field. Note the fiber shows as bright on the dark field, indicating birefringence. C is the same fiber rotated 90 degrees in bright field. D shows the fiber, again, in the dark field and with crossed polarizers. Approximate fiber diameter is 200μm.

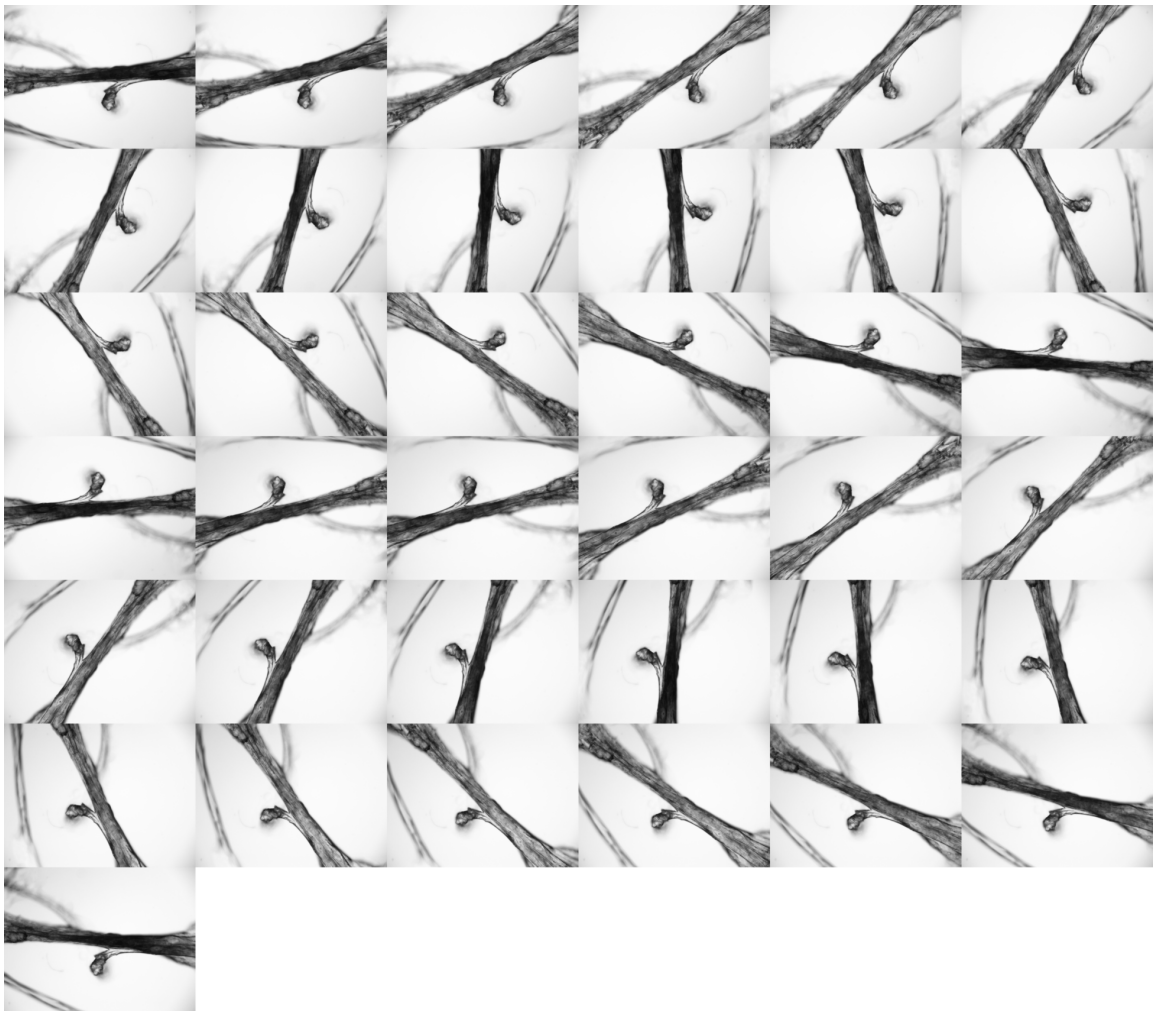

Figure 56. Montage of Chitin Gellatinous Fiber Rotations. A series of images showing the a chitin gelatinous fiber rotated through 360 degrees. An image was captured every ten degrees. The intensity change is visually apparent in this series of images. Approximate fiber diameter is 200μm.

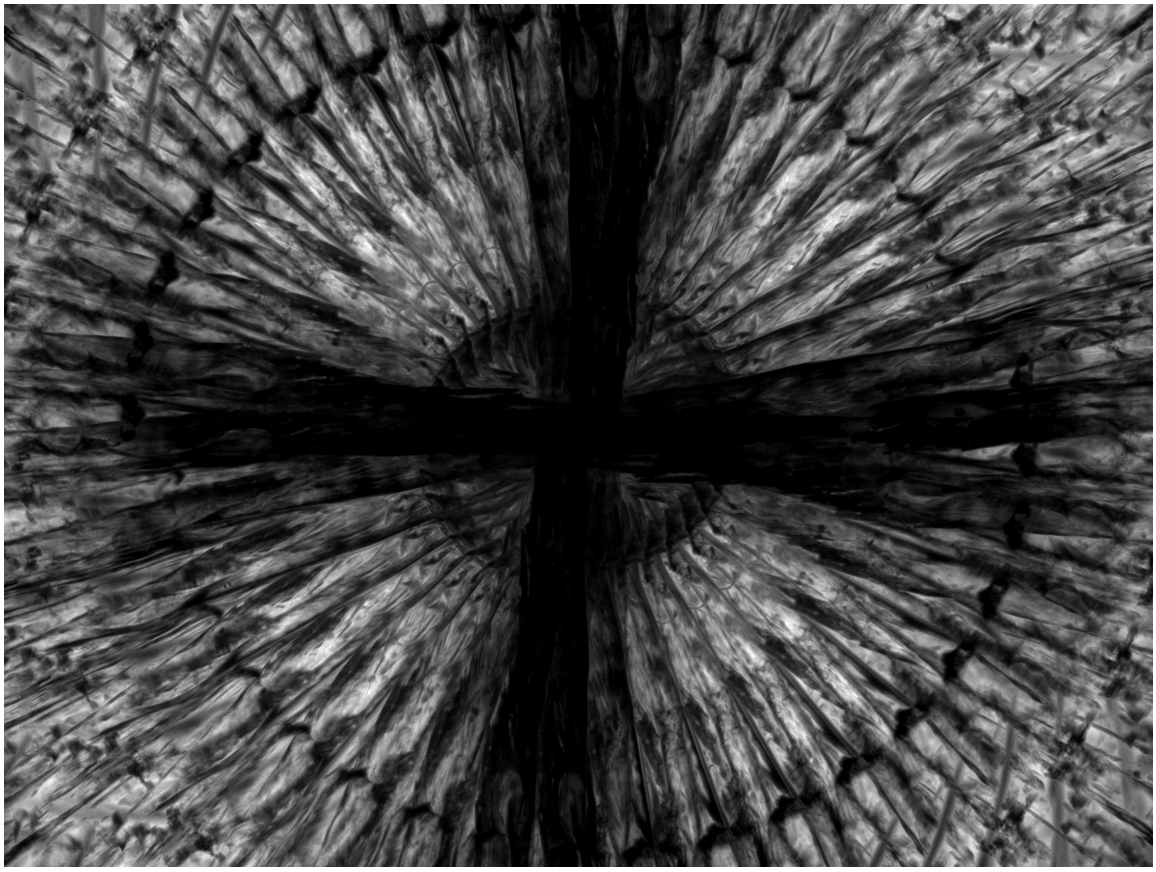

Figure 57. Maltese Cross. This Maltese Cross was created by overlaying all the images from Figure 35 into a single frame. The Maltese Cross pattern is indicative of birefringence in a material.

Table 5. Chitin Fiber Alignment. The tabular data from the Oval Profile plot of the five sections of the chitin gelatinous fiber. The average high angle is in the general direction of the long axis of the fiber.

	High Angle	**Value**
Fiber0	95.00	5972.25
Fiber1	93.00	5874.23
Fiber2	92.00	5855.98
Fiber3	95.00	5975.05
Fiber4	93.00	5725.17
Average	93.60	5880.54
Std Dev	1.34	102.63

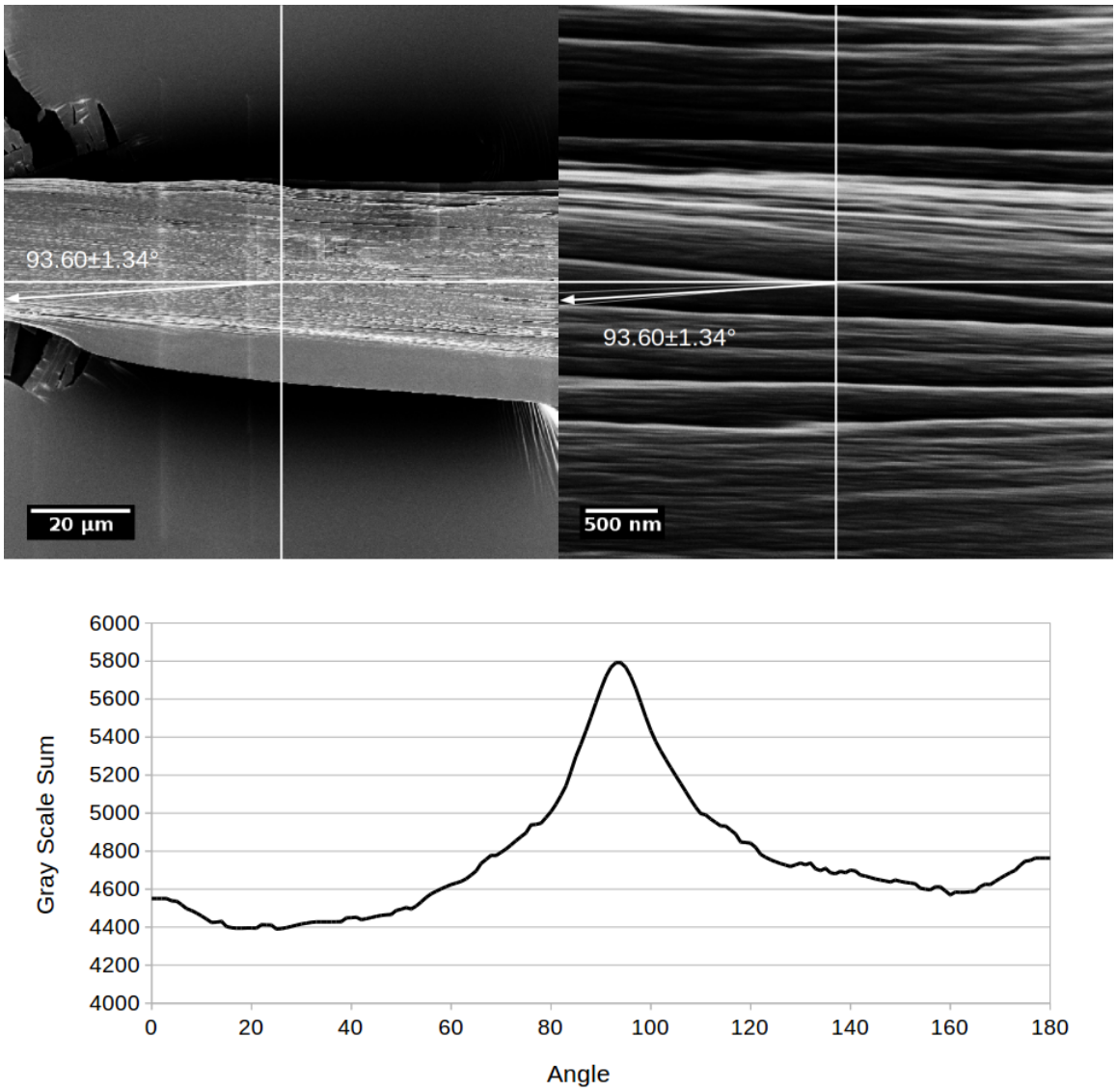

Figure 58. Extruded Chitin Gels. The top images are low and high resolution images of an extruded chitin gelatinous fiber. Note the aligned ridges oriented in the direction of the long axis of the fiber. The graph shows the Oval Profile plot of the alignment along the long axis of the fiber. In these images the zero/360 degree angle is in the 12 o'clock position.

6.6 Discussion

The manner of chitin gel formation is much simpler and less cumbersome than methods previously reported. This methods starts with chitin and ends with a chitin gel rather than starting with a chitin derivative, such as chitosan, gelling it and acetylating it to create a chitin gel. The HFIP solvent is easily removed through a simple bake-off process, leaving a clean, stable chitin hydrogel. These chitin gels and associated formations can be used for a manner of applications. Currently, in parallel within the lab, research is being conducted to use them as a means of nanoparticle separation and cell scaffolding.

These gels were then modified by introducing an extrusion event to produce fibrous gels. I was able to extrude the CGF's under acetone to create continuous fibers of several centimeters in length. Fibers extruded under other solvent conditions proved to be shorter and more broken up. This phenomenon can be attributed to the solvent interactions between the HFIP and the the solvent into which the fiber was extruded. The more rapidly the HFIP solvent is extracted from the fiber, the less chance it has of breakage resulting in a longer, more continuous fiber. A slow solvent extraction will allow for more breaks of the fiber do to instability in the gel matrix. This characteristic can be exploited to tailor the length of fibers for specific uses. Long continuous fibers tend to form into mats whereas shorter fibers can be more easily separated for individual use.

The key feature of the extruded fiber is the shear alignment induced by the extrusion event. As the fiber is pushed from the die head, the friction associated with the walls sets up an interaction zone. The fluid just at the fluid wall interface has a velocity of zero while the fluid moving in the center of the flow is moving with a fixed

velocity out of the syringe. At some distance above the wall, the velocity starts to decrease as a function of distance to the wall. This area of decreasing velocity defines the interaction zone (Figure 59). Within the interaction zone there is felt upon the liquid a shear stress which is defined radially as:

$$\tau(r) = \mu \frac{\partial u}{\partial r} \tag{6.2}$$

Where $\tau(r)$ is the radially dependent shear stress, μ is the viscosity of the fluid, and u is the velocity of the fluid. The shear felt in the interaction zone causes alignment of individual chitin fibers in the direction of extrusion.

The alignment of the chitin fibers is demonstrated with the use of a polarizing microscope by examining the fiber between two crossed polarizers. The birefringent fiber appears bright on a dark field. The birefringence is an indication of the anisotropic nature of the material causing a disparity between the indices of refraction. The anisotropy being attributed to the linear organization of the chitin fibers. A randomly oriented melange of fibers would produce a uniform index of refraction, bearing no dependence upon directionality.

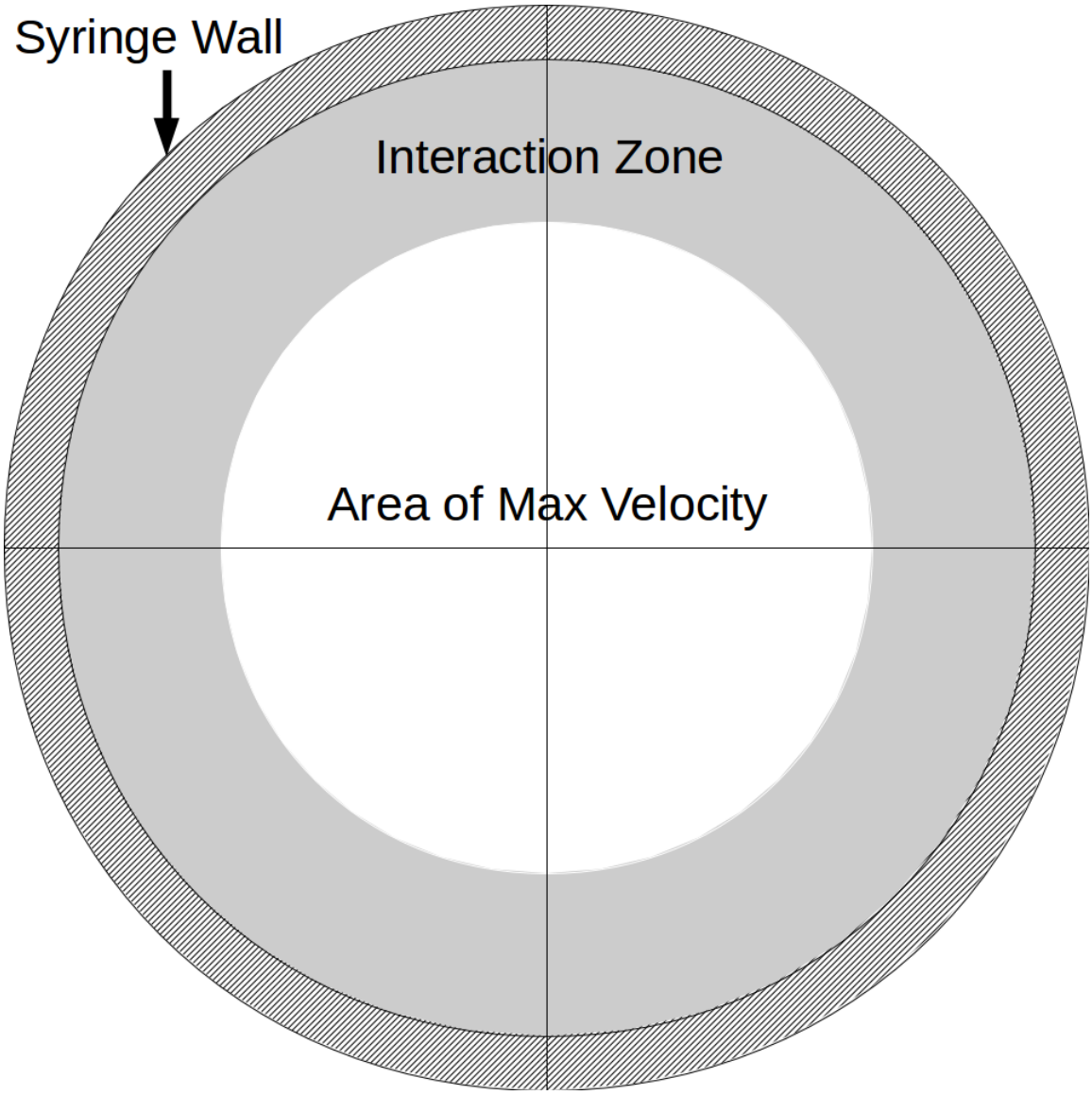

Figure 59. A Cross–Sectional Diagram of the Syringe Barrel. The barrel is the cross hatched area. The interaction zone is shown in gray and the central, white area is the area of maximum velocity of the fluid.

CHAPTER VII

CONCLUSIONS

I have demonstrated a new method for the study of chitin organization in situ. The Rakki Prep method of chitin preparation removes the extra-cellular matrix that binds and completes the composite of the cuticle. This allows for the study and quantification of the organization of cuticular structures through electron microscopy and image processing with ImageJ. The Oval Profile plugin has been shown to have the ability to quantify the alignment of fibers through the summing of gray scale at equal intervals about an oval selection. This technique was applied to the Rakki Prepped structures of the cicada to show that the alignment of chitin is different and variable depending upon the utilization of the structure.

The wing membranes of cicadas are a dynamic system with interesting optical properties. Light transmitted through the membrane is plane polarized. This polarization can be quantified using polarimetry and correlated to Malus' Law. Not only do the wings polarize light, the angle of polarization is not constant across the membrane. Polarized light is an integral part of the natural world. It has utility in the attraction of mates, navigation, and predator/prey relationships. Arthropods and other forms of life have the inherent ability to "see" polarized light. In a predator/prey scenario, it would be beneficial to minimize the amount of polarized light emanating from a large area structures, such as wings, in an attempt to help hide from predation. The polarization of the wing stems from the cuticle as a composite

material. It is due to the dichroism of the chitin and the extracellular matrix that the polarization occurs.

I have demonstrated an efficient method for the creation of chitin gels. Chitin gel systems are potentially valuable for use in cell scaffolding, tissue engineering, nanoparticle separation, and other applications. This method produces a mechanically sound and stable hydrogel that is easily stored for long periods of time. The gel is an optimal starting point for the artificial alignment and organization of chitin nanofibers. Gelatinous fibers were successfully extruded to reveal alignment of the chitin in the long axis of the fiber. The fiber alignment can be quantified via ImageJ processing using the Oval Profile plugin. The gelatinous fibers are birefringent, which arises from anisotropy in the index of refraction. This anisotropy is derived from the alignment of the chitin along the long axis of the gel fiber. Birefringence is a common method of showing polymer alignment in drawn fibers in the textile industry. The fibers show birefringence in accordance with AATCC Standard Method 20-2007.

The alignment of polymer nanofibers, in general, is an important step in the development of new materials to take human – kind into the future. The current methodology of polymer production and processing is costly in both materials and energy. The ability to process naturally occurring materials in a manner that is driven by self assembly is a valuable goal that deals with both the problems of solid waste and runaway energy consumption.

Solid plastic waste is an issue of major importance. The polymers that are the current state of the art do not readily degrade and are going to be with us for millions of years. It is for this reason that it is imperative to focus on renewable and biodegradable polymers such as chitin.

The self assembly of composite materials is the future of scientific and engineering endeavor. Spirited creativity and imagination are the requirements to drive houses and buildings that can erect themselves, machinery that can repair damaged parts automatically, and many other dreams that can be realized in a future of self assembled biopolymers.

REFERENCES

[1] Lydia Adour, Wassila Arbia, Abdeltif Amrane, and Nabil Mameri. Combined use of waste materialsâĂŤrecovery of chitin from shrimp shells by lactic acid fermentation supplemented with date juice waste or glucose. *Journal of chemical technology and biotechnology*, 83(12):1664–1669, 2008.

[2] Svend Olav Andersen and Torkel Weis-Fogh. Resilin. a rubberlike protein in arthropod cuticle. *Advances in insect physiology*, 2:1–65, 1964.

[3] Yasuyuki Arakane, Subbaratnam Muthukrishnan, Richard W Beeman, Michael R Kanost, and Karl J Kramer. Laccase 2 is the phenoloxidase gene required for beetle cuticle tanning. *Proceedings of the National Academy of Sciences of the United States of America*, 102(32):11337–11342, 2005.

[4] Chantal E Ayres, B Shekhar Jha, Hannah Meredith, James R Bowman, Gary L Bowlin, Scott C Henderson, and David G Simpson. Measuring fiber alignment in electrospun scaffolds: a user's guide to the 2d fast fourier transform approach. *Journal of Biomaterials Science, Polymer Edition*, 19(5):603–621, 2008.

[5] Emmanuel Belamie, Gervaise Mosser, Frédéric Gobeaux, and Marie-Madeleine Giraud-Guille. Possible transient liquid crystal phase during the laying out of connective tissues: α-chitin and collagen as models. *Journal of Physics: Condensed Matter*, 18(13):S115, 2006.

[6] Harold J Blumenthal and Saul Roseman. Quantitative estimation of chitin in fungi. *Journal of bacteriology*, 74(2):222, 1957.

[7] Michael J Bok, Megan L Porter, Allen R Place, and Thomas W Cronin. Biological sunscreens tune polychromatic ultraviolet vision in mantis shrimp. *Current Biology*, 24(14):1636–1642, 2014.

[8] Tamás Börzsönyi, Balázs Szabó, Gábor Törös, Sandra Wegner, János Török, Ellák Somfai, Tomasz Bien, and Ralf Stannarius. Orientational order and alignment of elongated particles induced by shear. *Physical review letters*, 108(22):228302, 2012.

[9] Y Bouligand. Twisted fibrous arrangements in biological materials and cholesteric mesophases. *Tissue and Cell*, 4(2):189–217, 1972.

[10] D Byrom. Polymer synthesis by microorganisms: technology and economics. *Trends in Biotechnology*, 5(9):246–250, 1987.

[11] Cristian Campos-Fernández, Daniel E Azofeifa, Marcela Hernández-Jiménez, Adams Ruiz-Ruiz, and William E Vargas. Visible light reflection spectra from cuticle layered materials. *Optical Materials Express*, 1(1):85–100, 2011.

[12] Diego Carlström. The crystal structure of α-chitin (poly-n-acetyl-d-glucosamine). *The Journal of biophysical and biochemical cytology*, 3(5):669–683, 1957.

[13] Krishan K Chawla. *Composite materials: science and engineering*. Springer, 2012.

[14] Po-Yu Chen, Albert Yu-Min Lin, Joanna McKittrick, and Marc André Meyers. Structure and mechanical properties of crab exoskeletons. *Acta biomaterialia*, 4(3):587–596, 2008.

[15] Daniel J Cosgrove. Growth of the plant cell wall. *Nature reviews molecular cell biology*, 6(11):850–861, 2005.

[16] Roger K Curtis and DONR TYSON. Human hair analysis. *J. Soc. Cosmet. Chem*, 27:411–431, 1976.

[17] Gregory D Edgecombe and David A Legg. Origins and early evolution of arthropods. *Palaeontology*, 57(3):457–468, 2014.

[18] Basil el Jundi, Keram Pfeiffer, Stanley Heinze, and Uwe Homberg. Integration of polarization and chromatic cues in the insect sky compass. *Journal of Comparative Physiology A*, 200(6):575–589, 2014.

[19] Michael Forsyth. *Materials and skills for historic building conservation*. John Wiley & Sons, 2008.

[20] James J Foster, Camilla R Sharkey, Alicia VA Gaworska, Nicholas W Roberts, Heather M Whitney, and Julian C Partridge. Bumblebees learn polarization patterns. *Current Biology*, pages 1450–20, 2014.

[21] Walter Friedrich, Paul Knipping, and Max Laue. Interferenzerscheinungen bei röntgenstrahlen. *Annalen der Physik*, 346(10):971–988, 1913.

[22] M-M Giraud-Guille. Fine structure of the chitin-protein system in the crab cuticle. *Tissue and Cell*, 16(1):75–92, 1984.

[23] Omacanda Hāndā. *Temple architecture of the western himalaya: Wooden temples*. Indus Publishing, 2001.

[24] Richard A Holland, Ivailo Borissov, and Björn M Siemers. A nocturnal mammal, the greater mouse-eared bat, calibrates a magnetic compass by the sun. *Proceedings of the National Academy of Sciences*, 107(15):6941–6945, 2010.

[25] Ian R Hooper, Peter Vukusic, and RJ Wootton. Detailed optical study of the transparent wing membranes of the dragonfly aeshna cyanea. *Optics express*, 14(11):4891–4897, 2006.

[26] Theodore L Hopkins and Karl J Kramer. Insect cuticle sclerotization. *Annual review of entomology*, 37(1):273–302, 1992.

[27] F Hoppe-Seyler. Ueber chitin und cellulose. *Berichte der deutschen chemischen Gesellschaft*, 27(3):3329–3331, 1894.

[28] M Iguchi, S Yamanaka, and A Budhiono. Bacterial celluloseâĂŤa masterpiece of nature's arts. *Journal of Materials Science*, 35(2):261–270, 2000.

[29] Eugene A Irene. *Electronic materials science*. John Wiley & Sons, 2005.

[30] James Irvine. A polarimetric method of identifying chitin. *Journal of the Chemical Society, Transactions*, 95:564–570, 1909.

[31] Jungho Jin, Valerie Reese, Rhea Coler, Darrick Carter, and Marco Rolandi. Chitin microneedles for an easy-to-use tuberculosis skin test. *Advanced healthcare materials*, 3(3):349–353, 2014.

[32] WJ Jung, GH Jo, JH Kuk, YJ Kim, KT Oh, and RD Park. Production of chitin from red crab shell waste by successive fermentation with lactobacillus paracasei kctc-3074 and serratia marcescens fs-3. *Carbohydrate Polymers*, 68(4):746–750, 2007.

[33] WJ Jung, JH Kuk, KY Kim, and RD Park. Demineralization of red crab shell waste by lactic acid fermentation. *Applied microbiology and biotechnology*, 67(6):851–854, 2005.

[34] Eric Kamst, Jens Pilling, Leonie M Raamsdonk, BJ Lugtenberg, and Herman P Spaink. Rhizobium nodulation protein nodc is an important determinant of chitin oligosaccharide chain length in nod factor biosynthesis. *Journal of bacteriology*, 179(7):2103–2108, 1997.

[35] Michiyo Kinoshita and Kentaro Arikawa. Color and polarization vision in foraging papilio. *Journal of Comparative Physiology A*, pages 1–14, 2014.

[36] Jolanta Kumirska, Małgorzata Czerwicka, Zbigniew Kaczyński, Anna Bychowska, Krzysztof Brzozowski, Jorg Thöming, and Piotr Stepnowski. Application of spectroscopic methods for structural analysis of chitin and chitosan. *Marine drugs*, 8(5):1567–1636, 2010.

[37] MR Mackley. Polymer processing: the physics of stretching chains. *Physics in Technology*, 9(1):13, 1978.

[38] Kurt H Meyer and Georg W Pankow. Sur la constitution et la structure de la chitine. *Helvetica Chimica Acta*, 18(1):589–598, 1935.

[39] Graham K Moore and George AF Roberts. Chitosan gels: 2. mechanism of gelation. *International Journal of Biological Macromolecules*, 2(2):78–80, 1980.

[40] Jacob LW Morgan, Joanna Strumillo, and Jochen Zimmer. Crystallographic snapshot of cellulose synthesis and membrane translocation. *Nature*, 493(7431):181–186, 2013.

[41] A Moropoulou, A Bakolas, and S Anagnostopoulou. Composite materials in ancient structures. *Cement and concrete composites*, 27(2):295–300, 2005.

[42] Bernard Moussian, Heinz Schwarz, Slawomir Bartoszewski, and Christiane Nüsslein-Volhard. Involvement of chitin in exoskeleton morphogenesis in drosophila melanogaster. *Journal of morphology*, 264(1):117–130, 2005.

[43] SB Murray and AC Neville. The role of ph, temperature and nucleation in the formation of cholesteric liquid crystal spherulites from chitin and chitosan. *International journal of biological macromolecules*, 22(2):137–144, 1998.

[44] Hong Kyoon No and Eun Young Hur. Control of foam formation by antifoam during demineralization of crustacean shell in preparation of chitin. *Journal of Agricultural and Food Chemistry*, 46(9):3844–3846, 1998.

[45] SN Patek and RL Caldwell. Extreme impact and cavitation forces of a biological hammer: strike forces of the peacock mantis shrimp odontodactylus scyllarus. *Journal of Experimental Biology*, 208(19):3655–3664, 2005.

[46] Anastassis Perrakis, Ivo Tews, Zbigniew Dauter, Amos B Oppenheim, Ilan Chet, Keith S Wilson, and Constantin E Vorgias. Crystal structure of a bacterial chitinase at 2.3 å resolution. *Structure*, 2(12):1169–1180, 1994.

[47] W Peters. Occurrence of chitin in mollusca. *Comparative Biochemistry and Physiology Part B: Comparative Biochemistry*, 41(3):541–550, 1972.

[48] CKS Pillai, Willi Paul, and Chandra P Sharma. Chitin and chitosan polymers: Chemistry, solubility and fiber formation. *Progress in Polymer Science*, 34(7):641–678, 2009.

[49] M Rhazi, J Desbrieres, A Tolaimate, A Alagui, and P Vottero. Investigation of different natural sources of chitin: influence of the source and deacetylation process on the physicochemical characteristics of chitosan. *Polymer International*, 49(4):337–344, 2000.

[50] Todd A Richmond and Chris R Somerville. The cellulose synthase superfamily. *Plant physiology*, 124(2):495–498, 2000.

[51] Marco Rolandi and Ranieri Rolandi. Self-assembled chitin nanofibers and applications. *Advances in colloid and interface science*, 207:216–222, 2014.

[52] Takanori Sannan, Keisuke Kurita, and Yoshio Iwakura. Studies on chitin, 2. effect of deacetylation on solubility. *Die Makromolekulare Chemie*, 177(12):3589–3600, 1976.

[53] Pawel Sikorski, Ritsuko Hori, and Masahisa Wada. Revisit of α-chitin crystal structure using high resolution x-ray diffraction data. *Biomacromolecules*, 10(5):1100–1105, 2009.

[54] Doekele G Stavenga, Atsuko Matsushita, Kentaro Arikawa, Hein L Leertouwer, and Bodo D Wilts. Glass scales on the wing of the swordtail butterfly graphium sarpedon act as thin film polarizing reflectors. *The Journal of experimental biology*, 215(4):657–662, 2012.

[55] Doekele G Stavenga, Bodo D Wilts, Hein L Leertouwer, and Takahiko Hariyama. Polarized iridescence of the multilayered elytra of the japanese jewel beetle, chrysochroa fulgidissima. *Philosophical Transactions of the Royal Society B: Biological Sciences*, 366(1565):709–723, 2011.

[56] Alison Sweeney, Christopher Jiggins, and Sönke Johnsen. Insect communication: polarized light as a butterfly mating signal. *Nature*, 423(6935):31–32, 2003.

[57] Hiroshi Tamura, Hideaki Nagahama, and Seiichi Tokura. Preparation of chitin hydrogel under mild conditions. *Cellulose*, 13(4):357–364, 2006.

[58] Laurent Vachoud, Nathalie Zydowicz, and Alain Domard. Formation and characterisation of a physical chitin gel. *Carbohydrate research*, 302(3):169–177, 1997.

[59] Julian FV Vincent. Arthropod cuticle: a natural composite shell system. *Composites Part A: Applied Science and Manufacturing*, 33(10):1311–1315, 2002.

[60] Julian FV Vincent and Ulrike GK Wegst. Design and mechanical properties of insect cuticle. *Arthropod Structure & Development*, 33(3):187–199, 2004.

[61] James C Weaver, Garrett W Milliron, Ali Miserez, Kenneth Evans-Lutterodt, Steven Herrera, Isaias Gallana, William J Mershon, Brook Swanson, Pablo Zavattieri, Elaine DiMasi, et al. The stomatopod dactyl club: a formidable damage-tolerant biological hammer. *Science*, 336(6086):1275–1280, 2012.

[62] Shinya Yoshioka and Shuichi Kinoshita. Polarization-sensitive color mixing in the wing of the madagascan sunset moth. *Optics express*, 15(5):2691–2701, 2007.

[63] Basel Younes, Alex Fotheringham, and Hassan M El-Dessouky. Birefringent approach for assessing the influence of the extrusion temperature profile on the overall orientation of as-spun aliphatic-aromatic co-polyester fibers. *Polymer Engineering & Science*, 49(12):2492–2500, 2009.

[64] Joseph Zaremba et al. Economics of the american lumber industry. *Economics of the American lumber industry*, page 232, 1963.

[65] Yongqin Zhang, Changhu Xue, Yong Xue, Ruichang Gao, and Xiuli Zhang. Determination of the degree of deacetylation of chitin and chitosan by x-ray powder diffraction. *Carbohydrate research*, 340(11):1914–1917, 2005.

[66] Chao Zhong, Ashleigh Cooper, Adnan Kapetanovic, Zhihua Fang, Miqin Zhang, and Marco Rolandi. A facile bottom-up route to self-assembled biogenic chitin nanofibers. *Soft Matter*, 6(21):5298–5301, 2010.